Copyright

By

Nicholas Bogart Richman

2009

Fatigue Life Investigation of High Performance Mast Arm Base Plate Connections

By

Nicholas Bogart Richman, B.S.

Thesis

Presented to the Faculty of the Graduate School

Of the University of Texas at Austin

In Partial Fulfillment

Of the Requirements

For the Degree of

Master of Science in Engineering

The University of Texas at Austin

May 2009

The Thesis committee for Nicholas Bogart Richman

Certifies that this is the approved version of the following thesis:

Fatigue Life Investigation of High Performance Mast Arm Base Plate Connections

APPROVED BY

SUPERVISING COMMITTEE:

Supervisor: Karl H. Frank

Todd A. Helwig

Dedication

To my family.

Tempus fugit.

Acknowledgements

I would like to thank the following people:

Dr. Karl H Frank, for the guidance he gave throughout my graduate education. It was a pleasure working as a grad student with him as my advisor.

Dr. Todd Helwig, whose Stability class was one of my favorite in graduate school.

Andrew Stam, for all the help and friendship he gave while we worked on our research. It was a great experience.

Steve Pool and James Kleineck, who ran tests while I ran analyses, and did plenty of other work around the lab.

Andrew Valentine, for all the hard work he put into our research and for his general attitude about everything.

Blake Stasney and Dennis Fillip, who know how to get everything done in the lab. Nothing would get done without them.

Fatigue Life Investigation of High Performance Mast Arm Base Plate Connections

by

Nicholas Bogart Richman, M.S.E

The University of Texas at Austin, 2009

SUPERVISOR: Karl H. Frank

Mast arm poles are typically connected to base plates using a structural fillet weld in a socket style connection. Previous research has shown that the fatigue performance of this connection is greatly dependent on the base plate thickness. Previous research has also indicated that the fatigue performance of a pole – to – base plate connection can be improved if a full penetration or external collar detail is used. This study was established to confirm these findings and to determine what variables affect the fatigue life of these higher performance details. Experimental tests were complimented with parametric studies using finite element models.

Results indicate that full penetration details can achieve excellent fatigue performance, and that both full penetration and external collar details perform better than a standard socket connection. It was found that the stiffness of the base plate played a role in the fatigue performance of the full penetration connection. Local bending in the pole occurs because of deflection of the base plate. This local bending creates high stresses in the pole near to the base plate, amplifying hot spot stresses at the weld toe of the full penetration connection, but not the hot spot stress in details that shift the hot spot stress away from the base plate.

Table of Contents

Chapter 1 Introduction 1

1.1 Background 1

1.2 Motivation 3

1.3 Scope of Research 4

Chapter 2 Test Setup and Procedure 6

2.1 Test Assumptions and Design 7

2.2 Description of Test Setup 8

2.3 Test Procedure 10

2.3.1 Calculation of Stress Ranges 10

2.3.2 Determination of Displacement Range 12

2.3.3 Limits and Failure Definition 12

2.3.4 Rotation of Failed Samples 13

Chapter 3 Test Specimen Design 14

3.1 Test Schedule 15

3.1.1 Nomenclature 15

3.1.2 Schedule of Mast Arms 17

3.2 Connection Detail 18

3.2.1 Full Penetration Detail 18

3.2.2 External Collar Detail 20

3.3 Bolt Pattern and Base Plate Geometry 21

3.4 Base Plate Thickness 25

3.5 Pole Diameter 26

3.6 Galvanization 26

3.7 Manufacturer 27

3.7.1 Pelco 27

3.7.2 Ameron and Union Metal 27

3.7.3 Valmont 27

Chapter 4 Experimental Test Results and Observations 28

4.1 Mill Test Results 28

4.1.1 Valmont Specimens 28

4.1.2 Pelco Specimens 29

4.1.3 Union Metal and Ameron Specimens 31

4.2 Prior Fatigue Test Results 31

4.3 Fatigue Life Coefficient and AASHTO Fatigue Categories 31

4.4 Fatigue Test Results 33

4.5 Typical Failures 36

4.5.1 Full Penetration 36

4.5.2 External Collar 40

4.6 Results and Observations 42

4.6.1 Comparison of Octagonal and Round Poles 43

4.6.2 Comparison of Base Plate Geometry 45
4.6.3 Comparison of External Collar and Full Penetration Details 49
4.6.4 Base Plate Thickness 52
4.6.5 Pole Diameter 54
4.6.6 Backing Ring Welds on Full Penetration Details 60
4.6.7 Comparison of Manufacturers 65
4.6.8 Comparison of Black, Galvanized, and Peened Specimens 66
4.7 Summary of Observations 68
Chapter 5 Analytical Methods 70
5.1 Finite Element Modeling 70
5.1.1 Parts 71
5.1.2 Assembly 74
5.1.3 Contact 74
5.1.4 Load and Boundary Conditions 76
5.1.5 Mesh 78
5.1.6 Global Model 79
5.1.7 Submodel 85
5.2 Evaluation of Stress Concentrations and Stress Concentration Factors (SCF) 87
5.2.1 Mesh Insensitivity Weld Toes 90
5.2.2 DNV Method 93

5.2.3 Dong Structural Stress Method 95

5.2.4 Convergence Study 96

Chapter 6 Results from Analytical Parametric Studies 100

6.1 Nomenclature Used in Parametric Studies 100

6.2 Results of Analytical Models 101

6.3 Full Penetration Weld Connection Stiffness 103

6.3.1 Base Plate Thickness 104

6.3.2 Pole Diameter 108

6.3.3 Pole Shape 110

6.3.4 Base Plate Geometry 114

6.3.5 Size of the Base Plate Hole in a Full Penetration Connection 115

6.3.6 Base Plate Stiffness 116

6.4 Failure Location 122

6.4.1 Presence of Backing Ring Fillet Welds 122

6.4.2 External Collar Base Plate Study 124

6.4.3 Effect of Base Plate Stiffness on SCF for Hot Spots Away From Base Plate 128

6.5 Evaluation of Fatigue Life Using Hot Spot Stress 130

6.6 Summary of Results of Parametric Studies 133

Chapter 7 Conclusions and Recommended Research 136

7.1 Conclusions 136

7.2 Recommendations for Future Research 137

7.3 Recommendations for Design of Mast Arm Structures 138

Appendix A Measured Dimensions of Specimens 140

Appendix B Summary of Results from Experimental and Analytical Research 142

Bibliography 144

List of Tables

Table 2-1: Moments of Inertia of 10-in Octagonal Poles with Varying Bend Radii 11

Table 3-1: Key of Nomenclature 16

Table 3-2: Test Schedule 17

Table 4-1: Valmont Tensile Data 28

Table 4-2: Valmont Chemistry Data 29

Table 4-3: Pelco Tensile Data 30

Table 4-4: Pelco Chemistry Data 30

Table 4-5: AASHTO Fatigue Constants 32

Table 4-6: Experimental Test Data 34

Table 4-7: Comparison of Round and Octagonal Full Penetration Details 45

Table 4-8: Comparison of *S* and *SR* Full Penetration Details 46

Table 4-9: Comparison of *S* and *R* Full Penetration Details 48

Table 4-10: Comparison of Full Penetration and External Collar Details 51

Table 4-11: Comparison of 2-in and 3-in Full Penetration Details 53

Table 4-12: Comparison of Pole Diameter, 2-in Base Plate Full Penetration Details 55

Table 4-13: Average Fatigue Coefficients for 8-in, 10-in, and 12-in Diameter Full Penetration Details 56

Table 4-14: Comparison of Pole Diameter, 3-in Base Plate Full Penetration Details 58

Table 4-15: Comparison of Pole Diameter, 2-in External Collar Details 59

Table 4-16: Variation in Backing Ring Weld, 10-3R-WY 61

Table 4-17: Variation of Backing Ring Weld, 8-2S-WY 64

Table 4-18: Comparison of Manufacturers, 10-3R-WY 66

Table 4-19: Comparison of Galvanized, Black, and Peened 10-3R-WY 67

Table 5-1: Results from Convergence Study 97

Table 6-1: Key of New Nomenclature Variables 101

Table 6-2: Computed Hot Spot Stresses and Stress Concentration Factors (SCF) 102

Table 6-3: Base Plate Stiffness and SCF 120

Table 6-4: Base Plate Stiffness and SCF for External Collar and Full Penetration with Backing Ring Fillet 129

Table 6-5: Fatigue Life and Hot Spot Stress Range 131

Table A-1: General Dimensions 140

Table A-2: Measured Weld Dimensions 141

Table B-1: Experimental Test Results 142

Table B-2: SCF and Base Plate Stiffness 143

List of Figures

Figure 1-1: A Typical Mast Arm Signal Structure (Anderson, 2007) 1

Figure 2-1: Typical loads on a mast arm (Anderson, 2007) 6

Figure 2-2: Simply supported beam approximating 2 cantilevers (Anderson, 2007) 8

Figure 2-3: Testing frame with mast arms in position (Anderson, 2007) 9

Figure 3-1: Typical Mast Arm 15

Figure 3-2: Sample Mast Arm Nomenclature 16

Figure 3-3: Full Penetration Detail (*WY* Detail) 19

Figure 3-4: Close Up of Full Penetration Weld 19

Figure 3-5: External Collar Detail (EC Detail) 21

Figure 3-6: *S* Detail 23

Figure 3-7: *R* Detail 24

Figure 3-8: *SR* Detail 25

Figure 4-1: Typical Weld Toe Failure of a Full Penetration Connection 36

Figure 4-2: Cross Section of a Typical Full Penetration Connection 37

Figure 4-3: Typical Failure at a Backing Ring Fillet Weld 38

Figure 4-4: An Etched Cross Section of a Full Penetration Connection with a Backing Ring Fillet Weld 38

Figure 4-5: Typical Failure at a Backing Ring Tack Weld 39

Figure 4-6: Cross Section of a Tack Weld Failure 40

Figure 4-7: Typical External Collar Failure 41

Figure 4-8: A Cross Section of a Typical External Collar Detail 41

Figure 4-9: Close Up of the Collar Weld (Etched) 42

Figure 4-10: Comparison of Round and Octagonal Full Penetration Details 44

Figure 4-11: Comparison of *S* and *SR* Full Penetration Details 46

Figure 4-12: Comparison of *S* and *R* Full Penetration Details 48

Figure 4-13: Comparison of Full Penetration and External Collar Details 50

Figure 4-14: Comparison of 2-in and 3-in Full Penetration Details 52

Figure 4-15: Comparison of Pole Diameter, 2-in Base Plate Full Penetration Details 55

Figure 4-16: Comparison of Pole Diameter, 3-in Base Plate Full Penetration Details 57

Figure 4-17: Comparison of Pole Diameter, 2-in External Collar Details 59

Figure 4-18: Variation of Backing Ring Weld, 10-3R-WY 60

Figure 4-19: Variation of Backing Ring Welds, 8-2S-WY 63

Figure 4-20: Comparison of Manufacturers, 10-3R-WY 65

Figure 4-21: Comparison of Galvanized, Black, and Peened 10-3R-WY 67

Figure 5-1: The Base Plate Assemblage Part 72

Figure 5-2: The Shell Pole Part 73

Figure 5-3: The Reaction Plate Part 73

Figure 5-4: The Completed Pole Assembly 74

Figure 5-5: Contact Surface between Pole Shaft and Backing Ring 75

Figure 5-6: The Symmetry Boundary Condition 77

Figure 5-7: The Fixed Edges of the Bolt Holes 78

Figure 5-8: A Typical Full Penetration Model 80

Figure 5-9: The Full Penetration Connection 81

Figure 5-10: An External Collar Model 82

Figure 5-11: The External Collar Connection 83

Figure 5-12: Typical Full Penetration Response 84

Figure 5-13: Typical External Collar Response 85

Figure 5-14: Submodel for a 12-1.5R-WY Model 86

Figure 5-15: The Variation of Stress near the Weld Toe (Full Penetration) 88

Figure 5-16: Through Thickness Stress at the Weld Toe (Full Penetration, Global Model)..... 89

Figure 5-17: Mesh Sensitivity of Finite Element Stresses at the Weld Toe (Full Penetration)..... 91

Figure 5-18: Close Up of Figure 9 near the Weld Toe 92

Figure 5-19: Mesh – Insensitivity shown in Through Thickness Stresses at the Weld Toe (Full Penetration) 93

Figure 5-20: DNV Extrapolation 94

Figure 5-21: The Assumed Stress Profile in the Dong Method (Dong 2001) 96

Figure 5-22: DNV Mesh Size Convergence 97

Figure 5-23: A Comparison of DNV and Dong Convergence (Hot Spot Stress)..... 98

Figure 5-24: A Comparison of DNV and Dong Convergence (SCF) 99

Figure 6-1: Typical Through Thickness Stress Profile..... 103

Figure 6-2: 8-XR-WY (SCF versus Base Plate Thickness) 105

Figure 6-3: 12-XR-WY (SCF versus Base Plate Thickness) 106

Figure 6-4: Bending of the Base Plate Connection (12-1.5R-WY)..... 107

Figure 6-5: Bending in the Base Plate Connection (12-3R-WY) 108

Figure 6-6: Pole Diameter Study (Hot Spot Stress versus Base Plate Thickness) 109

Figure 6-7: Pole Diameter Study (SCF versus Base Plate Thickness) 110

Figure 6-8: Typical Cross Section of Octagonal Pole 111

Figure 6-9: Pole Shape Study (SCF versus Base Plate Thickness) 112

Figure 6-10: Stress Distribution of a Typical Octagonal Pole (10-1.5R-WY) 113

Figure 6-11: Base Plate Geometries Studied..... 114

Figure 6-12: Base Plate Geometry Study (SCF) 115

Figure 6-13: Base Plate Hole Study (SCF versus Base Plate Thickness)..... 116

Figure 6-14: Approximate Behavior of Base Plate 117

Figure 6-15: Base Plate Moment of Inertia is Taken Through the Center of the Hole 119

Figure 6-16: SCF versus Base Plate Flexibility (Constant Applied Moment) 121

Figure 6-17: 10-3R-WY-FILLET Stress Distribution..... 123

Figure 6-18: 10-XR-WY-FILLET (SCF versus Base Plate Thickness)..... 124

Figure 6-19: 12-XS-EC (SCF versus Base Plate Thickness) 125

Figure 6-20: Comparison of External Collar and Full Penetration SCF 126

Figure 6-21: 12-1.5S-EC Stress Distribution 127

Figure 6-22: 12-3S-EC Stress Distribution 128

Figure 6-23: SCF versus Base Plate Flexibility for External Collar and Full Penetration with Fillet at Top of Backing Bar 129

Figure 6-24: Fatigue Life Plotted Against Hot Spot Stress Range..... 132

Chapter 1

Introduction

1.1 Background

This study investigated the fatigue performance of mast arms commonly used in traffic luminaries. Mast arms are used throughout the United States of America in cantilevered traffic signal structures. A typical structure is shown in Figure 1-1.

Figure 1-1: A Typical Mast Arm Signal Structure (Anderson, 2007)

Typical mast structures consist of a single vertical column supporting a tapered cantilevered mast arm. The horizontal mast arm supports traffic signals and signs. This type of traffic structure has

become popular due to its simplicity of design and aesthetics. The mast-type traffic signal structure is a flexible, non – redundant structure, however, and fatigue in the mast arm pole – to – base plate connection can become an issue.

A mast arm is a hollow tube that is cold worked from a steel plate. The plate is worked into shape and then a longitudinal seam weld closes the section. The tubular pole is then connected to a base plate using one of several connections. Typically, the pole – to – base plate connection is a fillet weld or a full penetration weld.

A fatigue crack grows when a structure cycles through a range of tensile stresses. The crack will start at an initial discontinuity and grow with each cycle of loading. Unlike the ultimate strength mode of failure, fatigue depends on the difference between the maximum and minimum stresses (called the stress range) that occur in a load cycle and not necessarily the maximum stress that occurs. Because of this, fatigue cycles can accumulate and a crack can grow even though stresses are well below the yield point of the material.

If the stress range that a structure experiences is below a certain level, called the constant amplitude fatigue limit (CAFL), no fatigue damage will accumulate. A structure that only experiences stress below the CAFL will have a theoretically infinite fatigue life, which is how AASHTO requires design for mast arms. Given in a nominal stress, the CAFL is different for different connections and connection geometries, accounting for the difference in local stress distribution between various details.

In mast arms, low stiffness and relatively low mass makes them susceptible to effects such as galloping which occur under a constant wind loading. Mast arms are also susceptible to vibration due to normal wind gusting (Koenigs, et al. 2003). The wind velocities that cause these effects are typically lower than the wind speed for ultimate strength design and could occur on a daily basis.

Most fatigue cycles will generally be accumulated under service loads; this means that fatigue failures can occur unexpectedly, under service conditions.

A fatigue crack anywhere in a traffic structure can be serious, due to the proximity to a roadway and the chance that the failed structure might end up in the right of way, possibly causing injury to a motorist. In cantilevered traffic signal structures, the failure tends to occur in the horizontal members, since the vertical members tend to be larger and experience an axial compressive load, which reduces the tension stress range that the vertical member sees (Koenigs, et al. 2003). Constant dead load moment due to self weight and the traffic attachments causes high tension stress near the pole – to – base plate connection on the top of the horizontal mast arm.

1.2 Motivation

Fatigue in mast arms has become an issue for several states. Researchers are aware of two mast arm failures that occurred in the state of Texas during the two years that this phase of research was ongoing.

Mast arms are designed to only experience stresses under the CAFL; the CAFL used for design is determined by matching the connection detail with examples of connections given in section 11 of AASHTO Luminaries 2006i. AASHTO provides two CAFLs for mast arms, one for socket connections and another for full penetration connections.

A failure of a mast arm indicates that the CAFL used in design did not accurately represent the fatigue behavior of the particular detail. Currently, CAFLs given in AASHTO do not account for any variable that may affect connection performance except connection detail.

Several studies at the University of Texas at Austin have researched fatigue of different mast arm connections. Previous research at the University of Texas at Austin focused on socket

connections, with other details such as full penetration connections, external stiffeners, and external collars also include in the research. It was found that fatigue performance of socket connections was highly dependent on the base plate thickness and that full penetration and external collar details exhibited much better fatigue performance (M. T. Koenigs 2003) (Anderson 2007).

This study was established to confirm the improved fatigue performance of full penetration and external collar details and to determine the variables that effect fatigue performance of these connections.

1.3 Scope of Research

This research was done for the pooled fund study "Investigation of the Fatigue Life of Steel Base Plate to Pole Connections for Traffic Structures". Funding for this research came from the following states: Texas, California, Pennsylvania, Wyoming, Iowa, Colorado, Minnesota, North Carolina, Wisconsin, and South Dakota. This is the second phase of research done under this study.

The details tested in this study were designed to have a high fatigue performance, based on the results of the prior phase of research as well as other research done at the University of Texas at Austin (M. T. Koenigs 2003) (Anderson 2007). The two connection details studied were a full penetration connection and an external collar connection. The objective of this research was to confirm the findings of previous studies and to determine the variables that influence the fatigue performance of these higher performance details.

In addition to experimental tests of mast arm specimens, Finite Element Analysis software was used to perform parametric studies. These parametric studies allowed the researchers to better understand the effects of individual variables on the fatigue performance of the mast arms.

The test setup and test specimen design are presented in Chapters 2 and 3, respectively. Chapter 4 presents the results material tension tests and of experimental fatigue tests. An introduction to the analytical models used in this study is given in Chapter 5. The results of parametric studies are given in Chapter 6. The conclusions that the researchers drew from this study and recommendations for future research are given in Chapter 7.

Chapter 2

Test Setup and Procedure

This chapter provides an overview of the experimental test setup and the procedures used to evaluate the fatigue performance of mast arms. This study used an existing test frame that had been used in two prior studies of mast-arm fatigue performance (M. T. Koenigs 2003) (Anderson 2007). An overview of the assumptions and general design of the test setup is given, followed by a discussion of the calculation of testing loads and the general test procedure

Figure 2-1: Typical loads on a mast arm (Anderson, 2007)

2.1 Test Assumptions and Design

Typical mast arm signal structures are cantilever structures as shown in Figure 2-1. The gravity loading consists of the self weight of the mast arm as well as point loads from the lights and signs. The gravity loads will cause a constant mean stress to be applied to the mast arm. Wind loading will occur due to wind effects such as galloping and will cause the stress in the mast arm to cycle about the mean dead load stress.

The resulting moment diagram can be approximated by a moment diagram that increases linearly from zero at the end of the pole to a maximum moment at the base plate, which is the moment diagram corresponding to a cantilever beam with a point load at the end. This is statically equivalent to the moment diagram of half of a simply supported beam with a point load of 2P as shown in Figure 2-2. A simply supported beam test setup was made by placing two mast arms back to back. This allowed two replicate mast arms could be tested at the same time under identical loads.

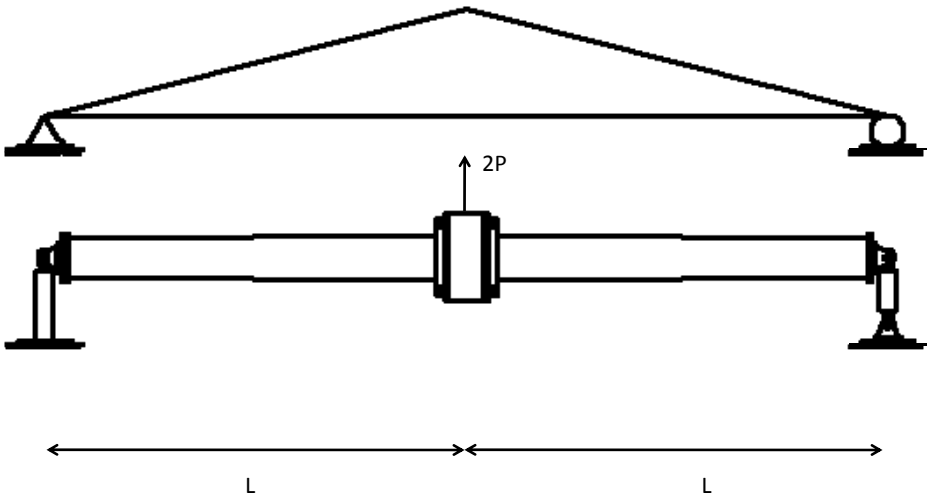

Figure 2-2: Simply supported beam approximating 2 cantilevers (Anderson, 2007)

2.2 Description of Test Setup

The test setup is shown in Figure 2-3. The setup consists of two mast-arms attached on either side of a load box to create a beam. The beam is simply supported by two end reactions with a load box in the middle that connects to a 22 kip hydraulic actuator. The actuator is supported by a steel portal frame that is anchored to the reaction floor. The load box serves as a rigid element (relative to the mast arms) that distributes the load from the actuator to the mast arms. The actuator is connected to a 20 gallon - per - minute hydraulic power supply. The test was designed so that the reaction ends would always remain in tension (the ram always pulling). This is similar to the loading that occurs in the field which is predominately a vertical dead load. The tension loading simplifies the end reactions by eliminating the need for restraining out of plane degrees of

freedom and rotation about the longitudinal axis of the specimens. The tension in the loading ram results in a stabilizing force which only produces reactions in the vertical plane perpendicular to the longitudinal axis of the beams.

Figure 2-3: Testing frame with mast arms in position (Anderson, 2007)

The length from one reaction to the other reaction is 16-ft, a distance chosen to fit the strong-floor bolt hole spacing of 4-ft on center. When the test setup was designed it was confirmed that a reaction-to-reaction distance of 16-ft gave appropriate variation in applied moment to produce the desired stress ranges for fatigue tests of mast arms. The samples were specified to be a length of 86.75-in. Smaller lengths could be tolerated by adding washers at the reaction end, but longer lengths could not be tolerated.

New bolt hole patterns at the base plate and reaction end were used in this phase of testing. At the reaction end, adapter plates were made to allow new reaction bolt patterns to be attached to the reaction clevises. Two different load boxes were available for use in the test to accommodate the new geometries. New holes were drilled in the load boxes to accommodate new bolt hole geometries tested in this phase of research. New holes were laid out on the load boxes in the way that minimized interaction with previously drilled holes. The change in the box stiffness due to the added holes was not considered to be significant.

2.3 Test Procedure

A test consists of loading the two mast arms through the load box until one mast arm fails from excessive growth of a fatigue crack in the pole – to – base plate connection. Once the test was stopped, the failed specimen is rotated to place the crack in compression and the test is continued until another failure occurs.

2.3.1 Calculation of Stress Ranges

Stress ranges were chosen based on prior knowledge of a connection detail's fatigue performance. The load range for the ram was determined by calculating the load that would produce the desired nominal stress at the weld toe at the base plate. Cross sectional properties used to determine the loads for fatigue testing were based on the nominal measurements called out in drawings. Measurements were made to verify the as built dimensions. When an external collar was present, it was treated as a fatigue performance attachment and was not included in the diameter of the pole. For all samples, the pole wall was nominally 7 ga (0.1793 –in) Diameters of round poles were measured using calipers. On polygonal poles two measurements characterize the overall shape of the pole: 1) corner – to – corner distance and 2) flat – to – flat distance. The corner – to – corner distance is the longest possible distance between two corners and is the diameter of a circle

that circumscribes the polygon. The flat – to – flat distance is the distance between two opposing faces and is the diameter of an inscribing circle. An ultrasonic transducer was used to confirm the thickness of the pole wall; in general a maximum discrepancy of approximately ±0.02 off of the nominal thickness was deemed ignored and the nominal thickness was used in calculations.

The taper of the specimen was ignored in the calculation of the nominal stress. Simple beam bending was assumed in this calculation, ignoring any geometric non-linearity or notch stress concentration. The moment of inertia of a round section was given by the equation $I = \frac{\pi}{4}(r_2^4 - r_1^4)$, where r_2 is the outer radius of the section and r_1 is the inner radius. When the moment of inertia of a polygonal cross section was required, a sketch of the cross section was made in AutoCad and the massprop function was used to determine the moment of inertia. When calculating the moment of inertia of the cross sections, sharp corners were assumed (a bend radius of 0-in) for simplicity. For reference, the moment of inertia of a mast arm with varying bend radii and the moment of inertia of a mast arm with a bend radius of 0-in (sharp corners) for a mast arm with a corner – to – corner distance of 10-in are compared in Table 2-1. The bend radius was not called out on dimension sheets and was not controlled during manufacture. The bend radius is difficult to measure, but most mast arms tested appear to have bend radii of approximately $^3/_8$-in.

Bend Radius	**Moment of Inertia**
0-in (Sharp Corners)	58.4037-in^4
$^3/_8$-in	59.2878-in^4
$^1/_2$-in	59.9303-in^4
2-in	62.7898-in^4

Table 2-1: Moments of Inertia of 10-in Octagonal Poles with Varying Bend Radii

2.3.2 Determination of Displacement Range

The tests were run under displacement control to maintain a high level of control of load cycle. In order to run a displacement control test, accurate measures of the displacements corresponding to the maximum and minimum loads must be made. The mast arms were loaded statically through several cycles until the connection settled and the displacements remained constant. From the deflections corresponding to maximum and minimum load, a mean deflection and amplitude were calculated and then entered in to the displacement control system as the set point and amplitude. The closed system maintained these deflections throughout the dynamic test. This allowed for the tests to be run at any speed without having to adjust for the reduction in required input load due to the dynamic amplification of the load.

2.3.3 Limits and Failure Definition

In order to maintain control over the setup while running the dynamic test, closed loop displacement control was used. Using an LVDT, the MTS control system can determine the difference between where the ram is relative to a programmed displacement function. This difference between where the ram displacement and the displacement function's command displacement is called the error. The control system then adjusts the position of the ram to reduce the error; the larger the error the larger the adjustment. This is done quickly and in repetition and produces a stable and accurate test.

Limits on the closed loop system were set on several variables during testing. When the variables exceeded the limits the system would shut down. The variables used in this study were ram force, displacement, and error. A 10% increase or decrease was used as the limit for force and displacement. A slightly larger increase or decrease was used for error depending on the amount

of signal noise observed in the specific test. The test was run under displacement control, so a considerable change in the displacement might indicate a loss of closed loop control of the test. A large amount of error reflects a loss of control of the system and can indicate a loss of stability. A change in load indicates a change in stiffness of the sample due which indicates that cracking of the specimen has occurred.

Using these limits, a failure was defined whenever a crack was large enough to cause a 10% drop in the load required to reach the minimum displacement. A loss of stiffness large enough to cause a 10% drop in the load corresponds to a crack that is easily observed and extended to about 1/3 the depth of the specimen.

2.3.4 Rotation of Failed Samples

At this point the failed specimen was rotated or "flipped" so that the crack was on the compression side. Displacements were re – determined to provide the required loads for continued testing at the same stress range. The test was then restarted and cycled until the second mast arm failed or a second failure occurred in the flipped specimen.

Chapter 3

Test Specimen Design

The mast arm specimens tested for the research outlined in this thesis were designed by the sponsors and researchers in the previous phase of the research. The mast arms were designed to have increased fatigue lives based on the results from the previous studies at the University of Texas at Austin (Anderson 2007). These previous studies found that the external collar and full penetration details greatly improved fatigue life over the typical socket connection and so all mast arms tested in this phase have external collar or full penetration base plate connection weld details

In addition to testing the connection detail, a few new variables were also tested. The effect of the geometry of the base plate and bolt hole pattern was investigated. Three types of base plate geometries were included: a rectangular base plate with a rectangular bolt pattern, a square base plate with a square bolt pattern, and a square base plate with a rectangular bolt pattern. Different manufacturers were also studied. Prior to the phase of research outlined in this thesis, only mast arms from one manufacturer were tested at the University of Texas at Austin. While the majority of the specimens tested were from the original manufacturer used in Anderson 2007, Valmont Industries, several mast arms from different manufacturers were tested to provide information on the effect of the producer upon the fatigue performance.

The lengths of the poles were determined by the test setup and were designed with a length of 86.75-in including the end plate. Longer poles could not be tested, but slightly smaller poles could be tested by placing extra washers between the reaction plate and the end plate. The design

pole wall thickness was 7-ga or 0.1793-in, which is typical for mast arms with a diameter of 10-in. A typical mast arm sample is shown in Figure 3-1.

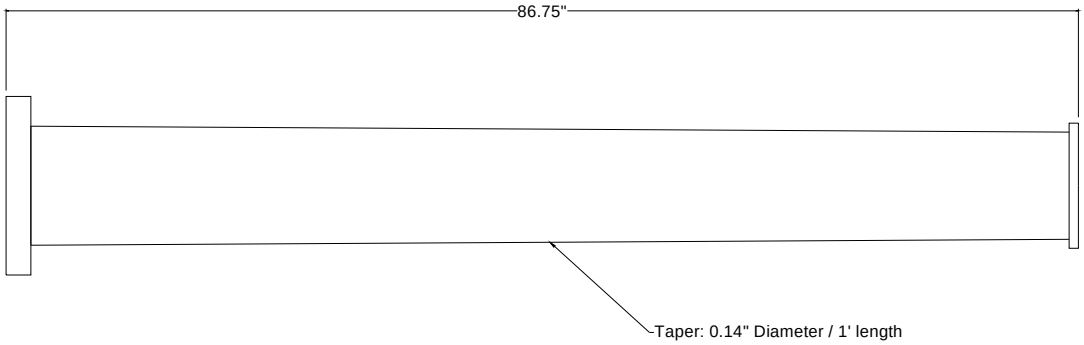

Figure 3-1: Typical Mast Arm

3.1 Test Schedule

3.1.1 Nomenclature

A number of variables were tested in this study. It was helpful to the researchers to name samples according to the features represented in each mast arm. All names followed the form: X_1 - X_2X_3 - X_4 - X_5X_6. The first characters represent pole diameter, the second characters represent base plate thickness and geometry, the third characters represent the connection detail, and the fourth characters represent the manufacturer and whether the mast arm was galvanized or black (not galvanized). For example, a sample mast arm name is given in Figure 3-2.

10-2S-WY-VG

Figure 3-2: Sample Mast Arm Nomenclature

Looking at each variable in Figure 2 at a time: 10 – this mast arm has a 10-in diameter pole. 2S – the base plate of this mast arm is 2-in thick and is square with a square bolt pattern. *WY* – this stands for Wyoming detail which consists of a full penetration weld. *VG* – indicates that this mast arm was made by Valmont Industries (*V*) and was galvanized (*G*). A complete key is given in Table 3-1. Specimens will be referred to by this nomenclature unless further explanation is required.

Connection Detail	
WY	Full Penetration ("Wyoming" Detail)
EC	External Collar
Base Plate Detail	
S	Square Base Plate / Square Bolt Pattern
R	Rectangular Base Plate / Rectangular Bolt Pattern
SR	Square Base Plate / Rectangular Bolt Pattern
Galvanizing	
G	Galvanized
B	Not Galvanized ("Black")
Manufacturer	
A	Ameron
P	Pelco
U	Union Metal
V	Valmont

Table 3-1: Key of Nomenclature

3.1.2 Schedule of Mast Arms

A complete schedule of mast arms tested in this phase of research is given in Table 3-2.

Specimen Code	Base Plate Thickness (in)	Arm Diameter (in)	Base Plate Geometry	Connection Detail	Galv.	Peened	Manufacturer	Backing Bar Weld Type
10-2S-WY-PB-A	2	10	S	Full Penetration	No	No	Pelco	Fillet
10-2S-WY-PB-B	2	10	S	Full Penetration	No	No	Pelco	Fillet
10-2S-WY-VG-A	2	10	S	Full Penetration	Yes	No	Valmont	None
10-2S-WY-VG-B	2	10	S	Full Penetration	Yes	No	Valmont	None
8-2S-WY-VG-A	2	8	S	Full Penetration	Yes	No	Valmont	Tack
8-2S-WY-VG-B	2	8	S	Full Penetration	Yes	No	Valmont	Tack
8-2S-EC-VG-A	2	8	S	External Collar	Yes	No	Valmont	N/A
8-2S-EC-VG-B	2	8	S	External Collar	Yes	No	Valmont	N/A
12-2S-WY-VG-A	2	12	S	Full Penetration	Yes	No	Valmont	Tack
12-2S-WY-VG-B	2	12	S	Full Penetration	Yes	No	Valmont	Tack
12-2S-EC-VG-A	2	12	S	External Collar	Yes	No	Valmont	N/A
12-2S-EC-VG-B	2	12	S	External Collar	Yes	No	Valmont	N/A
10-3R-WY-VG-A	3	10	R	Full Penetration	Yes	No	Valmont	
10-3R-WY-VG-B	3	10	R	Full Penetration	Yes	No	Valmont	
10-3R-WY-VP-A	3	10	R	Full Penetration	Yes	Yes	Valmont	None
10-3R-WY-VP-B	3	10	R	Full Penetration	Yes	Yes	Valmont	None
10-3R-WY-VB-A	3	10	R	Full Penetration	No	No	Valmont	None
10-3R-WY-VB-B	3	10	R	Full Penetration	No	No	Valmont	None
10-3R-WY-AG-A	3	10	R	Full Penetration	Yes	No	Ameron	None
10-3R-WY-UG-A	3	10	R	Full Penetration	Yes	No	Union Metal	None
ZZ88734-A	3	10	R	Full Penetration	Yes	No	Valmont	Fillet
ZZ88734-B	3	10	R	Full Penetration	Yes	No	Valmont	Fillet
ZZ88735-A	3	10	R	Full Penetration	Yes	Yes	Valmont	Fillet
ZZ88735-B	3	10	R	Full Penetration	Yes	Yes	Valmont	Fillet
10-2SR-WY-VG-A	2	10	SR	Full Penetration	Yes	No	Valmont	
10-2SR-WY-VG-B	2	10	SR	Full Penetration	Yes	No	Valmont	
10-2SR-EC-VG-A	2	10	SR	External Collar	Yes	No	Valmont	N/A
10-2SR-EC-VG-B	2	10	SR	External Collar	Yes	No	Valmont	N/A
10-3R-WY-PG-A	3	10	R	Full Penetration	Yes	No	Pelco	Tack
10-3R-WY-PG-B	3	10	R	Full Penetration	Yes	No	Pelco	Tack
10-2R-EC-PG-A	2	10	R	External Collar	Yes	No	Pelco	N/A
10-2R-EC-PG-B	2	10	R	External Collar	Yes	No	Pelco	N/A
12-3R-WY-PG-A	3	12	R	Full Penetration	Yes	No	Pelco	Tack
12-3R-WY-PG-B	3	12	R	Full Penetration	Yes	No	Pelco	Tack
12-2R-EC-PG-A	2	12	R	External Collar	Yes	No	Pelco	N/A
12-2R-EC-PG-B	2	12	R	External Collar	Yes	No	Pelco	N/A

Table 3-2: Test Schedule

3.2 Connection Detail

3.2.1 Full Penetration Detail

In previous phases of research at the University of Texas, mast arms that were connected to base plates using a full penetration weld outperformed those connected with a fillet weld in a socket connection (M. T. Koenigs 2003) (Anderson 2007). For the research study presented in this thesis, it was decided to use a full penetration detail specified by the Wyoming Department of Transportation (WyDOT), and is referred to in the nomenclature as *WY*. A typical *WY* detail is shown in Figure 3-3. The Wyoming detail calls for field applied caulking at the top of the backing ring. Before a mast arm is galvanized, it is dipped in an acidic pickling solution. This solution can get trapped in the space between the backing ring and the pole. When the mast arm is galvanized, the galvanizing material cannot penetrate into the space between the backing ring and the pole. This results in an unprotected area in an acidic environment which causes a problem for corrosion. The caulk seals out oxygen, and provides the protection against corrosion that is needed. Corrosion was not an issue in this phase of research, due to the relative short time between manufacture of the pole and testing, so the caulk was left off of the Wyoming details that were studied.

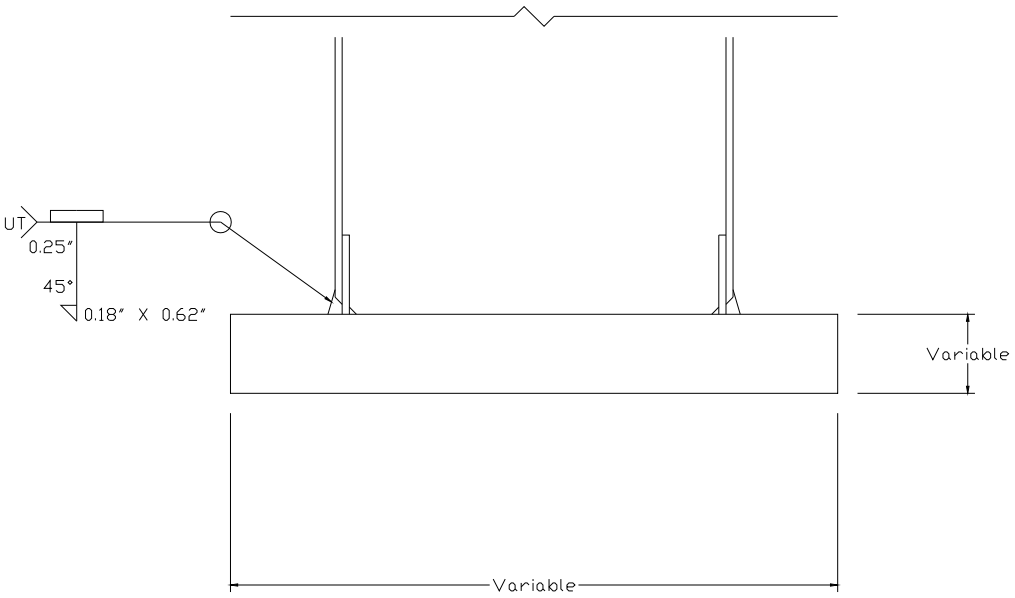

Figure 3-3: Full Penetration Detail (*WY* Detail)

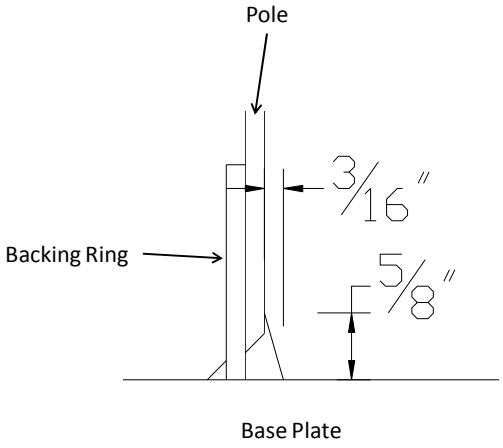

Figure 3-4: Close Up of Full Penetration Weld

The detail consists of first welding a backing ring on the base plate with a fillet weld. Then the mast arm is beveled at a 45° angle and fit over the backing ring. A root opening is left between the base plate and the beveled tip of the mast arm, and the full penetration weld is placed. The longer dimension of the weld is along the length of the pole and is 0.62-in or $^{5}/_{8}$-in. The weld leg dimension along the base plate is the same as the pole thickness, 0.1793-in or $^{3}/_{16}$-in. For this study it was specified that the backing ring remain unwelded to the pole at the top edge (away from the base plate). A close up of the full penetration weld is shown in Figure 3-4. Several samples received from Valmont that had been rejected due to a fillet weld at the top of the backing ring and were tested along with the other samples.

3.2.2 External Collar Detail

Previous phases also found that adding an external collar to a socket connection improved the fatigue life (M. T. Koenigs 2003) (Anderson 2007). External collars were seen as a large number of stiffeners evenly distributed around the mast arm (Anderson 2007). This detail is referred to as EC. The previous external collar detail used a scalloped collar that had a variable length around the pole; the distance from the base plate to the top of the collar varied (Anderson 2007). In this phase, all collars had a constant length around the pole; the distance from the base plate to the top of the collar was constant around the mast arm. A typical EC detail is shown in Figure 3-5.

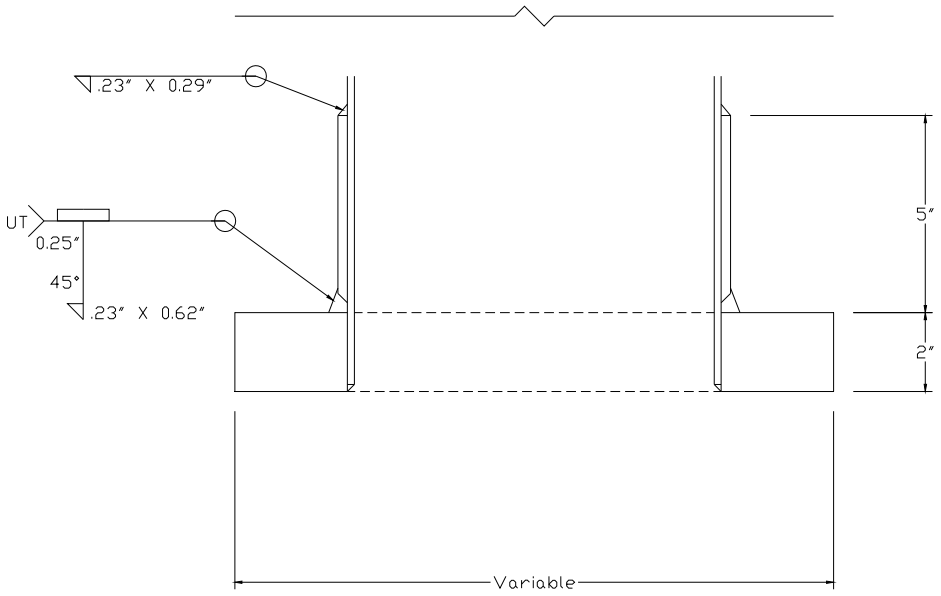

Figure 3-5: External Collar Detail (EC Detail)

The detail is similar to a socket connection. A hole is cut in the base plate and the mast arm is inserted into the hole and a seal fillet weld is placed connecting the mast to the back of the base plate. A 3-ga (0.2391-in) collar is then wrapped around mast and connected to the base plate with a full penetration weld using the mast arm as a backing plate. The collar is connected to the mast arm by a fillet weld at the top of the collar. Both the base plate weld and the weld at the top of the collar are unequal welds with the long edge in the direction of the mast arm. The long edge is 0.64-in on the base plate weld and 0.29-in on the weld at the top of the collar. The short dimension is equal to the thickness of the collar for both welds, 0.23-in.

3.3 Bolt Pattern and Base Plate Geometry

In prior studies at the University of Texas, one bolt pattern and base plate geometry were used throughout the entire study. A square pattern and geometry was used in Koenigs (M. T. Koenigs

2003) and a rectangular bolt pattern and geometry was used in Anderson (Anderson 2007). In order to determine if the bolt pattern or base plate geometry had an effect on fatigue life, multiple bolt patterns and base plate geometries were used in this study. A bolt pattern that is similar to the geometry of the base plate is typically used. For example, a rectangular bolt pattern is used with a rectangular base plate. This phase of research used a rectangular bolt pattern in a rectangular base plate and a square bolt pattern in a square base plate. Two specimens, a full penetration and an external collar had a rectangular bolt pattern in a square base plate. This was done in order to separate bolt pattern and base plate geometry as variables.

The rectangular bolt pattern used in the rectangular base plate measured 9-in horizontal by 15-in vertical and is the same pattern used in the previous phase of research done by Anderson. The square bolt pattern used in the square base plate measured 12.5-in by 12.5-in. In this study, these details were designated *R* and S, respectively. The rectangular bolt pattern that was used in a square base plate was tested and measured 9-in vertical by 12-in and was designated an *SR* detail. The bolt patterns and geometries can be seen in Figure 3-6, Figure 3-7, and Figure 3-8.

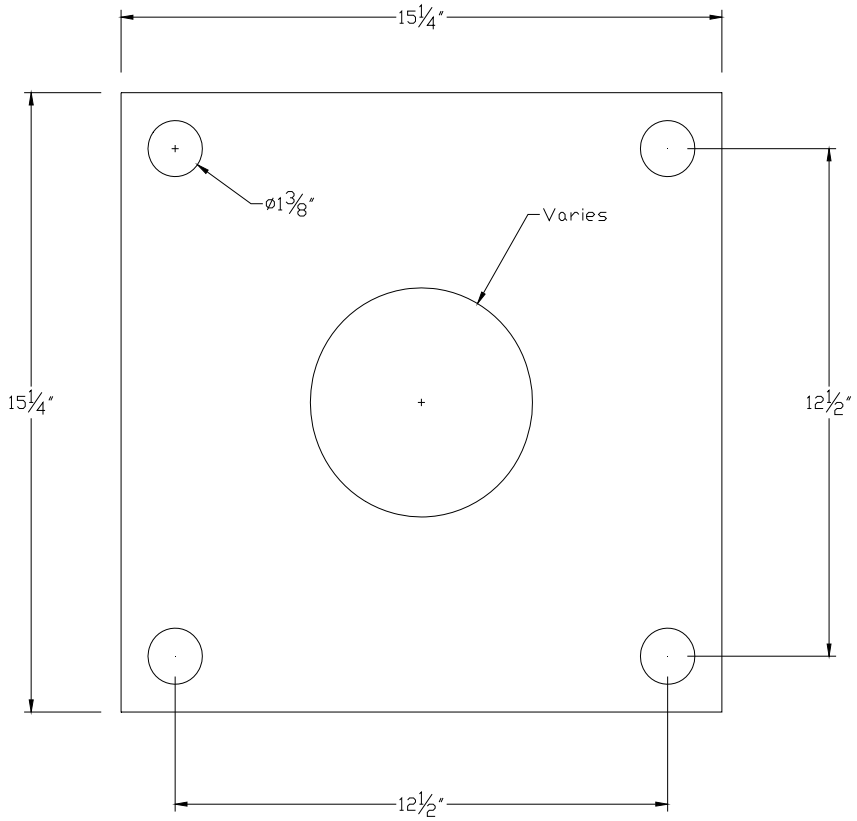

Figure 3-6: *S* Detail

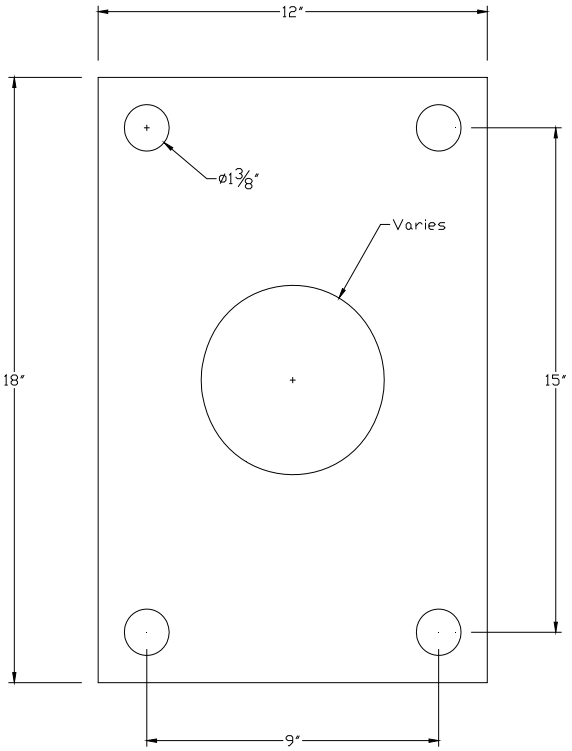

Figure 3-7: *R* Detail

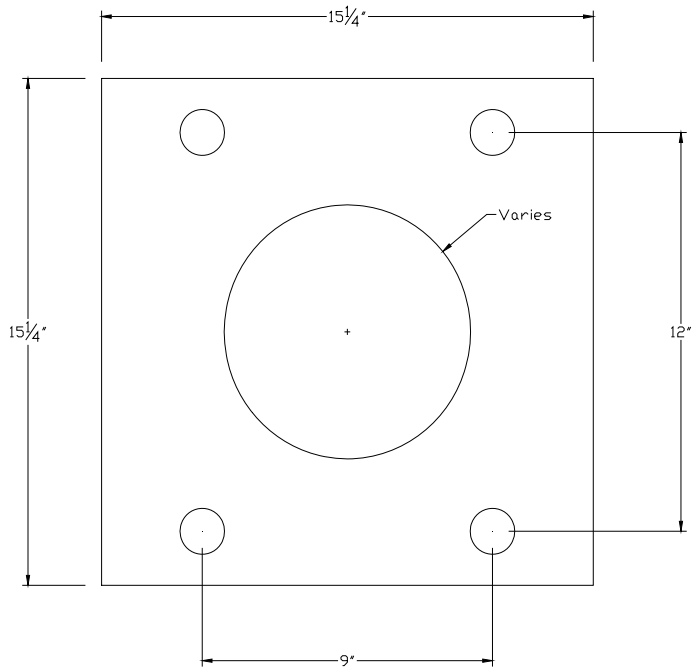

Figure 3-8: *SR* Detail

3.4 Base Plate Thickness

The findings of previous studies at the University of Texas indicate that the thickness of the base plate has a large influence on the stiffness of the entire connection. A thicker base plate produces a stiffer connection and will reduce the local bending close to the weld toe. With this in mind, the base plates of specimen tested in this phase were designed to be larger than base plates in typical mast arm connections.

All square, full penetration samples were tested with a 2-in thick base plate (2S-WY). All rectangular, full penetration samples were tested with a 3-in thick base plate (3R-WY). These base plates were the thickest tested in previous phases and approach the thickest practical base plate. All square, external collar details were tested with a 2-in base plate (2S-EC). Both

rectangular bolt pattern / square base plate were tested with a 2-in base plate (2SR-WY and 2SR-EC).

3.5 Pole Diameter

The earlier research at the University of Texas concentrated on only 10-in diameter poles. To determine the effect of pole diameter on the stiffness of the connection, the research presented in this thesis included pole diameters of 8-in, 10-in, and 12-in. The 8-in and 12-in diameter poles with external collar details and with 2-in thick base plates and full penetration details (8-2S-EC and 12-2S-WY, for example) were tested to compare with 10-in external collar and full penetration details from previous phases. The 10-in diameter poles with full penetration details with 3-in rectangular base plates (10-3R-WY) were tested to investigate base plate thickness in order to compare with data from the previous phase which used 2 inch base plates.

The corners of an octagonal pole create "hot spots" where the local stress is very high. In practice, an octagonal mast will not be designed with the corners at the extreme tension zone, since this is a worse fatigue detail. In this study, however, the corners were placed at the extreme tension fiber, since this was a more conservative detail.

3.6 Galvanization

Previous research at the University of Texas has indicated that galvanizing has a negative impact on fatigue performance (M. T. Koenigs 2003). Several pairs of samples were set to be black (not galvanized) to confirm this negative effect. However, a relative comparison of fatigue performance within this phase and the previous phase was desired and so most samples were specified to be galvanized. This gives a conservative estimation of fatigue performance when compared to black samples. Galvanization of mast arms is very common in service.

3.7 Manufacturer

Prior to the research documented in this thesis, all specimens in the University of Texas research had been manufactured by Valmont Industries. To determine if there is a manufacturer-specific effect on the fatigue performance of a mast arm, it was desirable to test mast – arms made by other manufacturers.

3.7.1 Pelco

A pair of 10-2S-WY-PB samples was tested. Pelco makes mast arms that are octagonal, as opposed to round. This is not indicated in the nomenclature of the mast arms, since Pelco was the only manufacturer that used an octagonal pole in this study. The difference between an octagonal pole and a round pole was looked at analytically and further discussion can be found in the chapters on analysis.

3.7.2 Ameron and Union Metal

Ameron and Union Metal produced a pair of samples each (10-3R-WY-AG and 10-3R-WY-UG). However, both pairs included a specimen that was too long for the setup. The remaining samples from each manufacturer were tested together.

3.7.3 Valmont

The majority of specimens tested were produced by Valmont. Valmont has produced samples for previous phases and has worked closely with the researchers to determine feasibly constructible details.

Chapter 4

Experimental Test Results and Observations

A large amount of data is presented in this chapter. The results of the material properties of the specimens are presented followed by the results of the fatigue tests.

4.1 Mill Test Results

4.1.1 Valmont Specimens

Mill test results for Valmont mast arms are presented in Table 4-1 and Table 4-2.

Use	Heat	Yield (ksi)	Ultimate (ksi)	Elongation (%)	
				2"	8"
3-in Plate	B4K666	46	76	38	
		45	74	31	
	Average:	45.5	75	34.5	
0.75-in Plate	6102039	45	73.6		19.8
		44.6	74.4		19.3
	Average:	44.8	74		19.55
2-in Plate	6105420	43.4	72.2		22
		41.3	72.4		24.1
	Average:	42.35	72.3		23.05
10-in Diameter Pole	B61906	62.7	76.3	35	
8-in Diameter Pole	91840C	64.3	79.1	36	
12-in Diameter Pole	664119	67.4	70.9	33	

Table 4-1: Valmont Tensile Data

Use	Heat	C	Mn	P	S	Si	Ni	Cr	Mo	Al
3-in Plate	B4K666	0.16	0.93	0.016	0.003	0.26	0.1	0.13	0.03	0.028
0.75-in Plate	6102039	0.17	0.83	0.014	0.009	0.03	0.1	0.12	0.01	0.028
2-in Plate	6105420	0.17	0.83	0.018	0.004	0.2	0.08	0.12	0.01	0.009
10-in Diameter Pole	B61906	0.22	0.81	0.01	0.00	0.01	0.01	0.05		
8-in Diameter Pole	91840C	0.22	0.84	0.00	0.01	0.00				
12-in Diameter Pole	664119	0.05	0.49	0.01	0.01	0.01				

Use	Heat	V	Nb	Cu	Ti	B	N	Ca	Sn
3-in Plate	B4K666	0.065	0.003	0.25	0.007	0.0002	0.007		
0.75-in Plate	6102039	0.006	0.001	0.31	0.001	0.0003		0.0004	0.01
2-in Plate	6105420	0.005	0.002	0.24	0.001	0.0003		0.0012	0.008
10-in Diameter Pole	B61906			0.02					
8-in Diameter Pole	91840C			0.02					

Table 4-2: Valmont Chemistry Data

4.1.2 Pelco Specimens

Mill test reports for Pelco are given in Table 4-3 and Table 4-4. Mill test reports for Specimen 10-2S-WY-PB were not available.

Use	Heat	Yield (ksi)	Ultimate (ksi)	Elongation (%)	
				2"	8"
3-in Base Plate	8103966	40.6	76.7	29	
		39.6	76.2	30	
	Average:	40.1	76.45	29.5	
0.75-in Plate	8107037	46.5	74.6		22.3
		45.8	74.8		20
	Average:	46.15	74.7		21.15
2-in Base Plate	8101830	44.6	69		22.3
		46.3	73.4		20.1
	Average:	45.45	71.2		21.2
Pole	06758C	75	89.5	22	
		76	90.5	22	
	Average:	75.5	90	22	
External Collar / Backing Bar	A453961	67.8	82.2	29.4	
		82	92.5	24	
	Average:	74.9	87.35	26.7	

Table 4-3: Pelco Tensile Data

Use	Heat	C	Mn	P	S	Si	Ni	Cr	Mo	Al
3-in Plate	8103966	0.19	0.87	0.014	0.005	0.2	0.05	0.1	0.02	0.013
0.75-in Plate	8107037	0.2	1.04	0.011	0.006	0.19	0.08	0.11	0.02	0.034
2-in Plate	8101830	0.18	0.83	0.013	0.005	0.18	0.09	0.1	0.02	0.007
Pole	06758C	0.15	1.16	0.007	0.00	0.021	0.01	0.03		0.043
EC / Backing	A453961	0.06	1.3	0.02	0.007	0.03	0.04	0.08	0.02	0.023

Use	Heat	V	Nb	Cu	Ti	B	N	Ca	Sn
3-in Plate	8103966	0.002	0.004		0.001			0.0016	0.009
0.75-in Plate	8107037	0.004	0.002	0.26	0.002		0.0002	0.0008	0.005
2-in Plate	8101830	0.003	0.003	0.22	0.001	0.0001		0.0017	0.006
Pole	06758C	0.051	0.04	0.03		0.0001	0.004		
EC / Backing	A453961	0.026	0.041	0.12	0.001	0.0001	0.0079		0.009

Table 4-4: Pelco Chemistry Data

4.1.3 Union Metal and Ameron Specimens

Mill tests reports were not available for the Union Metal and Ameron specimens.

4.2 Prior Fatigue Test Results

The research outlined in this thesis complemented previous phases of research. The results presented in this chapter are mainly the results of this phase, but results from this phase will be compared with previous work at the University of Texas at Austin where applicable. Complete records of previous fatigue studies are contained in the theses of Koenigs and Anderson (M. T. Koenigs 2003) (Anderson 2007) and TxDOT report FHWA/TX-04/0-4178-2 (Koenigs, et al. 2003).

4.3 Fatigue Life Coefficient and AASHTO Fatigue Categories

When a specimen is tested in fatigue, two variables are recorded. The independent variable that is selected by the researcher is the nominal stress range (S_r) that the specimen was tested at. The dependant variable that is then recorded is the number of cycles (N) that the specimen experienced before failure at the selected stress range. For a given detail an S-N plot can be produced by plotting S_r on the vertical axis and N on the horizontal axis, usually shown with a log – log scale. Above a threshold stress range, called the constant amplitude fatigue limit, under which fatigue life is theoretically infinite, the equation used to relate stress range and number of cycles is: $N = AS_r^{-3}$, where A is a constant that depends on detail geometry and size and pervasiveness of inherent defects. The coefficient A is used to designate fatigue life categories, ranging from Category A to Category E'. A list of AASHTO Fatigue Categories and corresponding values of the constant A is given in Table 4-5.

AASHTO Category	Fatigue Constant, A
A	250×10^8
B	120×10^8
C	44×10^8
D	22×10^8
E	11×10^8
E’	3.9×10^8

Table 4-5: AASHTO Fatigue Constants

A simple way to compare the fatigue life of different specimens is to compare the coefficient *A* of the sample. Using the equation $A = NS_r^3$, values of *A* were calculated for each specimen using the stress range and fatigue life recorded from the test. These were then compared with each other and the AASHTO fatigue categories in order to quantify the fatigue performance of each detail. This allowed for the comparison of samples that were tested at different stress ranges. The coefficient *A* will vary somewhat, due to scatter, but allows for a convenient way to compare the fatigue performance of two details tested at different stress ranges.

When comparing fatigue performance, it is also necessary to consider the threshold stress range. If a specimen is cycled at a low enough stress range, the specimen will have an extended life or will simply not fail during the experiment. The calculation of the coefficient *A* will not account for this extended life at lower stress ranges and it is necessary to plot data points against the curves given for the AASHTO fatigue categories. The AASHTO categories account for the effect

of extended life experienced at lower stress ranges by designating a threshold stress range (S_{th}) under which infinite life can be expected from the detail.

4.4 Fatigue Test Results

A total of 26 full penetration samples (12 pairs and two singles) of varying base plate thicknesses were tested. All 3 base plate and bolt geometries (*S*, *R*, and *SR*) were used and 3 pole diameters were tested (8-in, 10-in, and 12-in). As well as varying geometry, 2 pairs of samples had no galvanizing on it (10-2S-WY-PB, 10-3R-WY-VB) and one pair of samples had the full penetration weld peened after galvanizing (10-3R-WY-VP).

A total of 10 external collar samples (5 pairs) were tested. All samples had a 2-in thick base plate, with either the *S* or *SR* geometry.

The complete results of the experimental tests are given in Table 4-6. The sample name is given along with the stress range tested and the cycles to failure. Using the equation $A = NS_r^3$, values of A were calculated. These values of A do not account for the threshold stress effect. The location of the failure crack is indicated along with the presence of a fillet weld or tack weld at the top of the backing ring of a full penetration weld. In one case the mast arm failed at a pock mark on the pole wall, away from a weld. This is indicated by the word “Shaft” in the crack location box.

Specimen Code	S_r	$N_{failure}$	A	Category	Crack Location	Backing Bar Weld Type
10-2S-WY-PB-A	12	6,734,487	1.164E+10	C	Weld Toe	Fillet
10-2S-WY-PB-B	12	5,219,304	9.019E+09	C	Weld Toe	Fillet
10-2S-WY-VG-A	12	**12,602,940**	**2.178E+10**	**B**	N/A	None
10-2S-WY-VG-B	12	**12,602,940**	**2.178E+10**	**B**	N/A	None
8-2S-WY-VG-A	12	**12,464,800**	**2.154E+10**	**B**	Weld Toe	Tack
8-2S-WY-VG-B	12	**12,464,800**	**2.154E+10**	**B**	Weld Toe	Tack
8-2S-WY-VG-A	24	856,122	1.184E+10	C	Backing	Tack
8-2S-WY-VG-A (flip)	24	747,510	1.033E+10	C	Weld Toe	Tack
8-2S-WY-VG-B	24	**1,603,632**	**2.217E+10**	**B**	N/A	Tack
8-2S-EC-VG-A	18	512,860	2.991E+09	D	Collar	N/A
8-2S-EC-VG-B	18	653,208	3.810E+09	D	Collar	N/A
12-2S-WY-VG-A	18	1,053,554	6.144E+09	C	Weld Toe	Tack
12-2S-WY-VG-B	18	880,807	5.137E+09	C	Weld Toe	Tack
12-2S-EC-VG-A	18	**805,991**	**4.701E+09**	**C**	N/A	N/A
12-2S-EC-VG-B	18	468,601	2.733E+09	D	Collar	N/A
12-2S-EC-VG-B (flip)	18	337,390	1.968E+09	E	Collar	N/A
10-3R-WY-VG-A	18	**8,037,420**	**4.687E+10**	**A**	N/A	
10-3R-WY-VG-B	18	**8,037,420**	**4.687E+10**	**A**	N/A	
10-3R-WY-VG-A	24	439,511	6.076E+09	C	Weld Toe	None
10-3R-WY-VG-B	24	343,175	4.744E+09	C	Weld Toe	None
10-3R-WY-VP-A	24	**10,055,123**	**1.390E+11**	**A**	N/A	None
10-3R-WY-VP-B	24	**10,055,123**	**1.390E+11**	**A**	N/A	None
10-3R-WY-VB-A	19.07	2,232,742	1.548E+10	B	Weld Toe	None
10-3R-WY-VB-A (flip)	24	490,061	6.775E+09	C	Weld Toe	None
10-3R-WY-VB-B	21.14	3,516,775	3.322E+10	A	Shaft	None
10-3R-WY-AG-A	24	222,649	3.078E+09	D	Weld Toe	None
10-3R-WY-AG-A (flip)	24	212,891	2.943E+09	D	Weld Toe	None
10-3R-WY-UG-A	24	1,873,499	2.590E+10	A	Weld Toe	None
ZZ88734-A	24	677,763	9.369E+09	C	Backing	Fillet
ZZ88734-B	24	633,458	8.757E+09	C	Backing	Fillet
ZZ88735-A	28	286,526	6.290E+09	C	Backing	Fillet
ZZ88735-B	28	123,072	2.702E+09	D	Backing	Fillet
ZZ88735-B (flip)	28	129,090	2.834E+09	D	Backing	Fillet
10-2SR-WY-VG-A	12	**9,881,390**	**1.708E+10**	**B**	Weld Toe	
10-2SR-WY-VG-B	12	3,051,996	5.274E+09	C	N/A	
10-2SR-EC-VG-A	12	**10,652,284**	**1.841E+10**	**B**	N/A	N/A
10-2SR-EC-VG-B	12	**10,652,284**	**1.841E+10**	**B**	N/A	N/A
10-3R-WY-PG-A	24	1,272,665	1.759E+10	B	Weld Toe	None
10-3R-WY-PG-B	24	1,210,499	1.673E+10	B	Backing Bar	Tack
10-2R-EC-PG-A	24	137,220	1.897E+09	E	Collar	N/A
10-2R-EC-PG-B	24	244,763	3.384E+09	D	Collar	N/A
12-3R-WY-PG-A	24	292,468	4.043E+09	D	Weld Toe	Tack
12-3R-WY-PG-B	24	328,833	4.546E+09	C	Weld Toe	Tack
12-2R-EC-PG-A	24	169,059	2.337E+09	D	Collar	N/A
12-2R-EC-PG-B	24	119,289	1.649E+09	E	Collar	N/A

Table 4-6: Experimental Test Data

One test (10-3R-WY-VB) was inadvertently tested at a stress range of 16.37-ksi for 1,630,300 cycles. When this was realized, the test was stopped and continued at a stress range of 24-ksi until failure. Miner's Rule was used to determine effective stress ranges for the total number of cycles applied to the specimens.

Samples that did not fail during a test were declared "run outs" are indicated in bold red text that is underlined. Some specimens ran out at a lower stress range and were tested again at a higher stress range. The cycle counts reported for these retests are shown ignoring the cycles at the lower stress range. Ignoring these initial cycles at a lower stress range is conservative since any damage that may have occurred at the original, low stress range is ignored. The cycle count may be lower than the cycle count would have been had the test been run at the higher stress range originally. However, when a test is declared a run out, it is assumed that the test could have run for an infinite amount of cycles. This implies that no damage occurred, since the fraction of damage occurring per cycle would be infinitely small.

When one mast arm failed in the setup, it was rotated or "flipped" so that the crack was on the compression side and the cycles were continued until the other mast arm failed. In some cases, the flipped mast arm failed before the other mast arm failed. A data point from a flipped specimen is indicated next to the specimen name. The number of fatigue cycles reported for the failure of a flipped specimen is the number of cycles that specimen experienced after being flipped. Due to residual stresses in the weld toe, there may be some tension stress cycled on the bottom of the mast arm; however this is conservatively ignored when reporting the number of cycles a flipped specimen experienced before failing.

4.5 Typical Failures

4.5.1 Full Penetration

Full penetration details typically failed at the weld toe. A typical failure is given in Figure 4-1. The crack initiated at the top of the tension region and propagated down either side of the mast arm, perpendicular to the maximum principle tension.

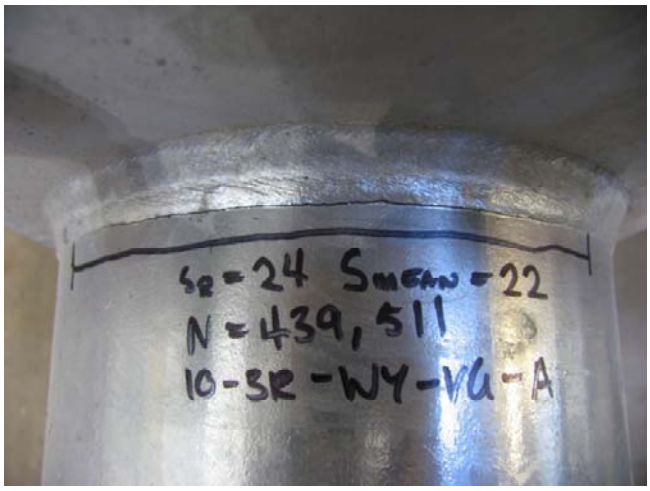

Figure 4-1: Typical Weld Toe Failure of a Full Penetration Connection

An etched cross section of a typical full penetration detail is given in Figure 4-2.

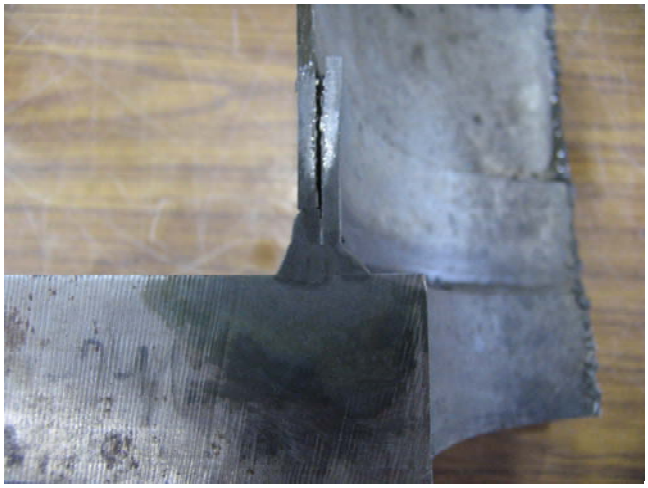

Figure 4-2: Cross Section of a Typical Full Penetration Connection

Some full penetration details received had welds at the top of the backing ring which were not called out on the details, but were tested anyway.

Several specimens had fillet welds at the top of the backing bar. All specimens with fillet welds at the top of the backing ring failed at the toe of the fillet weld. A typical failure is seen in Figure 4-3.

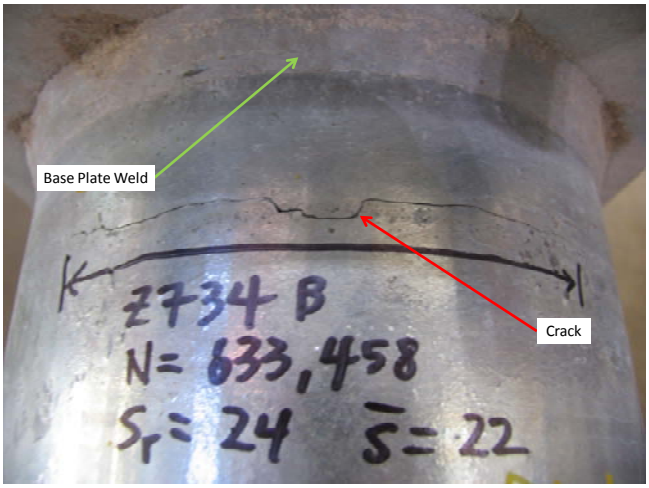

Figure 4-3: Typical Failure at a Backing Ring Fillet Weld

An etched cross section of a failed full penetration specimen with a fillet weld at the top of the backing ring is shown in Figure 4-4.

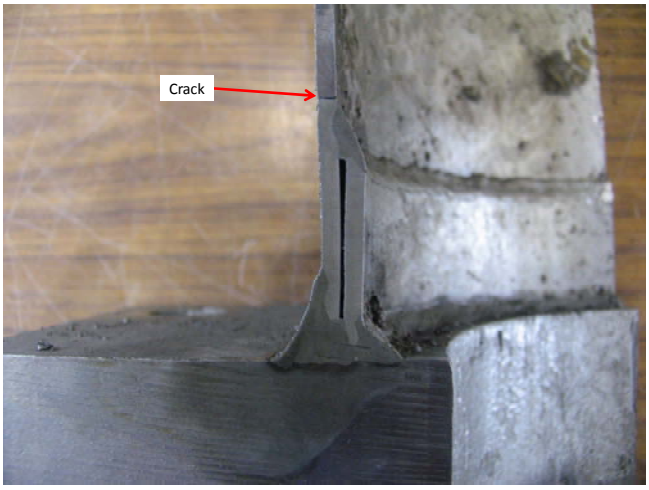

Figure 4-4: An Etched Cross Section of a Full Penetration Connection with a Backing Ring Fillet Weld

Some specimens had a tack weld connecting the top of the backing ring to the inside of the pole wall. Some of these tacked welded specimens failed at the toe of the tack weld, while others failed at the base plate weld. A typical failure is shown in Figure 4-5 and a cross section through the crack is shown in Figure 4-6.

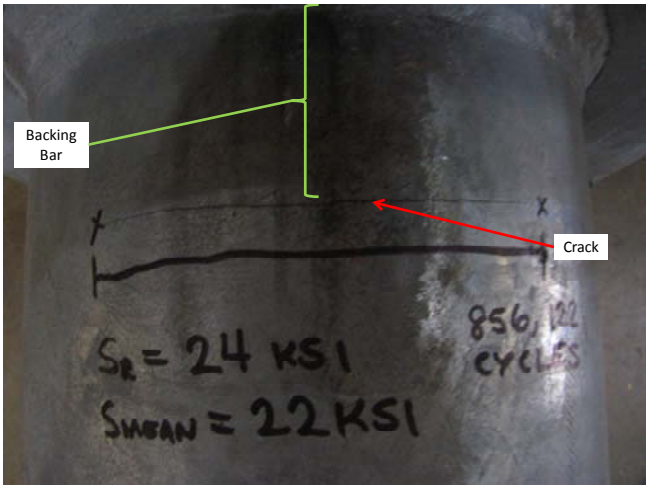

Figure 4-5: Typical Failure at a Backing Ring Tack Weld

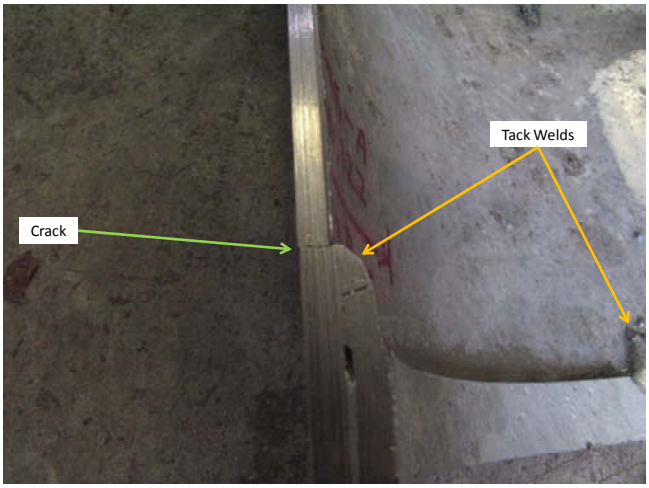

Figure 4-6: Cross Section of a Tack Weld Failure

The crack initiation of the backing ring fillet or tack weld failures begin on the inside of the pole wall at the toe of the weld. The crack propagates through the wall, to the outside, and then down the sides of the mast arm perpendicular to the maximum principal tensile stress.

4.5.2 External Collar

All of the external collars tested in this phase failed at the toe of the fillet weld connecting the top of the collar to the pole wall. A typical failure is shown in Figure 4-7. Similar to the full penetration failure, the crack initiates at the extreme tension fiber and propagates down both sides, perpendicular to the maximum principal tension.

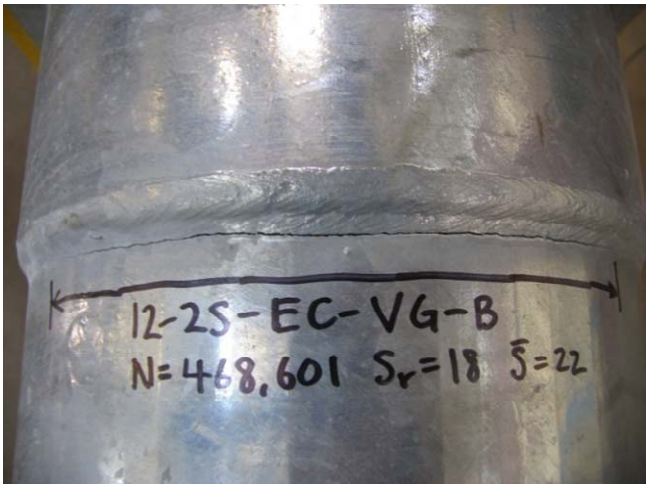

Figure 4-7: Typical External Collar Failure

Etched cross sections of a typical external collar detail are given in Figure 4-8 and Figure 4-9.

Figure 4-8: A Cross Section of a Typical External Collar Detail

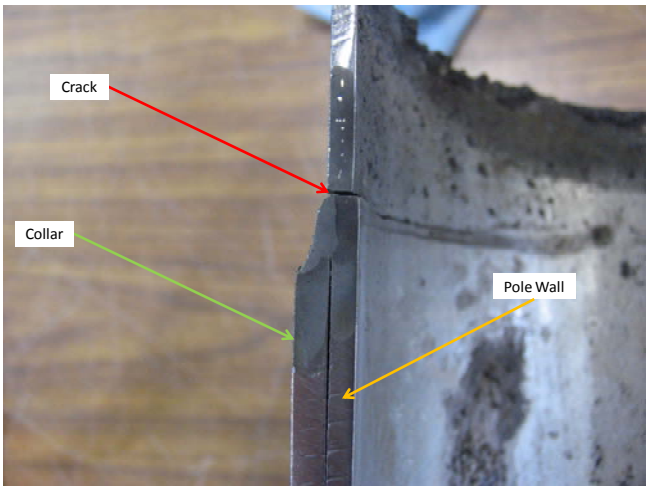

Figure 4-9: Close Up of the Collar Weld (Etched)

Previous external collar specimens had scalloped collars. A scalloped collar means that the distance from the base plate to the top of the collar varied around the pole. All scalloped external collars failed at the base plate weld except for two run outs and one that failed at the toe of the fillet weld that connects the top of the collar to the pole. In addition, no comparison of the scalloped collars and the collars tested in this phase of research exists where the type of collar is the only variable. Because of the lack of comparable data and the different failure mechanism, scalloped external collars are not compared with the external collars tested in this phase of research, which had a constant distance from the base plate to the top of the collar. Typical failures of scalloped external collars can be seen in Anderson, 2007.

4.6 Results and Observations

A list of all fatigue test results is presented in Section 4.4 in Table 4-6.

In all comparisons, it is important to only compare specimens that are similar. It is necessary to only change one variable when specimens are being compared in order to reduce convolution of the data. In this phase of research, many different variables were tested which presented some difficulties in arranging the results into meaningful comparisons. The comparisons are arranged based on observations of the effects of specific variables and the findings from the computer modeling discussed in Chapters 5 and 6.

4.6.1 Comparison of Octagonal and Round Poles

4.6.1.1 Full Penetration Details

Round and octagonal poles with 3-in base plates and 10-in diameter poles (10-3R-WY) were studied with both full penetration details and external collar details. A comparison of full penetration pole shape can be seen in Figure 4-10. The round full penetration detail contains data from 3 manufacturers. The two pairs of round specimens that performed between a Category B and a Category A were 10-3R-WY-UG (Union Metal) and 10-3R-WY-VG (Valmont). The Union Metal specimen was tested at 24-ksi to 1,873,499 cycles before failing and the Valmont specimen experienced 8,037,420 cycles at a stress range of 18-ksi and did not fail (the two data points lie on top of each other on the graph and appear as one point). The two round data points that performed between a Category C and a Category B were the second tests of the 10-3R-WY-VG specimens, when the stress range was increased to 24-ksi. The stress range and cycle count reported for these specimens does not account for any fatigue damage that occurred during the first test at the 18-ksi stress range. This seems to be the case, since in the second test, the specimens did not perform in the same fatigue category as they did in the first test. The two round data points that performed between a Category D and a Category C were 10-3R-WY-AG (Ameron).

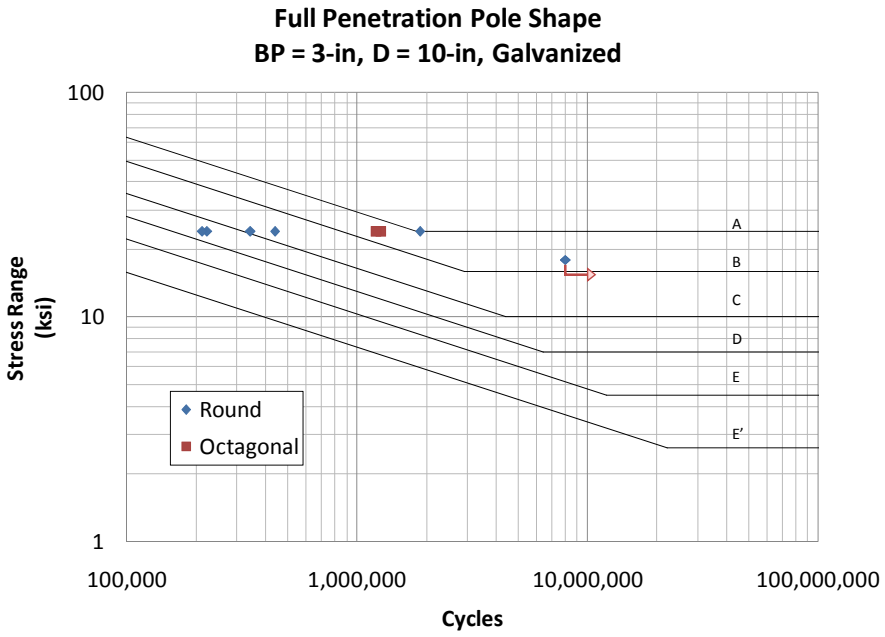

Figure 4-10: Comparison of Round and Octagonal Full Penetration Details

Only two octagonal specimens were tested at 10-3R-WY and were 10-3R-WY-PG (Pelco). These specimens performed between a Category B and a Category A.

A comparison of the coefficient *A* for each detail tested is given in Table 4-7. Specimens were tested in pairs and the mean value of *A* is given. The AASHTO categories given in Table 4-7 were determined only by comparing the coefficient A and does not account for the constant amplitude fatigue region. This is typical throughout this chapter.

Specimen	Fatigue Coefficient *A*	AASHTO Category
10-3R-WY-VG (S_r = 18-ksi)	**4.687 X 10^{10}**	**A**
10-3R-WY-VG (S_R = 24-ksi)	5.412 X 10^{9}	C
10-3R-WY-UG	2.590 X 10^{10}	B
10-3R-WY-AG	3.011 X 10^{9}	D
10-3R-WY-PG (Octagonal)	1.716 X 10^{10}	B

Table 4-7: Comparison of Round and Octagonal Full Penetration Details

Computer models were analyzed to compare round full penetration mast arms with octagonal full penetration mast arms and it was found that there is no large difference between round and octagonal full penetration details. This is discussed in detail in Chapters 5 and 6.

In light of the similar performance from the Pelco, Union Metal, and Valmont specimens tested at a stress range of 18-ksi, and the results from the computer models, the full penetration detail shows no practical difference between octagonal poles and round poles. In subsequent figures, octagonal poles are grouped together with round poles of similar geometries.

4.6.1.2 External Collar Details

No valid comparison of round and octagonal poles can be made for external collars, because no comparison exists where the shape of the pole is the only variable.

4.6.2 Comparison of Base Plate Geometry

4.6.2.1 Full Penetration

4.6.2.1.1 Comparison of *S* and *SR*

A comparison of *S* and *SR* geometries for full penetration details with 2-in base plates and 10-in diameter poles is shown in Figure 4-11.

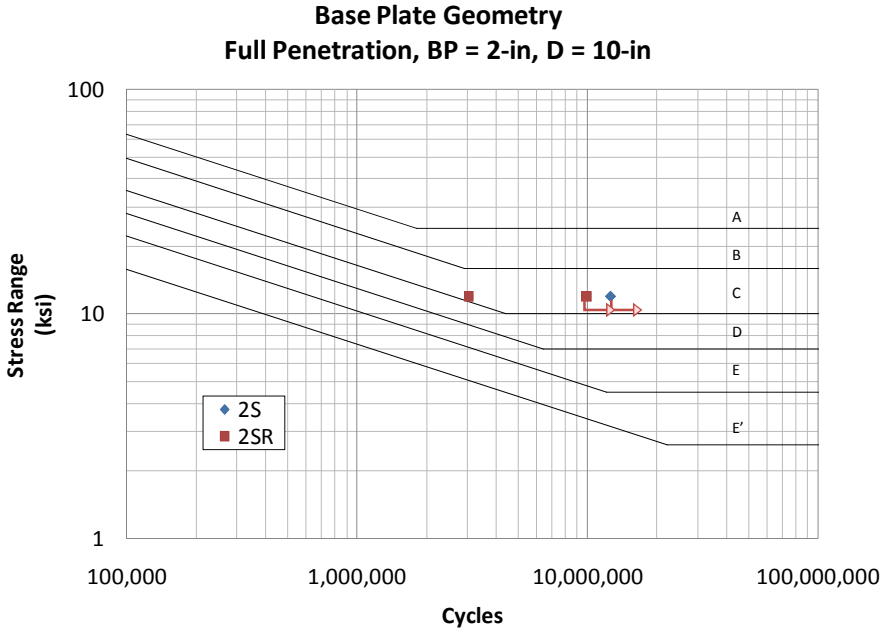

Figure 4-11: Comparison of *S* and *SR* Full Penetration Details

One pair of mast arms each was tested for *S* and *SR* base plate geometries. The specimens tested were 10-2S-WY-VG and 10-2SR-WY-VG. A comparison of the mean values of the coefficient *A* is presented in Table 4-8. The *A* value for 10-2SR-WY-VG is the average of a run out test and a test that failed, and is labeled as a run out in the table. This was a typical encountered while evaluating this data.

Specimen	Fatigue Coefficient A	AASHTO Category
10-2S-WY-VG	2.178×10^{10}	B
10-2SR-WY-VG	1.118×10^{10}	C

Table 4-8: Comparison of *S* and *SR* Full Penetration Details

It appears that there may be a slight difference between the two base plate geometries. The cutoff for a Category B detail is $A = 1.2 \text{ X } 10^{10}$, and the 10-2SR-WY-VG specimens are within 2% of that cutoff. In addition, both geometries had at least one specimen that did not fail at the stress range tested.

Computer models of full penetration details with 10-in diameter holes and 2-in base plates was performed on the effect of the bolt geometry on square base plates, and found that an *SR* detail only had an 8% increase in the stress at the weld toe over the *S* detail. This study is discussed in detail in Chapter 6.

Given the experimental and analytical data, an *S* detail performs slightly better than an *SR* . The difference is small, however, and *S* and *SR* full penetration details are grouped together in this chapter.

4.6.2.1.2 Comparison of *S* and R

A comparison of *S* and *R* geometries for full penetration mast arms with 2-in base plates and 10-in diameter poles is given in Figure 4-12.

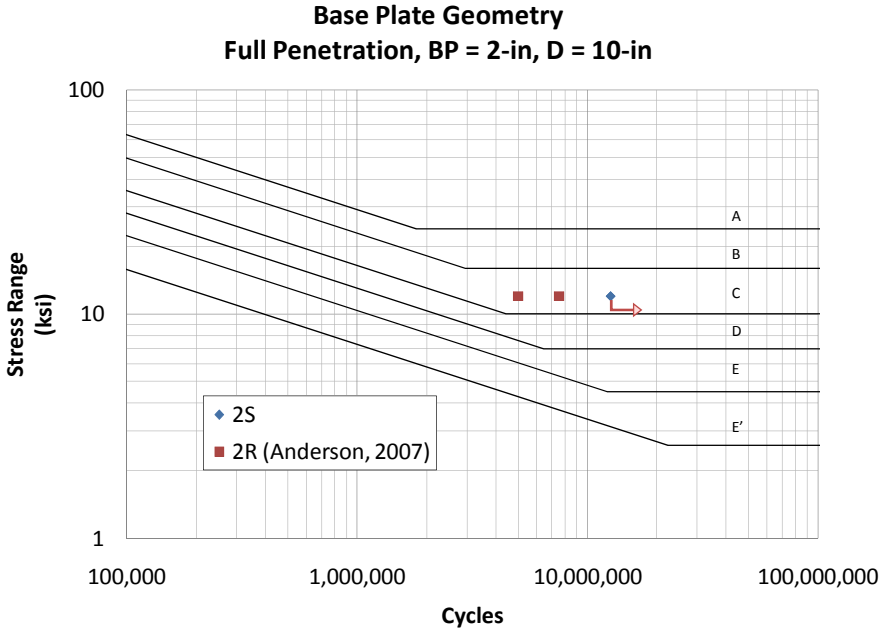

Figure 4-12: Comparison of *S* and *R* Full Penetration Details

One pair of 10-2S-WY-VG samples is compared with one pair of 10-2R-WY-VG samples from Anderson, 2007. A table of the mean coefficient *A* for each detail compared is given in Table 4-9.

Specimen	Fatigue Coefficient A	AASHTO Category
10-2S-WY-VG	**2.178×10^{10}**	**B**
10-2R-WY-VG	1.082×10^{10}	C

Table 4-9: Comparison of *S* and *R* Full Penetration Details

Both the 10-2S-WY-VG and the 10-2R-WY-VG specimens lie between a Category C and a Category B on the plot of fatigue performance. In Table 4-9, coefficient *A* of the 10-2R-WY-VG

specimens misses the cutoff for Category B by about 10%, which is noteworthy, but small enough that scatter in the data may account for the difference.

Computer models, discussed in detail in Chapters 5 and 6, of 10-2S-WY and 10-2R-WY mast arms show that the *R* detail increases stress at the weld toe by less than 1%.

In light of the computer models, and the small sample size (only 2 mast arms of each geometry) it appears that if there is a difference between full penetration details with *R* geometries and *S* geometries, it is only a small difference.

4.6.2.2 External Collar Details

No valid comparison of base plate geometry can be made for external collars, because no comparison exists where base plate geometry is the only variable.

4.6.3 Comparison of External Collar and Full Penetration Details

A comparison of external collar and full penetration details with 2-in thick base plates and 10-in diameter poles is given in Figure 4-13. There is a limited amount of data: only 3 pairs full penetration mast arms (including 2 from this phase of testing and 1 from Anderson, 2007) and two pairs of external collar details. In addition, 2 pairs of socket connections from Anderson, 2007 are presented for comparison.

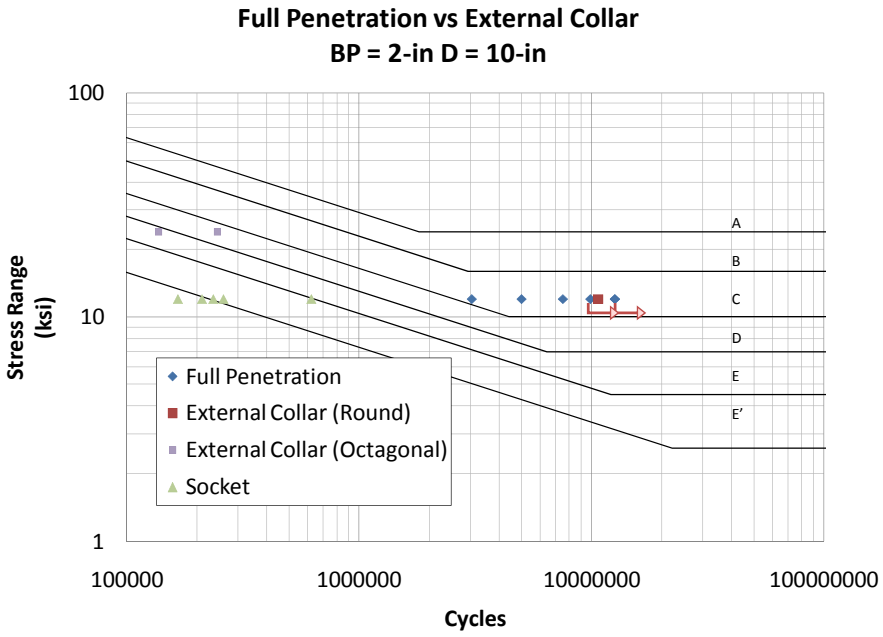

Figure 4-13: Comparison of Full Penetration and External Collar Details

As discussed earlier in this chapter, different full penetration base plate geometries are grouped together. In this plot, external collars with different pole geometries and base plate geometries are presented. The round external collars are 10-2SR-EC-VG and the octagonal external collars were 10-2R-EC-PG. The 10-2SR-EC-VG (round external collar) specimens experienced fatigue lives similar to the full penetration details while the 10-2R-EC-PG (octagonal external collar) specimens experienced lower fatigue performance than the full penetration details.

The presence of several variables in the external collars somewhat confounds the data. The two pairs of external collar specimens have different base plate geometries, different pole diameters, and different manufacturers. No valid comparison can be made from the physical data for the variables present in the two sets of external collars, however computer models of external collars

with varying base plate thicknesses (with *S* base plate geometry) suggest that the base plate stiffness does not play the same large role in external collar details as it does in full penetration details. Further discussion of these models is found in Chapters 5 and 6. In light of these computer models the large difference in the two external collar specimens may be due to the pole geometry. More experimental data would be needed to confirm or refute this statement, and to see if there is a difference in the manufacturers of external collars and octagonal poles.

The fatigue coefficients for each specimen in the comparison are given in Table 4-10. The large difference between the two external collar specimens presented is clear.

Specimen	Fatigue Coefficient A	AASHTO Category
10-2S-WY-VG	**2.178×10^{10}**	**B**
10-2SR-WY-VG	**1.118×10^{10}**	**C**
10-2R-WY	2.165×10^{10}	B
10-2SR-EC-VG	1.841×10^{10}	B
10-2R-EC-PG	1.993×10^{9}	E
Socket Details	3.472×10^{8}	Worse than E'
	6.303×10^{8}	E'

Table 4-10: Comparison of Full Penetration and External Collar Details

Given the presence of the run out full penetration details, a round full penetration detail may perform somewhat better than a round external collar. The octagonal external collars performed worse than round full penetration and external collar details. More details of similar geometries would be needed to compare the effect of round and octagonal poles and the effect of manufacturers on external collar details.

4.6.4 Base Plate Thickness

4.6.4.1 Comparison of 2-in and 3-in Base Plates Full Penetration Details

Of the 26 full penetration details, 10 had a base plate thickness of 2-in and 16 had a base plate thickness of 3-in. The effect of base plate thickness in full penetration details is plotted in Figure 4-14.

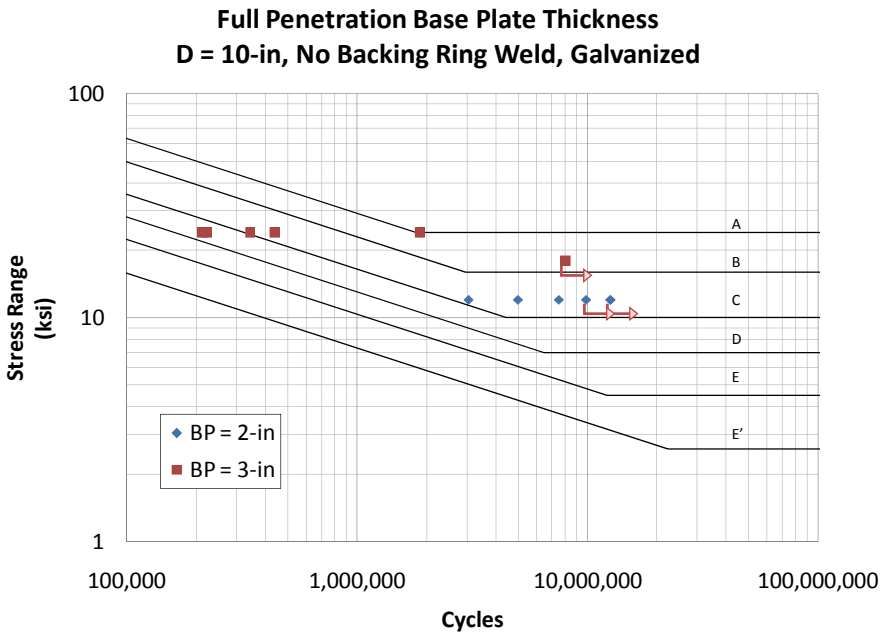

Figure 4-14: Comparison of 2-in and 3-in Full Penetration Details

The mean fatigue coefficients for each specimen tested are given in Table 4-11. *S* and *R* details are grouped together as well as octagonal and round poles. The 3-in base plate specimens consist

of three different manufacturers. One of the 10-2SR-WY-VG specimens failed and the other ran out. In table X the 10-2SR-WY-VG data is indicated as a run out.

Specimen	Fatigue Coefficient A	AASHTO Category
10-3R-WY-VG (S_r = 18-ksi)	**4.687 X 10^{10}**	**A**
10-3R-WY-VG (S_r = 24-ksi)	5.410 X 10^{9}	C
10-3R-WY-AG	3.012 X 10^{9}	D
10-3R-WY-UG	2.59 X 10^{10}	A
10-2S-WY-VG	**2.17 X 10^{10}**	**B**
10-2SR-WY-VG	**3.491 X 10^{10}**	**B**
10-2R-WY-VG (Anderson, 2007)	1.082 X 10^{10}	C

Table 4-11: Comparison of 2-in and 3-in Full Penetration Details

There is a large amount of scatter in the 3-in base plate data, due to the low performance of the 10-3R-WY-AG specimens and the conservatively low fatigue life reported for the second test of the 10-3R-WY-VG specimens (S_r = 24-ksi) which was discussed earlier in this chapter.

Ignoring the 10-3R-WY-VG test 2 and 10-3R-WY-AG in the 3-in base plate data, it can be seen in Table 4-11 that the 3-in base plate full penetration details perform somewhere around a Category A, and the 2-in base plate full penetration details perform somewhere between a high Category C to Category B.

Computer models of full penetration details that analyzed different base plate thicknesses strongly indicate the increased fatigue performance that moving from a 2-in base plate to a 3-in base plate causes. These models are discussed in detail in Chapters 5 and 6. The correlation between fatigue performance and base plate thickness found analytically suggests that the low performance of the 10-3R-WY-AG may be due to a fabrication issue.

Ignoring the low outliers it can be observed that an increase in base plate thickness from 2-in to 3-in improves the fatigue life of full penetration specimens. This agrees with prior research that has shown that the thickness of the base plate as an important variable in the fatigue life for mast arms that fail at the base plate weld (M. T. Koenigs 2003) (Anderson 2007).

4.6.4.2 Effect of Base Plate Thickness in External Collar

All external collar specimens had a base plate thickness of 2-in, so no comparison across base plate thickness of external collars can be made in study. Anderson tested 1.75-in and 2-in scalloped external collar and found that the base plate thickness did have an effect, however, all scalloped external collar failures occurred at the base plate weld except one which failed at the top of the collar. This different failure mechanism and the fact that no comparison external collars in both phases can be made where the type of collar is the only variable, mean that no conclusion can be drawn about the external collars tested in this phase of research.

Computer models, discussed in Chapters 5 and 6, indicate that the base plate thickness has little effect on the fatigue performance of constant length external collar specimens.

4.6.5 Pole Diameter

Poles with 8-in, 10-in, and 12-in diameters of varying base plate thicknesses and geometries were tested.

4.6.5.1 Comparison of Pole Diameters in Full Penetration Details with 2-in Base Plates

The variation of pole diameter for 2-in full penetration details is plotted in Figure 4-15

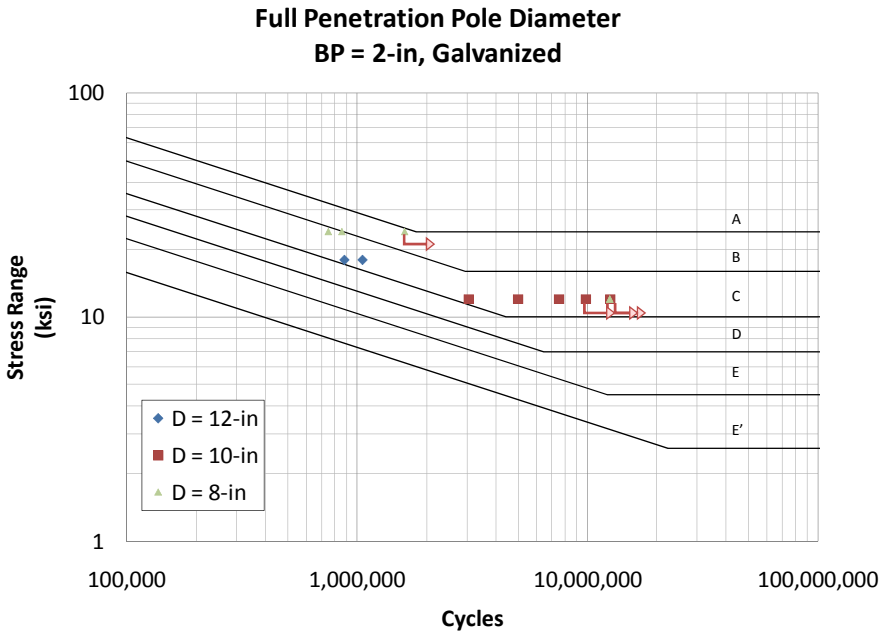

Figure 4-15: Comparison of Pole Diameter, 2-in Base Plate Full Penetration Details

Comparisons are made across various base plate geometries. The average fatigue coefficients for each specimen in this comparison are given in Table 4-12.

Specimen	Fatigue Coefficient, A	AASHTO Category
12-2S-WY-VG	5.641×10^{9}	C
10-2S-WY-VG	**2.178×10^{10}**	**B**
10-2SR-WY-VG	**1.118×10^{10}**	**C**
10-2R-WY-VG (Anderson, 2007)	1.082×10^{10}	C
8-2S-WY-VG (S_r = 12-ksi)	**2.154×10^{10}**	**B**
8-2S-WY-VG (S_r = 24-ksi)	1.478×10^{10}	B

Table 4-12: Comparison of Pole Diameter, 2-in Base Plate Full Penetration Details

In some pairs of specimens, one mast arm failed and the other ran out. In table X, these are indicated as run outs. The 8-2S-WY-VG specimens had tack welds at the top of the backing ring, but only 8-2S-WY-VG mast arm failed at the tack weld. This failure occurred in the second test (S_r =24-ksi) and is included in this data because of the similar fatigue life of the same mast arm after it was flipped.

The average fatigue coefficients of the different diameters of full penetration details with 2-in base plate are given in Table 4-13.

Pole Diameter	Fatigue Coefficient, A	AASHTO Category
12-in	5.64×10^{9}	C
10-in	1.63×10^{10}	B
8-in	1.82×10^{10}	B

Table 4-13: Average Fatigue Coefficients for 8-in, 10-in, and 12-in Diameter Full Penetration Details

There is only one pair of 12-in diameter specimens and one pair of 8-in diameter specimens (that were tested and ran out, then re-tested at a higher stress range, where one of the mast arms ran out again). The low amount of 12-in and 8-in specimens that can be compared may introduce error due to scatter in the data.

It can be seen that decreasing the pole diameter from 12-in to 10-in improves the fatigue performance. Decreasing the pole diameter again, from 10-in to 8-in, somewhat improves the fatigue performance and the added benefit has started to level off.

In computer models, discussed in Chapters 5 and 6, that were analyzed to compare the effect of pole diameter on full penetration details, it was found that for a given nominal stress range (the

stress ranges reported in this chapter are nominal stress ranges) the 8-in diameter should perform better than the 10-in and 12-in diameter poles which should have similar fatigue performance.

This difference between the computer model and the experimental data may be due to scatter in the experimental test or could indicate that the computer models are not accounting for some variable in the real specimens.

4.6.5.2 Comparison of Pole Diameters in Full Penetration Details with 3-in Base Plates

The variation of pole diameter for full penetration details with 3-in base plate is given in Figure 4-16.

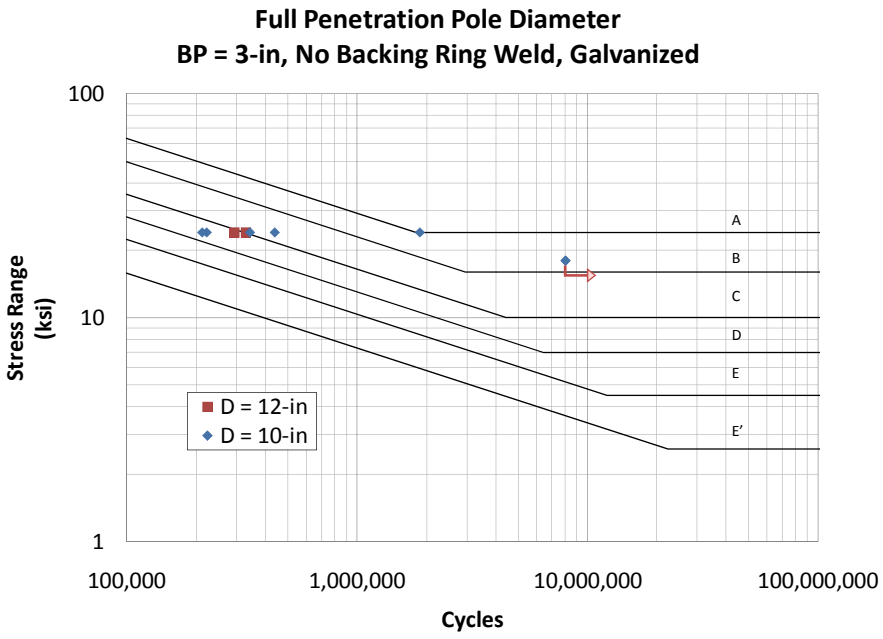

Figure 4-16: Comparison of Pole Diameter, 3-in Base Plate Full Penetration Details

Specimens, along with average values of the fatigue coefficient for each specimen, are listed in Table 4-14

Specimen	Fatigue Coefficient, A	AASHTO Category
10-3R-WY-VG (S_r = 18-ksi)	**4.687 X 10^{10}**	**A**
10-3R-WY-VG (S_r = 24-ksi)	5.410 X 10^{9}	C
10-3R-WY-AG	3.012 X 10^{9}	D
10-3R-WY-UG	2.590 X 10^{10}	A
12-3R-WY-PG	4.295 X 10^{9}	D

Table 4-14: Comparison of Pole Diameter, 3-in Base Plate Full Penetration Details

Only one pair of 12-in diameter specimens was tested, which could lead to errors in the data due to scatter in the data. These 12-in diameter specimens had tack welds at the top of the backing ring, in the zone of highest tension stresses, but failed at the base plate weld toe and are therefore assumed to be comparable.

As discussed earlier, there is a large amount of scatter in the 10-in diameter, 3-in base plate data, however, the 10-3R-AG samples and the second test (S_r = 24-ksi) of the 10-3R-WY-VG samples may be able to be ignored, as low outliers. If the lower outliers are ignored, the 10-in diameter poles exhibit significantly better fatigue performance than the 12-in diameter poles for 3-in base plates.

This disagrees with computer models, which are discussed in Chapters 5 and 6, which predict that there should be no significant difference between the 12-in and the 10-in diameter poles.

4.6.5.3 Comparison of Pole Diameter in External Collar Details with 2-in Base Plates

The variation of pole diameter for 2-in external collars details is plotted in Figure 4-17

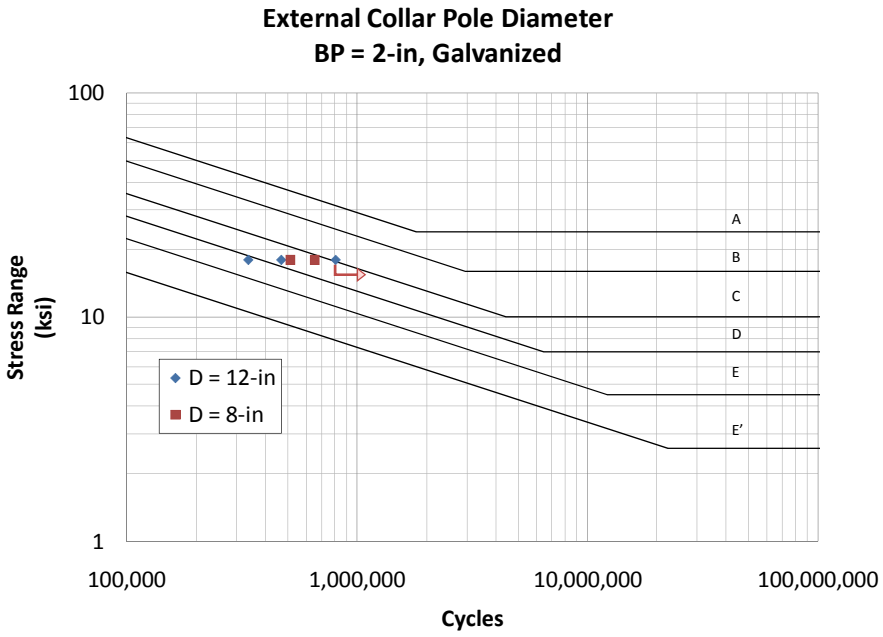

Figure 4-17: Comparison of Pole Diameter, 2-in External Collar Details

Specimens compared, along with average values of the fatigue coefficient for each specimen, are listed in Table 4-15.

Specimen	Fatigue Coefficient, A	AASHTO Category
12-2S-EC-VG	3.314×10^9	D
8-2S-EC-VG	3.401×10^9	D

Table 4-15: Comparison of Pole Diameter, 2-in External Collar Details

Only four mast arms are compared, which could lead to error due to scatter in the fatigue data. Barring any scatter, there is no significant difference in the fatigue performance of 12-in and 8-in diameter poles in external collar mast arms.

4.6.6 Backing Ring Welds on Full Penetration Details

Several samples received had welds on the top of the backing ring. Two types of backing ring welds occurred. Some specimens with backing ring welds had a fillet weld completely around the top of the backing ring and others simply had tack welds.

4.6.6.1 Full Penetration Details with 3-in Base Plate, 10-in Diameter

The variation of backing ring weld type for 3-in base plate, 10-in diameter, full penetration details is plotted in Figure 4-18.

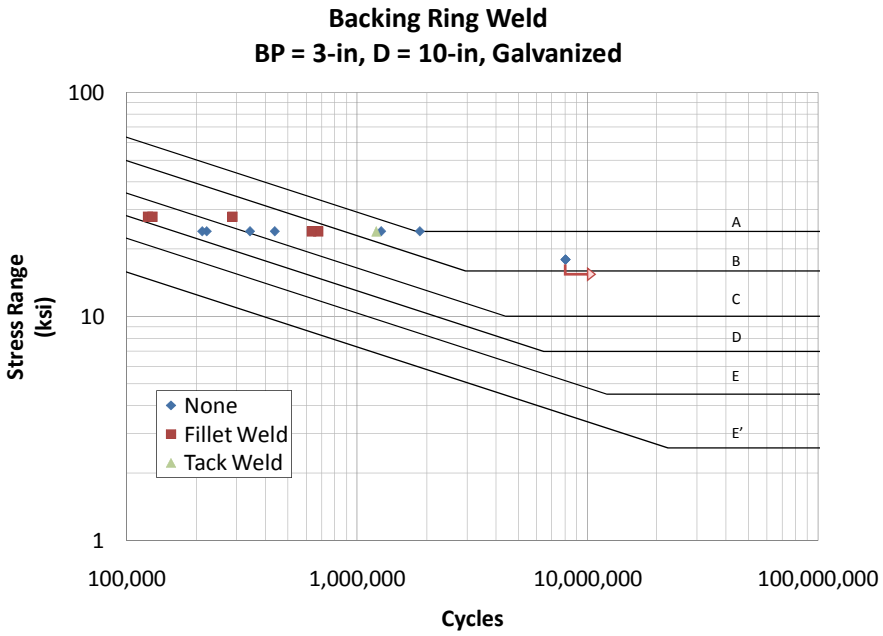

Figure 4-18: Variation of Backing Ring Weld, 10-3R-WY

Specimens compared, along with average values of the fatigue coefficient for each specimen, are listed in Table 4-16. Type of backing ring weld is also listed.

Specimen	Fatigue Coefficient, A	AASHTO Category	Backing Ring Weld
10-3R-WY-VG (S_r = 18-ksi)	**4.687 X 10^{10}**	**A**	None
10-3R-WY-VG (S_r = 24-ksi)	5.410 X 10^{9}	C	None
10-3R-WY-AG	3.012 X 10^{9}	D	None
10-3R-WY-UG	2.590 X 10^{10}	A	None
ZZ88734	9.063 X 10^{9}	C	Fillet
ZZ88735	3.942 X 10^{9}	D	Fillet
10-3R-WY-PG	1.759 X 10^{10}	B	None
10-3R-WY-PG	1.673 X 10^{10}	B	Tack

Table 4-16: Variation in Backing Ring Weld, 10-3R-WY

Ignoring the low outliers in the 10-3R-WY data as previously discussed, it can be seen that the presence of a fillet weld at the top of the backing ring of a full penetration detail with a 3-in base plate reduces the fatigue performance of the mast arm. Full penetration details with 3-in base plates and fillet welds at the top of the backing ring performed at about the level of a Category C detail. Full penetration details with no weld at the top of the backing ring perform at the level of a Category B detail (ignoring the low outliers), with one specimen performing just below a Category A detail.

Computer models discussed in Chapters 5 and 6, which focused on different values of base plate thickness, showed that the reduction in fatigue performance that a full penetration weld with a fillet weld would exhibit was dependant on base plate thickness. In the case of full penetration details with 3-in base plates, the performance of full penetration details with fillet welds was found to be worse than in those without fillet welds, which corresponds to the experimental data.

One of the 10-3R-WY-PG specimens tested had a tack weld at the top of the backing ring at the maximum tension fiber of the mast arm (octagonal mast arms were oriented with a corner at the

highest point, and the tack weld was located in the corner). The other specimen had no weld at the top of the backing ring. As indicated, both samples performed essentially the same, at the level of a Category B. In this test, there was no difference between a full penetration detail with no backing ring weld and one with a tack weld at the top. Only one tack welded specimen was tested, however and more would need to be tested to make a conclusion. The tack weld is essentially an unregulated weld and a great deal of variability is expected if a tack weld study was to be done.

4.6.6.2 Full Penetration Details with 2-in Base Plate, 8-in Diameter Pole

Two 8-2S-WY-VG specimens were tested and both had tack welds at the top of the backing ring. The specimens were designated A and B. Both specimens had tack welds were located at top, bottom, and sides of the masts arms. During tests, the highest tension stresses occur at the top of the pole. This meant that there was a tack weld present on the inside of the pole where the highest tension stresses were located.

The variation of backing ring weld type for 2-in base plate, 8-in diameter full penetration details is plotted in Figure 4-19

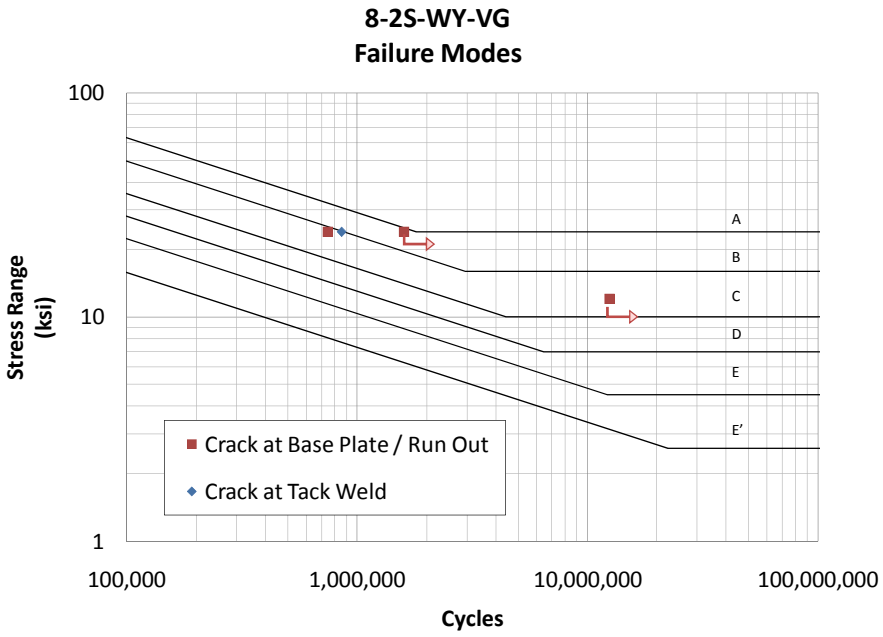

Figure 4-19: Variation of Backing Ring Welds, 8-2S-WY

Each test compared is listed, along with values of the fatigue coefficient for each specimen, in Table 4-17. The location of failure is also listed. The individual specimen name is added to the end of the specimen designation.

Specimen	Fatigue Coefficient, A	AASHTO Category	Location of Failure
8-2S-WY-VG-A (S_r = 12-ksi)	**2.154 X 10^{10}**	**B**	**Run Out**
8-2S-WY-VG-B (S_r = 12-ksi)	**2.154 X 10^{10}**	**B**	**Run Out**
8-2S-WY-VG-A (S_r = 24-ksi)	1.184 X 10^{10}	C	Tack Weld
8-2S-WY-A (S_r = 24-ksi) FLIP	1.033 X 10^{10}	C	Base Plate Weld Toe
8-2S-WY-B (S_r = 24-ksi)	**2.217 X 10^{10}**	**B**	**Run Out**

Table 4-17: Variation of Backing Ring Weld, 8-2S-WY

The specimens ran out at a lower stress range (S_r = 12) and were then retested at a higher stress range (S_r = 24-ksi). The number of cycles reported for the second test only accounts for cycles accumulated at the second stress range. This assumes that no damage occurred during the run out test i.e., the specimens would have experienced infinite life at that stress range. During the second test, Specimen A failed and was flipped. The side that was under compression cycling then failed before Specimen B could fail. This caused specimen B to be a run out test. This also indicates that the assumption that no damage occurred was correct since the original "bottom" of Specimen A had accumulated no fatigue damage and exhibited similar fatigue performance to the original "top" of Specimen A. In addition, the data points from the second test lie in the same or AASHTO category as the run out test, which may not be the case if fatigue damage had been accumulated in the first test.

This data indicates that the presence of a tack weld at the top of the backing ring has little effect on the fatigue life. With only two specimens (although multiple tests were run on the specimens) it is impossible to rule out the presence of error due to scatter in the fatigue data.

4.6.7 Comparison of Manufacturers

One pair of 10-3R-WY details was received from four different manufacturers; Ameron, Pelco, Union Metal and Valmont. The results for each manufacturer are shown in Figure 4-20.

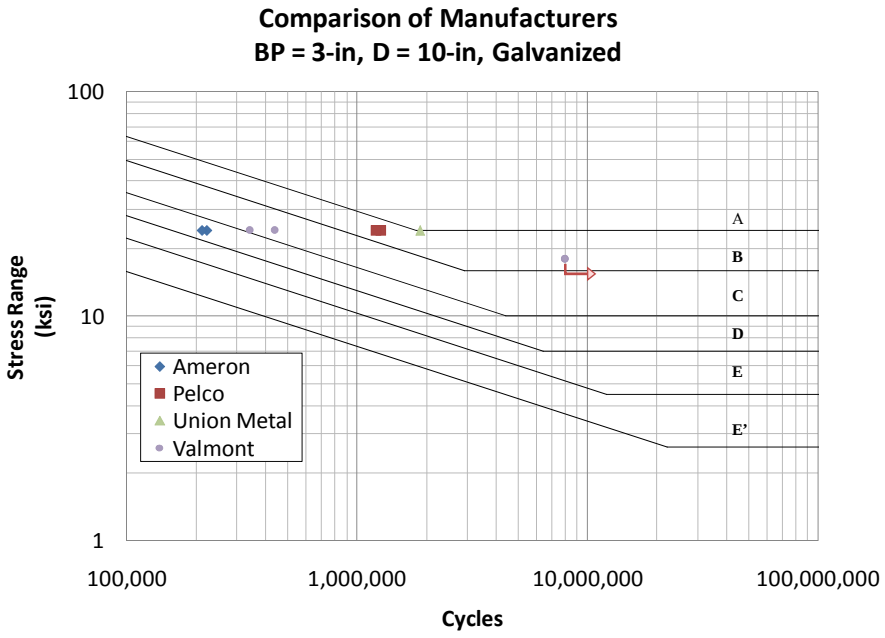

Figure 4-20: Comparison of Manufacturers, 10-3R-WY

Specimens compared, along with average values of the fatigue coefficient for each specimen, are listed in Table 4-18.

Specimen	Fatigue Coefficient, A	AASHTO Category
10-3R-WY-AG	3.012×10^{9}	D
10-3R-WY-PG	1.716×10^{10}	B
10-3R-WY-UG	2.590×10^{10}	A
10-3R-WY-VG (S_r = 18-ksi)	**4.687×10^{10}**	**A**
10-3R-WY-VG (S_r = 24-ksi)	5.410×10^{9}	C

Table 4-18: Comparison of Manufacturers, 10-3R-WY

A large amount of scatter exists between the manufacturers, however all manufacturers produced specimens that made it past Category B, except Ameron. The Valmont specimen was tested at a stress range of 18-ksi and did not fail. It was then tested again at a stress range of 24-ksi and failed. The cycles reported for the second test (S_r = 24-ksi) only account for the cycles that were accumulated at 24-ksi. This is conservative, because it assumes that no fatigue damage was accumulated during the first test. It appears that this may be overly conservative, since although the first test ran out, the specimens still performed better than a Category B detail. Had there been no damage, it could be expected that the specimens would perform better than a Category B on the second test as well.

It should be noted that the Pelco samples had tack welds at the top of the backing ring. One sample failed at the tack weld, while the other failed at the base plate weld. Both specimens achieved the same fatigue performance for practical purposes.

4.6.8 Comparison of Black, Galvanized, and Peened Specimens

All samples were tested as galvanized with the exception of one sample that was left black (not galvanized) and one that was galvanized and then peened. Results are shown in Figure 4-21.

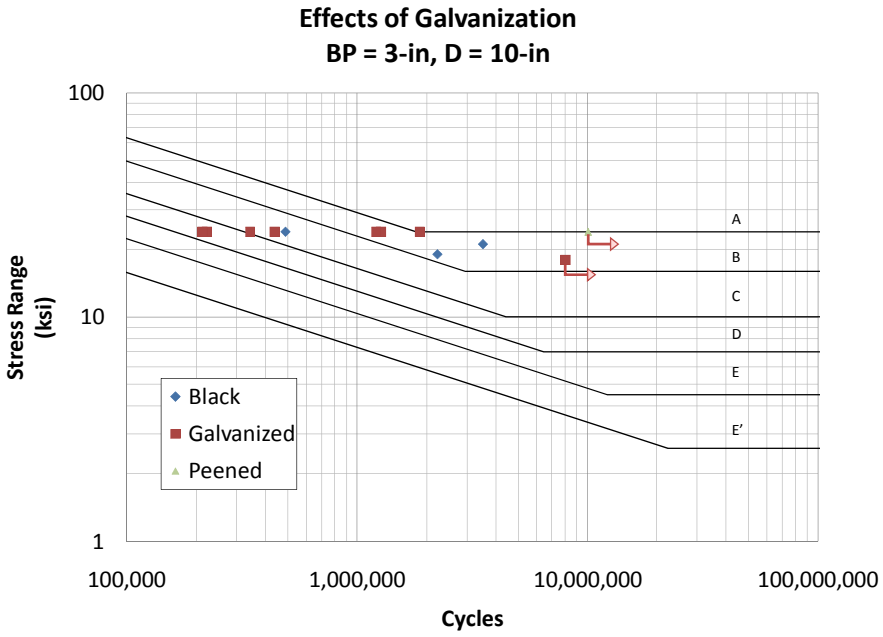

Figure 4-21: Comparison of Galvanized, Black, and Peened 10-3R-WY

Specimens compared, along with mean values of the fatigue coefficient for each specimen, are listed in Table 4-19.

Specimen	Fatigue Coefficient, A	AASHTO Category
10-3R-WY-VB	1.849×10^{10}	B
10-3R-WY-VG (S_r = 18-ksi)	**4.687×10^{10}**	**A**
10-3R-WY-VG (S_r = 24-ksi)	5.410×10^{9}	C
10-3R-WY-AG	3.012×10^{9}	D
10-3R-WY-UG	2.590×10^{10}	A
10-3R-WY-PG	1.716×10^{10}	B
10-3R-WY-VP	**1.390×10^{11}**	**A**

Table 4-19: Comparison of Galvanized, Black, and Peened 10-3R-WY

In the specimens tested, it appears that galvanizing has little effect on the fatigue performance of a mast arm. Ignoring the lower outliers of the galvanized full penetration specimens with 3-in base plate and 10-in diameter pole, as discussed earlier, the galvanized and black poles all performed better than a Category B detail.

Peening improved fatigue life. The peened specimen was tested at a stress range of 24-ksi (which is the Constant Amplitude Fatigue Limit of Category A) and ran out. Therefore, the peened sample is a Category A detail.

4.7 Summary of Observations

- There is no practical difference in the fatigue performance of full penetration details with round or octagonal poles.
- The shape of the base plate and orientation of bolt holes in full penetration details has a slight effect on the fatigue performance on the connection but is a relatively minor factor.
- Round full penetration details, octagonal full penetration details, and external collars exhibit similar fatigue performance and all perform much better than a socket connection. Octagonal external collars may not perform as well as round external collars.
- Thicker base plates improve the fatigue performance of full penetration connections.
- There may be a reduction of fatigue performance when using a 12-in diameter pole in full penetration connections. Further tests would be needed to conclusively state this. No effect on the fatigue performance of external collar details was found.
- In the 3-in base plate full penetration details tested, the presence of a fillet weld at the top of the backing ring reduced the fatigue life of the connection.

- The two specimens that failed at a tack weld connecting the top of the backing ring to the pole in the tension zone of the mast arm performed similar to specimens that did not fail at the backing ring. This may indicate that a tack weld does not have an effect on the fatigue performance of the connection. A tack weld that occurs in the compression region will have no effect on the fatigue life.
- The mast arms received from Pelco, Union Metal, and Valmont performed equally. The mast arm manufactured by Ameron performed significantly worse.
- Galvanization had little effect on fatigue performance in this study.
- The peened sample performed exceptionally well.

Chapter 5

Analytical Methods

Finite element models were developed to supplement the physical test data. Due to local bending in the pole near the connection to the base plate, high stress concentrations occur in the pole at the weld toe. The local bending cannot be detected during the physical tests of the mast arms without the use of strain gauges, and a finite element analysis provides a great deal of insight about how specific details behave under fatigue loading.

It is necessary to support analytical results with experimental data. The experimental program covered a large range of variables and analysis can be used to fill in gaps in the data and further investigate trends that were found in experimental data. Analysis also provides a powerful numerical tool that allows the researcher to quantify the effect of various geometric variables on the stress distribution in the mast arm.

5.1 Finite Element Modeling

Models of the mast arms that were tested were created for the analytical study. Using symmetry, only half of the mast arm needed to be analyzed. In order to accurately quantify hot spot stresses a submodel of the point of interest was created and driven by the deflections of the global model. A linear elastic material was used with a modulus of $E = 29{,}000$-ksi

The model was created in ABAQUS using the following steps: First parts are created using the CAD features in ABAQUS. These parts were then grouped together in an assembly, which created the full mast arm. Loads and boundary conditions, such as symmetry and contact were then applied to the assembly. Finally, the model was meshed.

A submodel was used to allow the mesh size to be reduced. Reducing the mesh size increases the number of elements and increases the computation time. A submodel allows only the part of the structure that is of interest to be modeled, which reduces the amount of elements required.

5.1.1 Parts

The mast arm was comprised of 3 parts, which were drawn in ABAQUS. A solid reaction plate where the load was applied, a shell pole, and a solid base plate assemblage, which included the base plate, connection and first 10-in of the pole. Pictures of the three parts are given in Figure 5-1, Figure 5-2, and Figure 5-3.

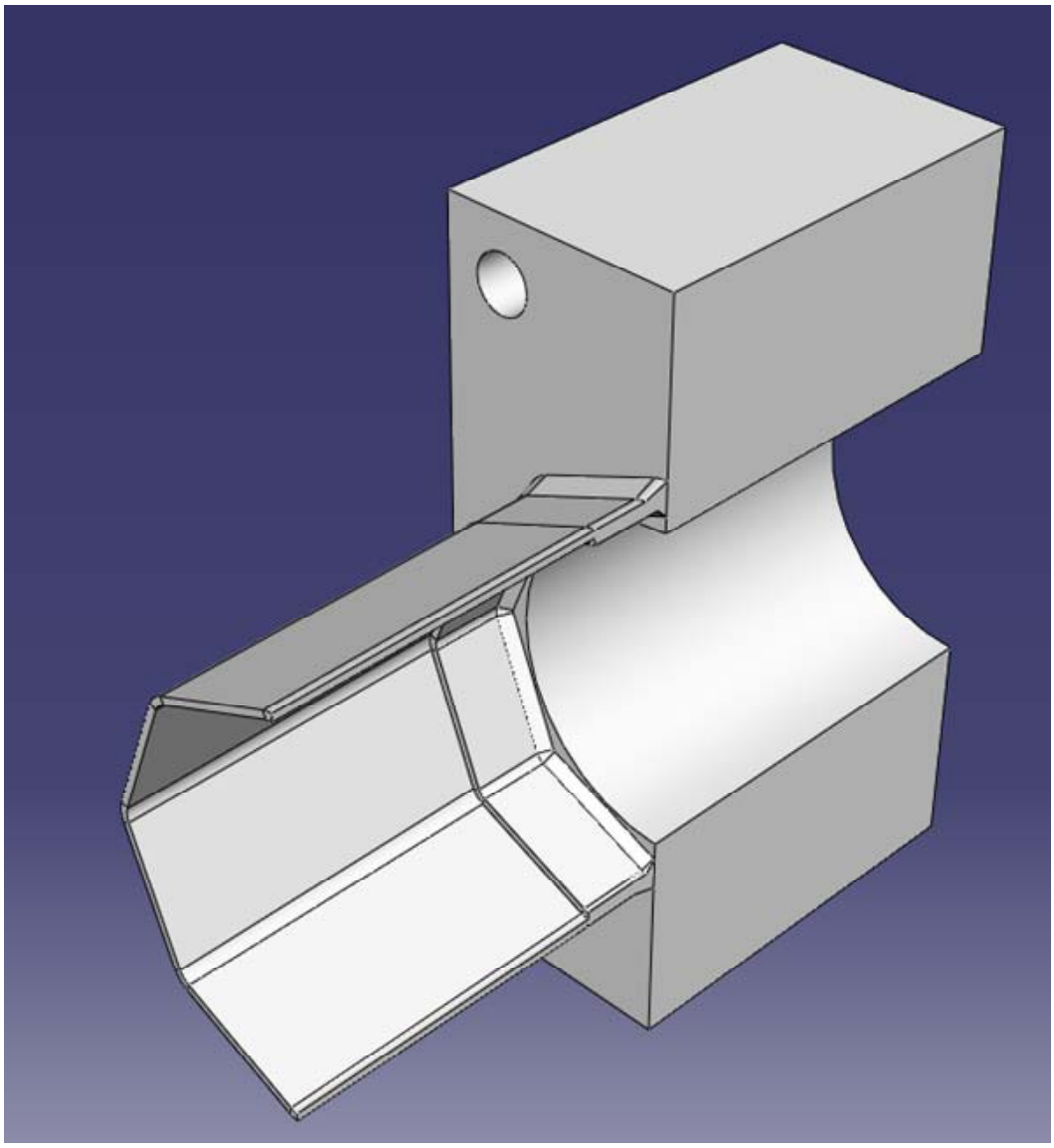

Figure 5-1: The Base Plate Assemblage Part

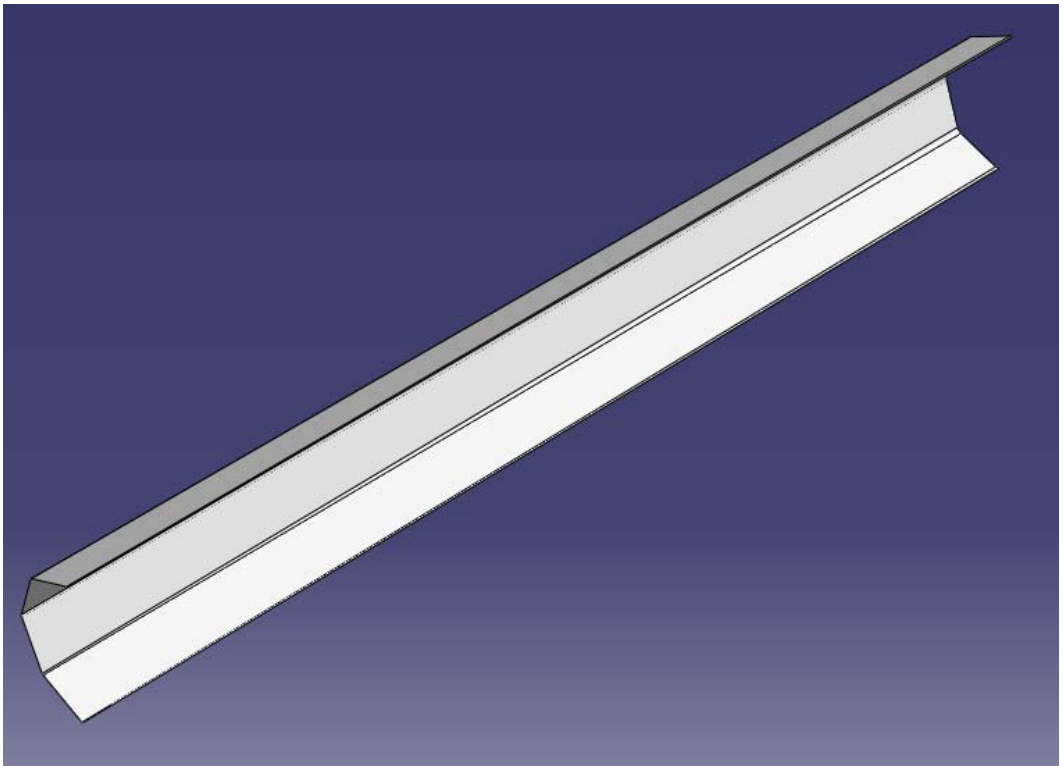

Figure 5-2: The Shell Pole Part

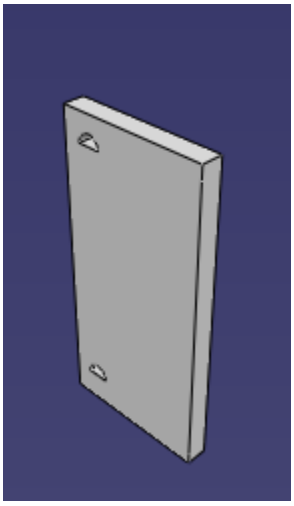

Figure 5-3: The Reaction Plate Part

5.1.2 Assembly

The 3 parts were connected using shell-to-solid ties. Partitions were created to guide the mesh and denote seams and contact surfaces. A complete assembly is shown in Figure 5-4.

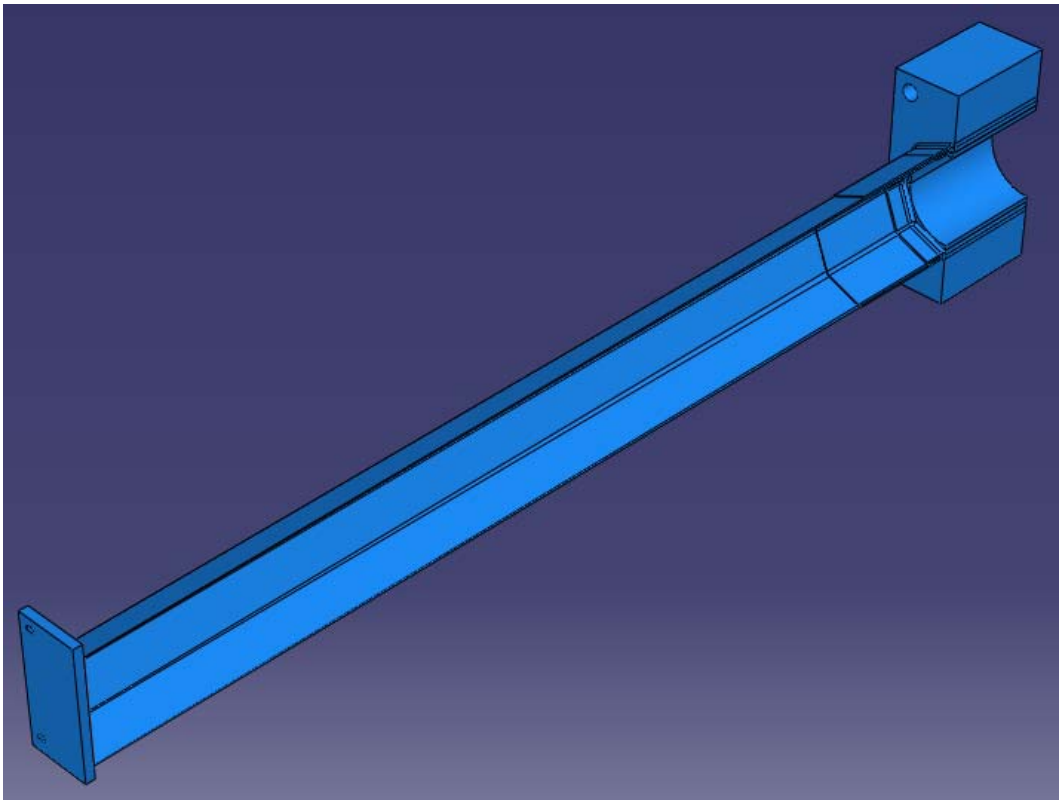

Figure 5-4: The Completed Pole Assembly

5.1.3 Contact

The full penetration detail was modeled with a seam between the backing ring and the pole in the base plate assemblage. A contact surface was set between the backing ring and the pole. This method allowed the backing ring to be created with the base plate assemblage, but still act as a

separate entity from the pole. The contact surface was used to capture the stiffness of the backing ring in the connection model. A similar contact surface exists between the external collar and the wall of the pole. A typical contact surface is shown in Figure 5-5.

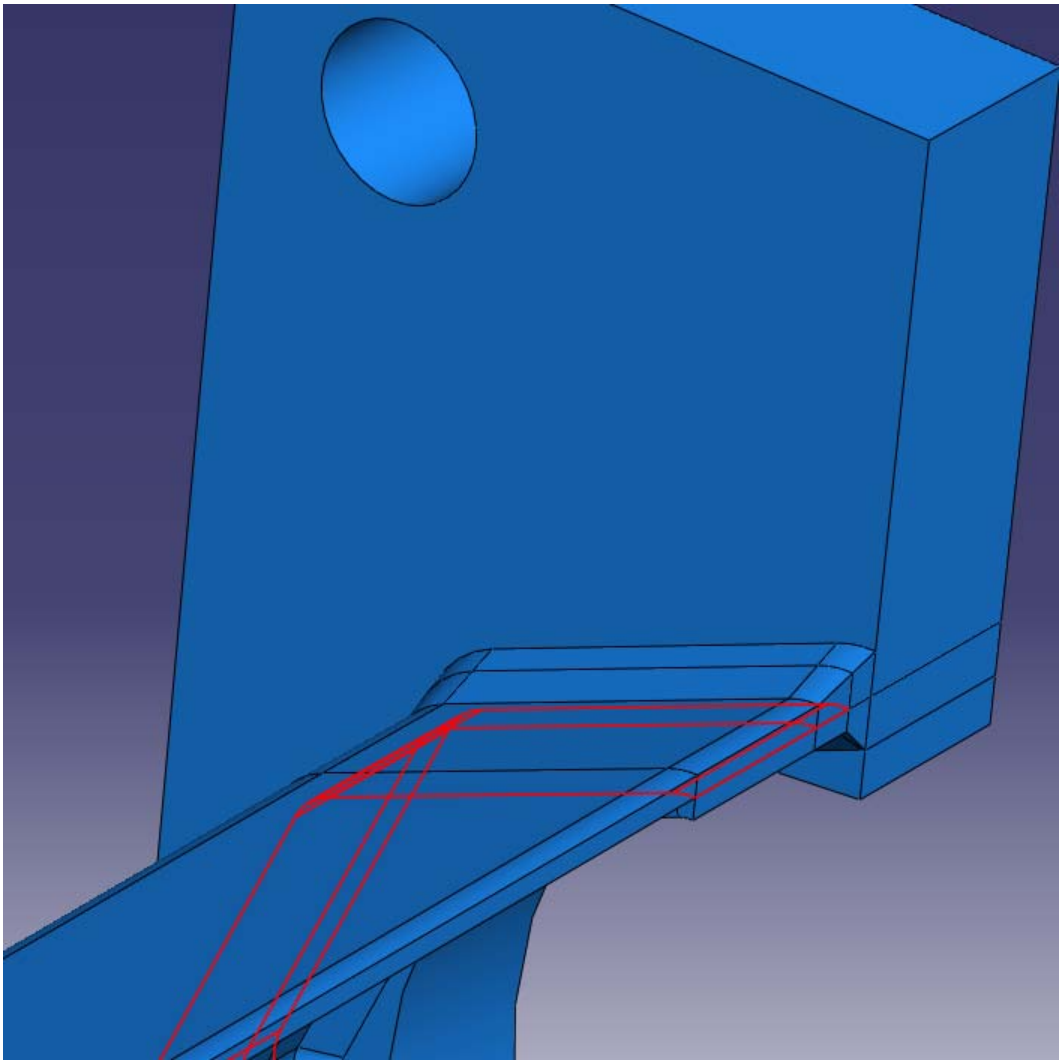

Figure 5-5: Contact Surface between Pole Shaft and Backing Ring

It was found in the external collar detail that defining a contact surface between the collar and the pole changed the hot spot stress by only 1%. In order to save computation time, the contact relationship was ignored in external collars. The contact relationship between the backup bar and pole in full penetration models did not significantly increase the computation time and was employed in the all the models with a back up bar.

5.1.4 Load and Boundary Conditions

In order to save on computation time, half the mast arm was modeled and a symmetry boundary condition enforced symmetry along the vertical plane along the centerline of the mast arm. Using symmetry reduced the number of elements by half, resulting in a large saving in terms of computation time. The symmetry planes selected for the symmetry boundary condition are shown in Figure 5-6.

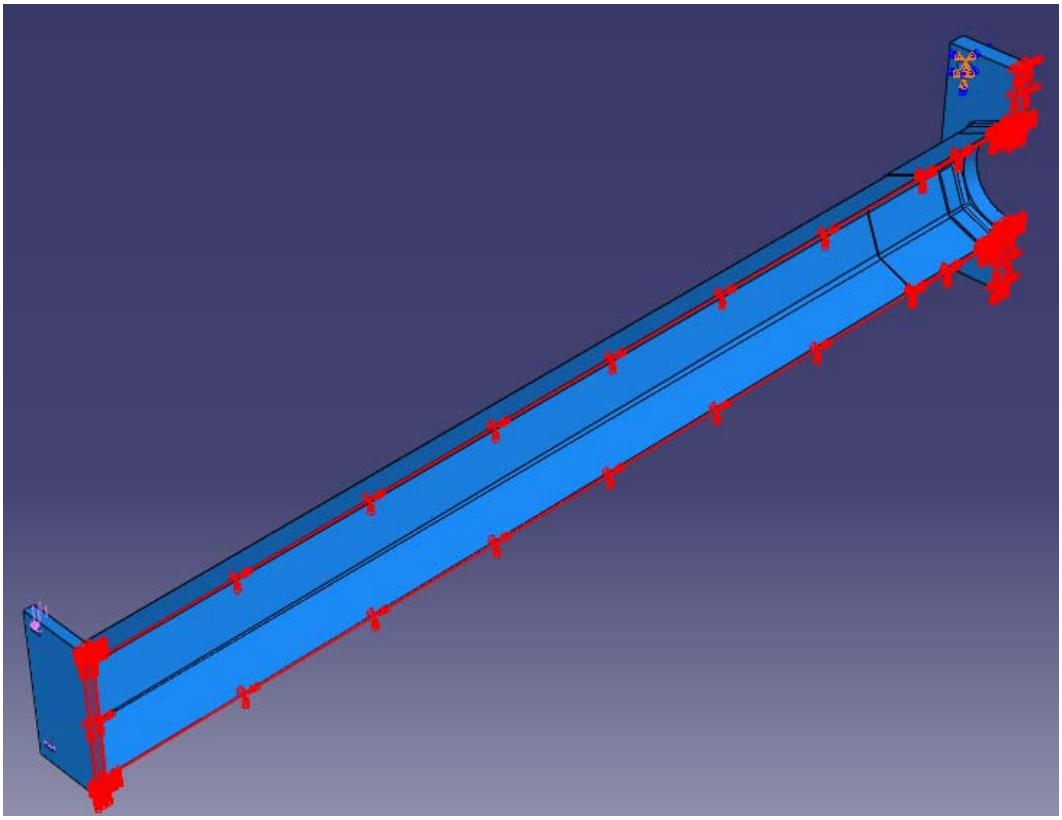

Figure 5-6: The Symmetry Boundary Condition

Load from the reaction bolts was simulated by modeling the reaction bolt holes as half circles with a horizontal surface where the center of the bolt would be at the far end of the model. Downward pressure was applied to this surface in order to create 0.5-k per bolt. With four bolts in the reaction plate (2 in the model plus 2 symmetric bolts) producing a total load of 2-kip.

Base plate bolts were simulated by fixing the front and back edges of the base plate bolt holes. This was compared to fixing a region that would simulate a washer and was found to produce hot spot stresses that were about 5% larger than the fixed "washer" boundary condition. For

simplicity, fixing the edges was chosen. The fixed edges of the bolt holes are highlighted in Figure 5-7.

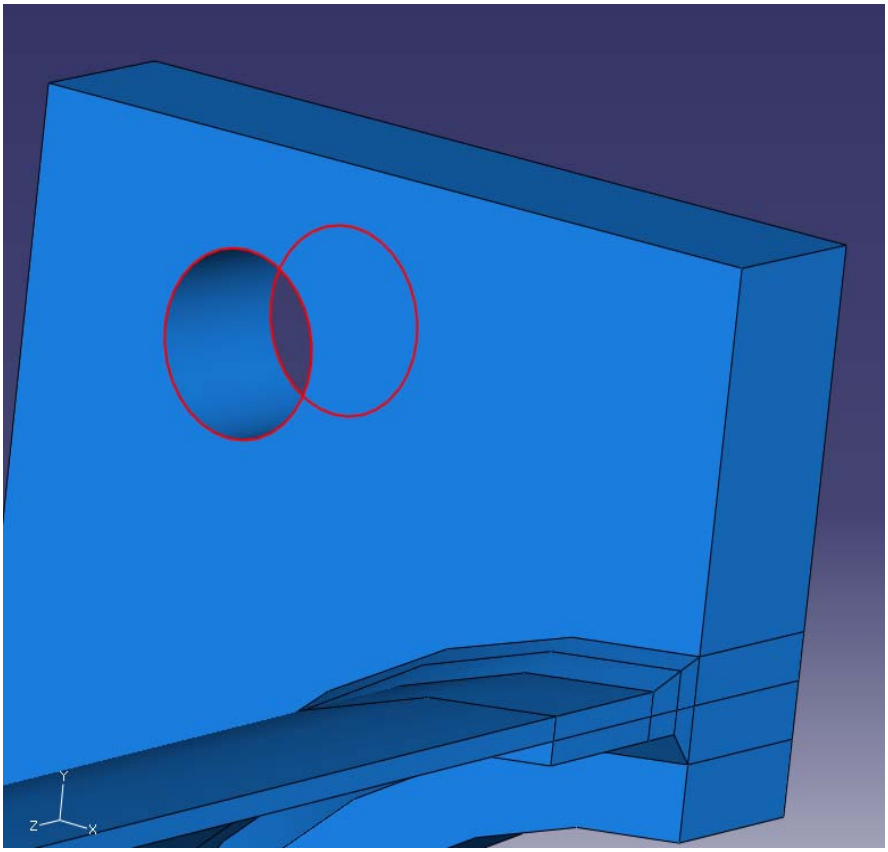

Figure 5-7: The Fixed Edges of the Bolt Holes

5.1.5 Mesh

Two major types of elements were used in the analytical model, solid brick elements and shell elements. Twenty node quadratic solid elements were used in the solid parts and eight node quadratic shell elements were used for the shell part. In many cases, a structured brick mesh,

adapted by ABAQUS from the mesh of a simple shape, was used. In cases where a structured mesh was not feasible or practical, like the base plate, a swept brick mesh was used. A swept mesh creates a mesh on a face of the object and sweeps the mesh along a line normal to the face. Most welds were modeled using brick elements and a structured mesh, but some needed to be modeled using wedge elements, which could only be swept.

Element sizes varied throughout the model. In the reaction plate and the shell pole, the elements were approximately 0.7172-in ($4t$). In the pole near the weld toe, elements were approximately 0.1793-in (t). In the base plate the largest elements were approximately 0.5-in to 0.7-in. In the submodel, the elements were all approximately 0.044825 ($t/4$)

5.1.6 Global Model

A completed finite element model of a full penetration connection is shown in Figure 5-8 and Figure 5-9. An external collar model is shown in Figure 5-10 and Figure 5-11.

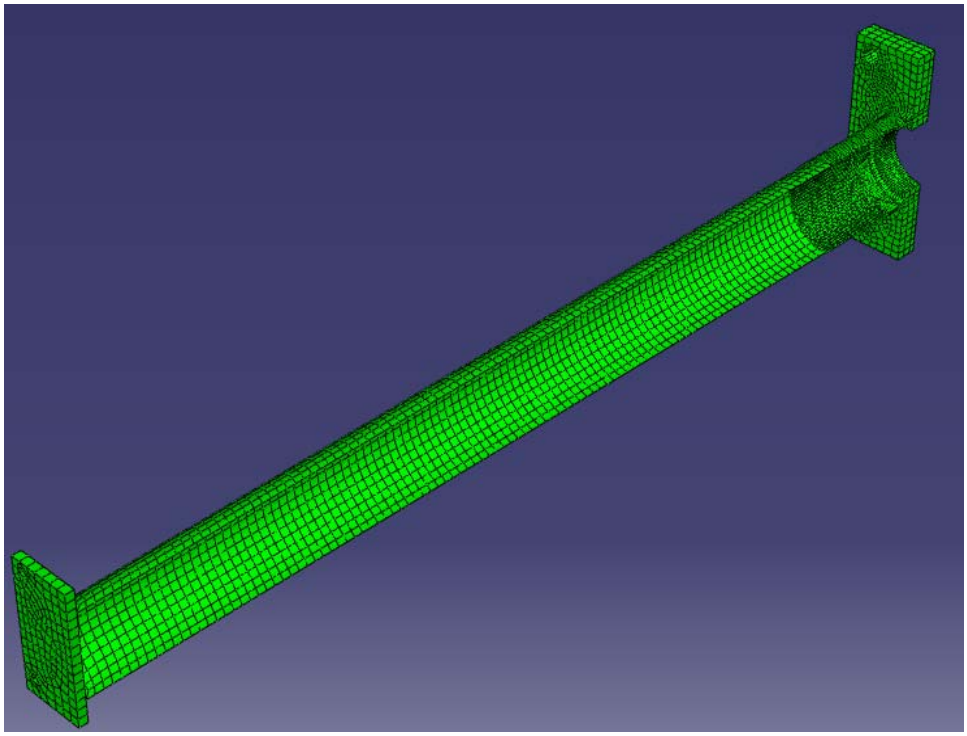

Figure 5-8: A Typical Full Penetration Model

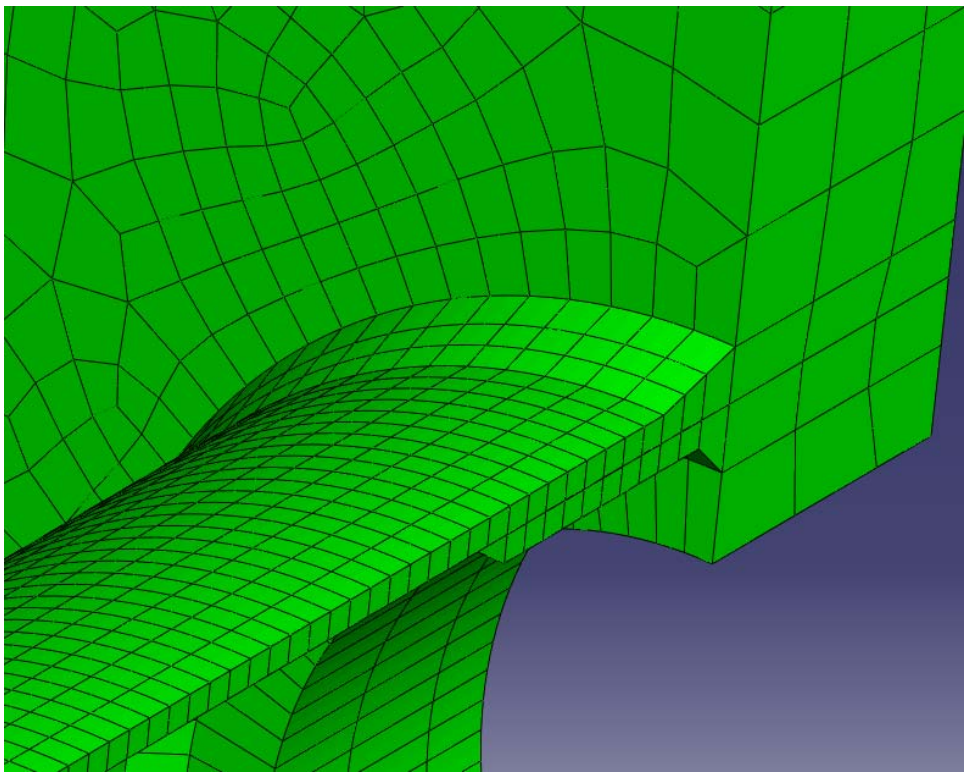

Figure 5-9: The Full Penetration Connection

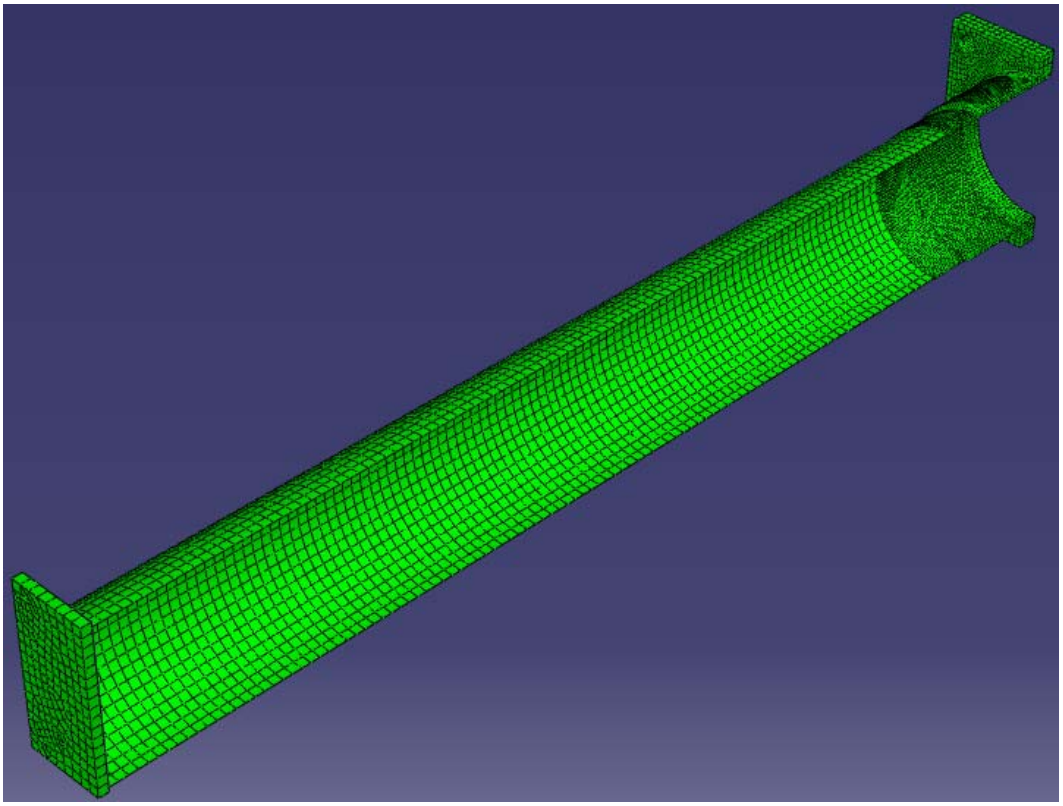

Figure 5-10: An External Collar Model

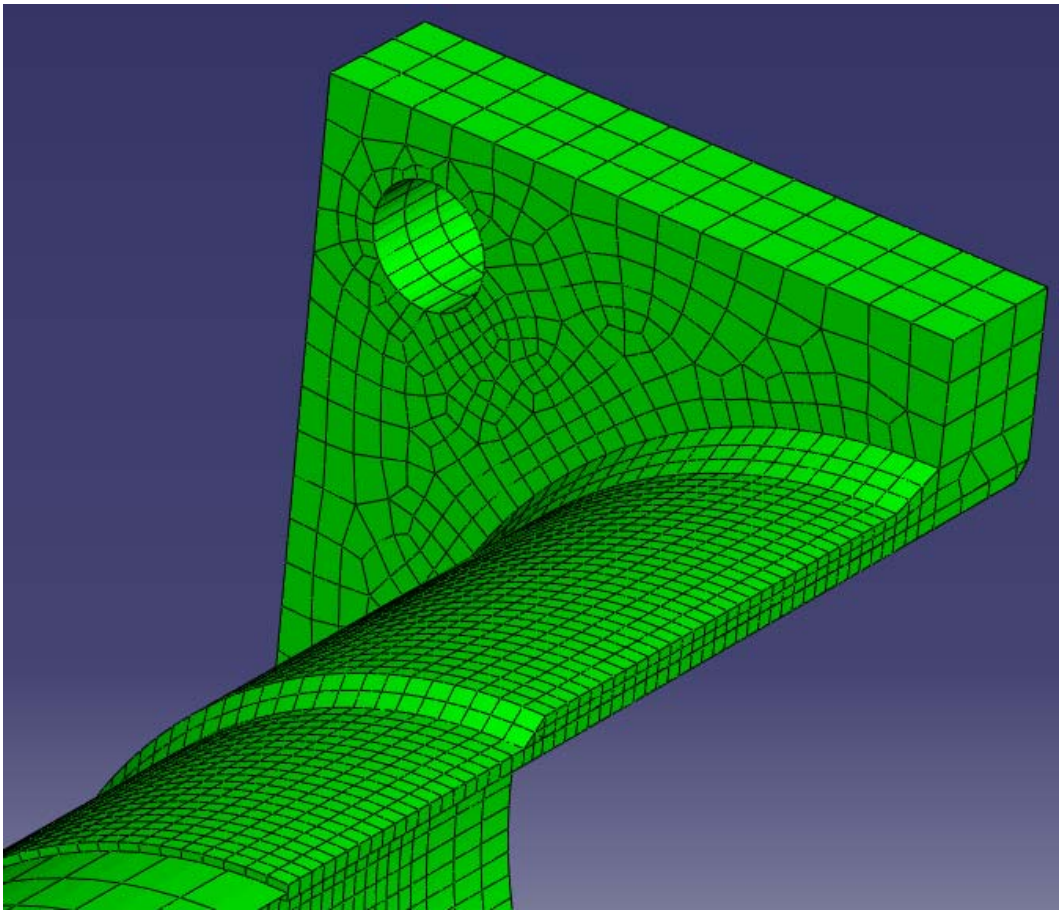

Figure 5-11: The External Collar Connection

The stress pattern and local deflection of a full penetration detail under a cantilever loading is seen in Figure 5-12**.** The stress pattern of an external collar detail can be seen in Figure 5-13. In the external collar picture, note that in addition to the high stress at the fillet weld connecting the top of the collar to the pole, high stresses also occur at the base plate weld.

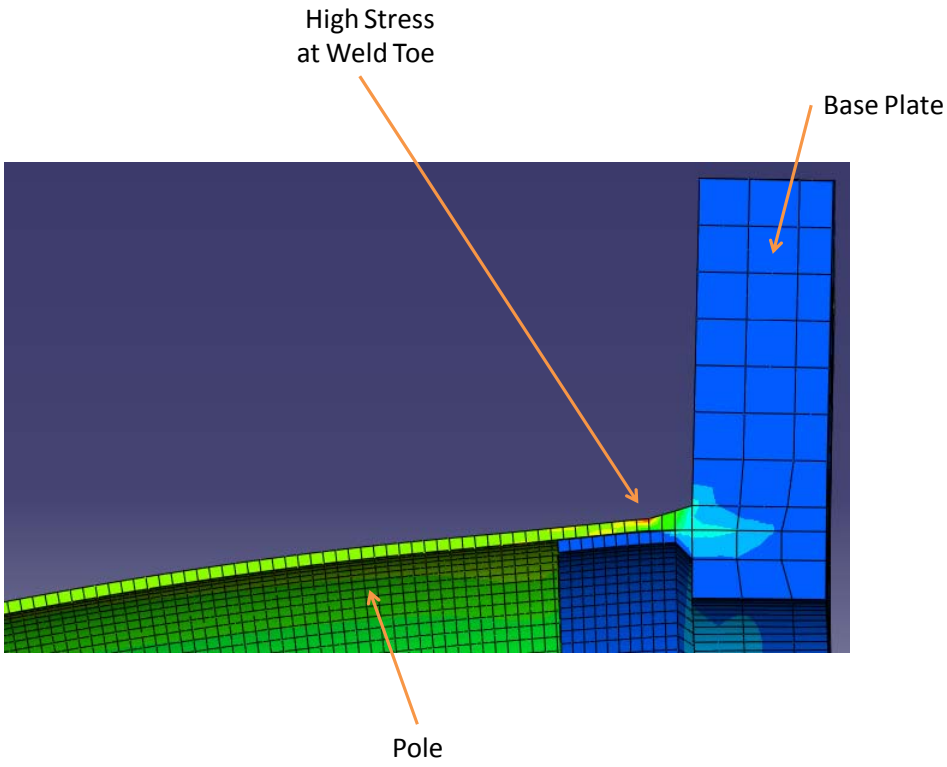

Figure 5-12: Typical Full Penetration Response

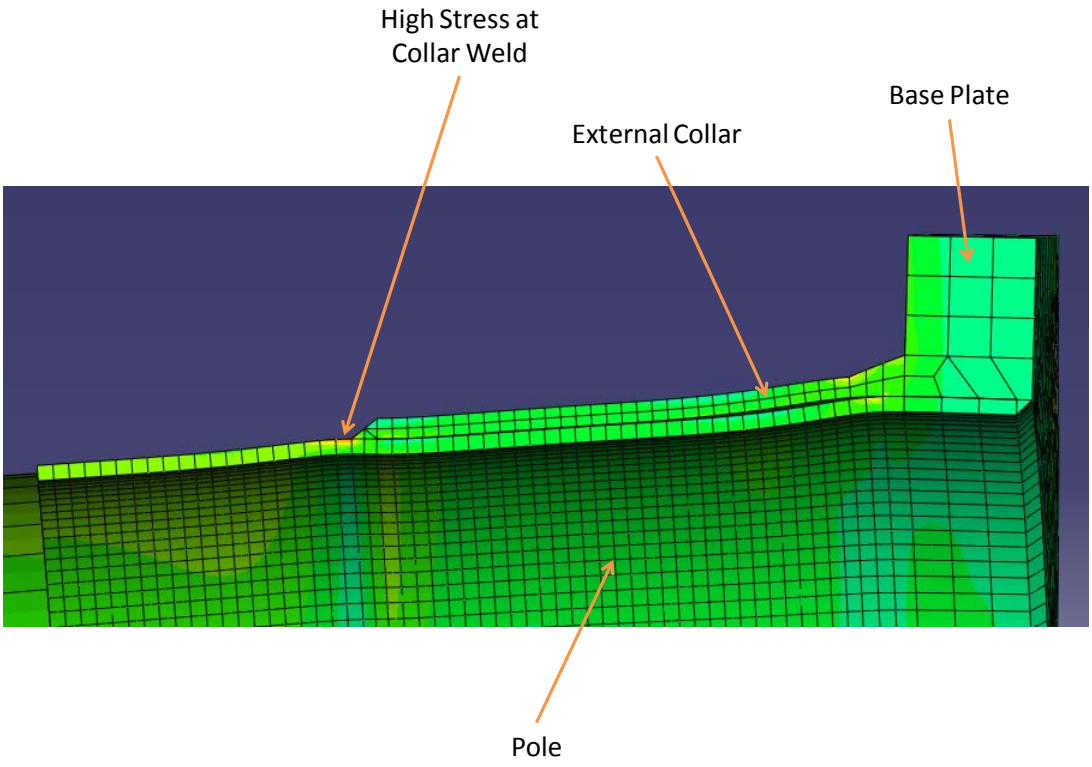

Figure 5-13: Typical External Collar Response

5.1.7 Submodel

In order to accurately account for the hot spot stress, a submodel was created. The submodel allowed smaller elements to be used than would be feasible on the larger, global model. A typical submodel is shown in Figure 5-14.

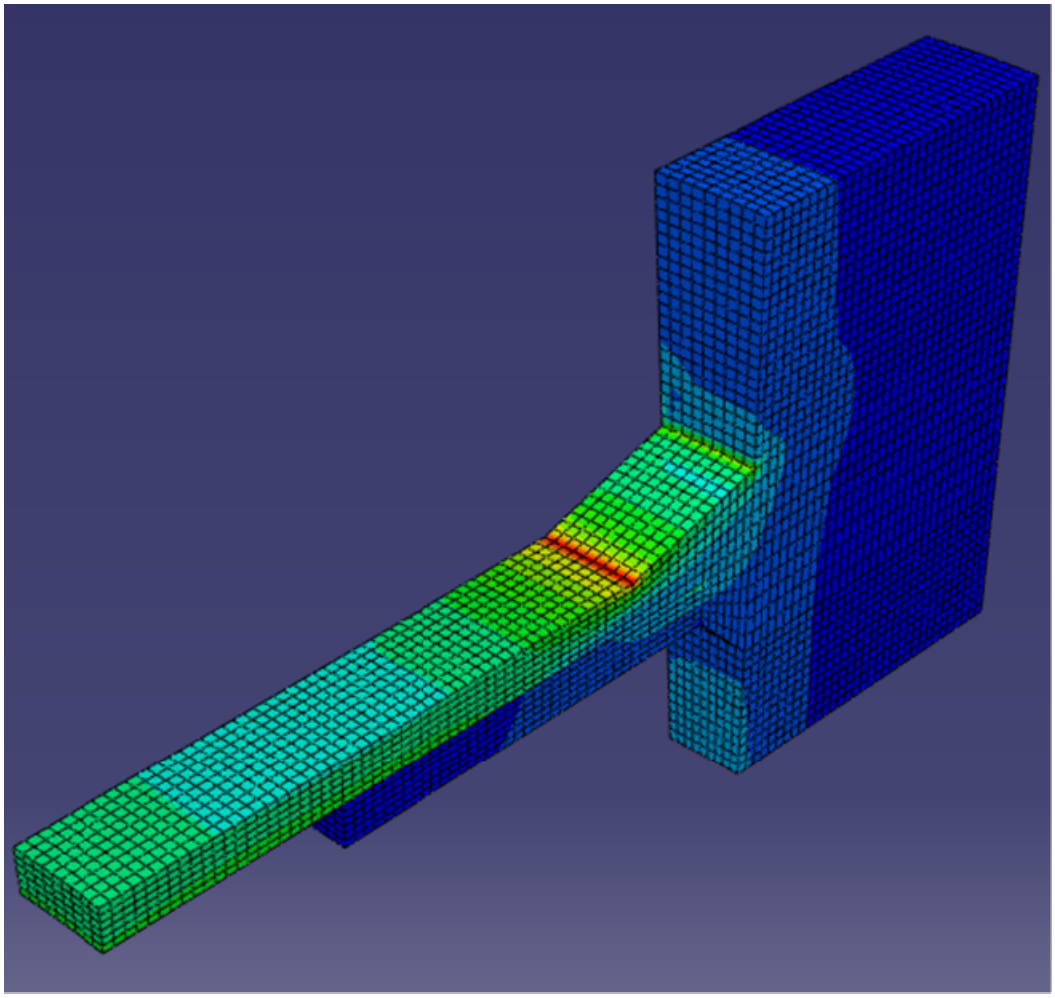

Figure 5-14: Submodel for a 12-1.5R-WY Model

A copy of the base plate assemblage was created and then cut down to leave only what was necessary for the submodel. The new surfaces created were grouped together and had the submodel boundary condition applied to them, which enforced displacements of those surfaces as if they were still part of the global model. The submodel boundary condition enforced displacements as if the submodel was still part of a global model. Aside from symmetry (since the point of interest was always at the top of the mast arm), no other boundary condition was applied

Submodels were typically created with the arc length of the outer surface of the pole as 0.1793-in. This created a mesh that was 4 elements across. The length of a submodel was chosen to include about 1.5-in of the base plate and about 3-in to 4-in of the pole. This was twice the distance of the backing ring, which was 2-in long. In early studies, some submodels included the entire length of the solid pole. This was changed since the larger submodel included regions that were mesh – insensitive and could be accurately modeled with the global model.

5.2 Evaluation of Stress Concentrations and Stress Concentration Factors (SCF)

The term stress concentration refers to a local maximum in the stress profile, and is also referred to as a hot spot stress. These stress concentrations are not accounted for if simple beam theory is used to calculate the stresses in the mast arm. Referred to as the nominal stress, a designer typically uses the stress computed from simple beam theory when designing a mast arm.

In mast arms, stress concentrations occur at weld toes due to the abrupt change in geometry and the large amount of local bending near the weld toe. The stress concentration occurs at the weld toe on the outer surface of the pole wall. A typical stress profile from a model of a mast arm is plotted in Figure 5-15. The nominal stress is given for comparison. A typical through thickness stress profile is given in Figure 5-16. As shown in Figure 5-16, the highest stress occurs on the outside of the pole; the stress on the inside of the pole is actually less than the nominal. This is due to the local bending in the pole.

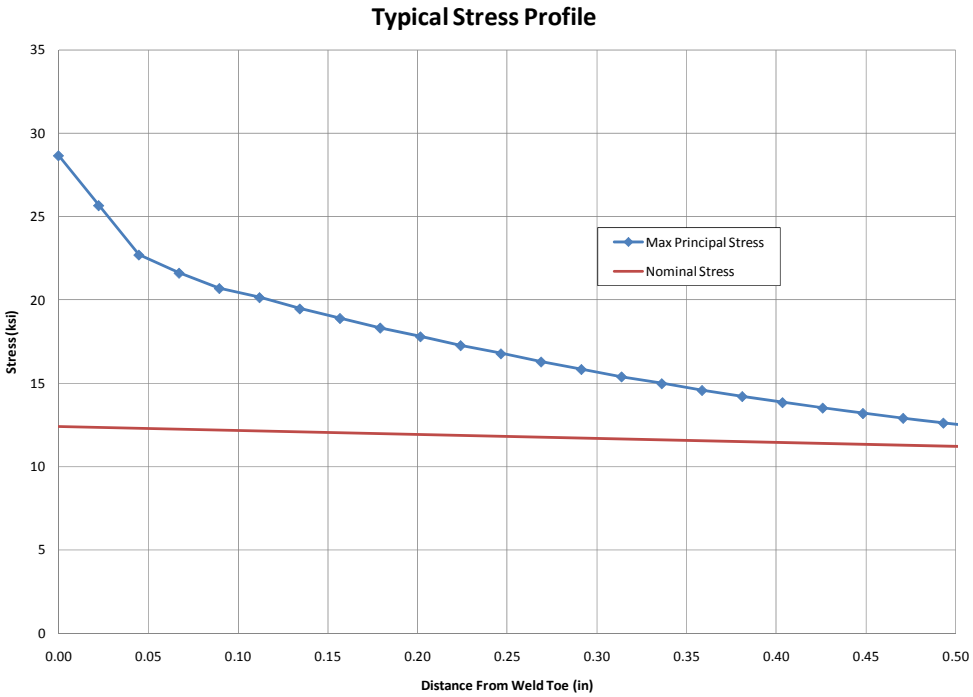

Figure 5-15: The Variation of Stress near the Weld Toe (Full Penetration)

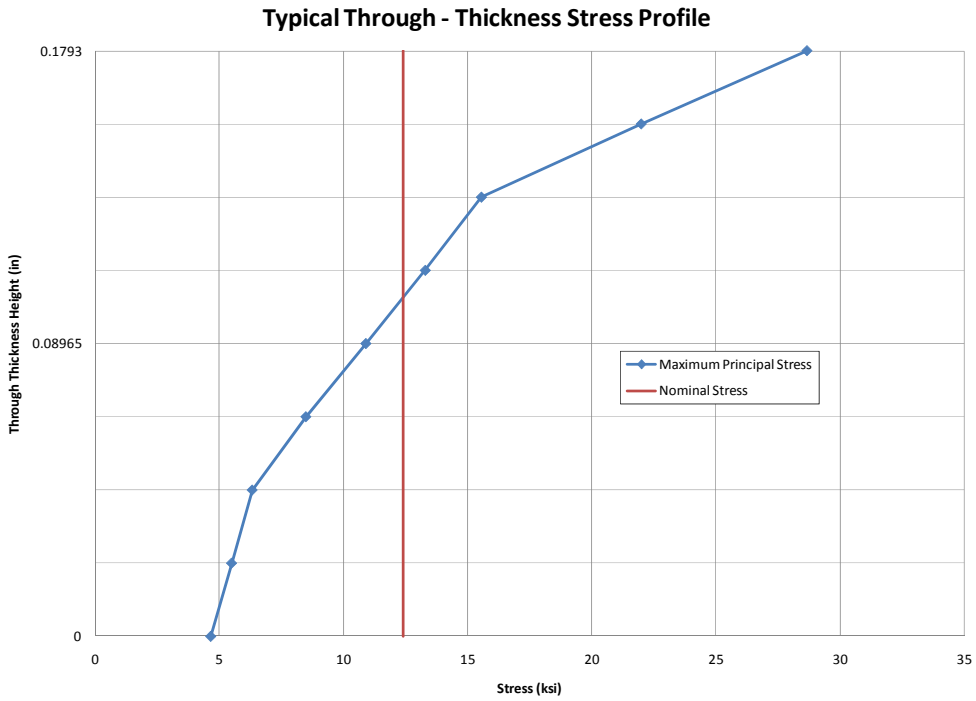

Figure 5-16: Through Thickness Stress at the Weld Toe (Full Penetration, Global Model)

The actual stress profile of the mast arm differs from the nominal in the region close to the weld toe, increasing nonlinearly and culminating in the hot spot stress or stress concentration occurs at the weld toe. Away from the weld toe, the stress profile approaches the nominal stress. Fatigue cracks propagate perpendicular to the maximum tensile stress, so stress concentrations in the maximum principle stress were of concern.

Stress concentration factors (SCFs) provide a convenient way to describe a stress concentration. An SCF is simply the hot spot stress divided by the nominal stress at that location. The different pole diameters and connection details produce varying moments of inertia and therefore produce

different nominal stresses. SCFs can be used to compare the effect a variable has across a wide variety of diameters and connection details.

The mast arms were all modeled with the same bending moment. This allows both the hot spot stress and SCF to be used to compare details. The lower the hot spot stress at a critical point in the mast arm (like the base plate weld in a full penetration connection), the longer the fatigue life will be. In general, a low SCF will produce longer fatigue life but this is not always the case and it is important to consider both the hot spot stress and the SCF when determining the fatigue performance of a detail. The hot spot stress is simply the nominal stress multiplied by the SCF. If the nominal stress is high enough, a detail with a low SCF could still produce a high hot spot stress. This is especially true when comparing different diameter poles (which have different moments of inertia and different nominal stresses) but also important in comparing details since the external collar details have a different moment of inertia than full penetration details.

5.2.1 Mesh Insensitivity Weld Toes

Welds profile were modeled as triangular shapes, producing a kink at the weld toe. Because of the kink, the stresses near the weld toe are mesh – sensitive. As the mesh size decreases, the stress at the weld toe increases to infinity. An example of this can be seen in Figure 5-17. The stress near the weld toe increases as the mesh size is decreased. A close up of the stresses near the weld toe in Figure 5-18clearly shows this effect. However, the stresses away from the weld toe are not as sensitive to the mesh size. Through thickness stresses are shown in Figure 5-19. The hot spot occurs at the surface of the pole. The mesh size influences the shape of the stress distribution through the thickness and magnitude of the stress at the weld toe.

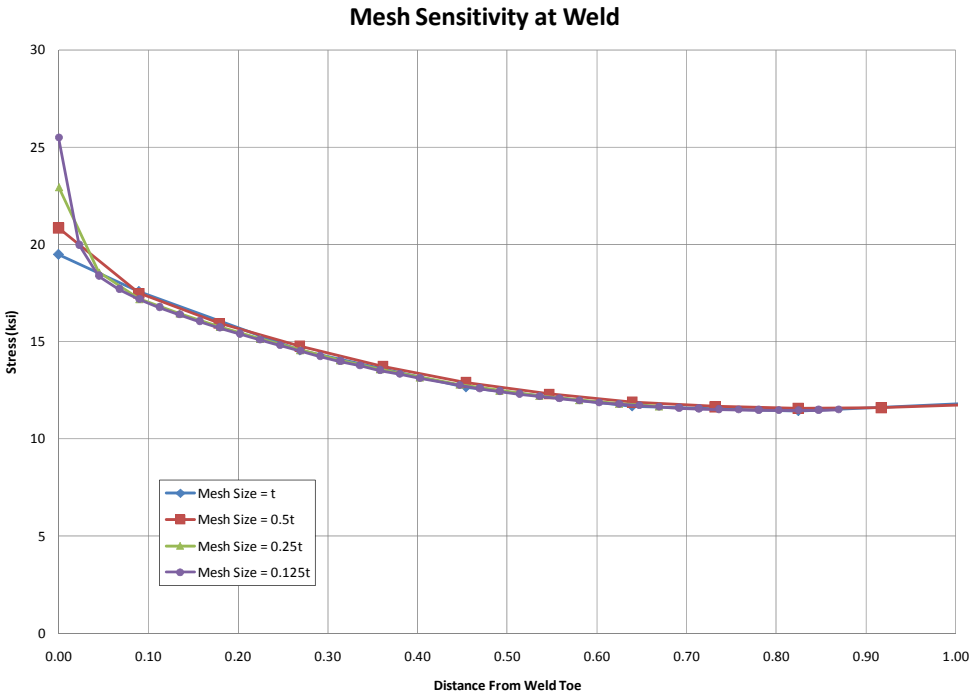

Figure 5-17: Mesh Sensitivity of Finite Element Stresses at the Weld Toe (Full Penetration)

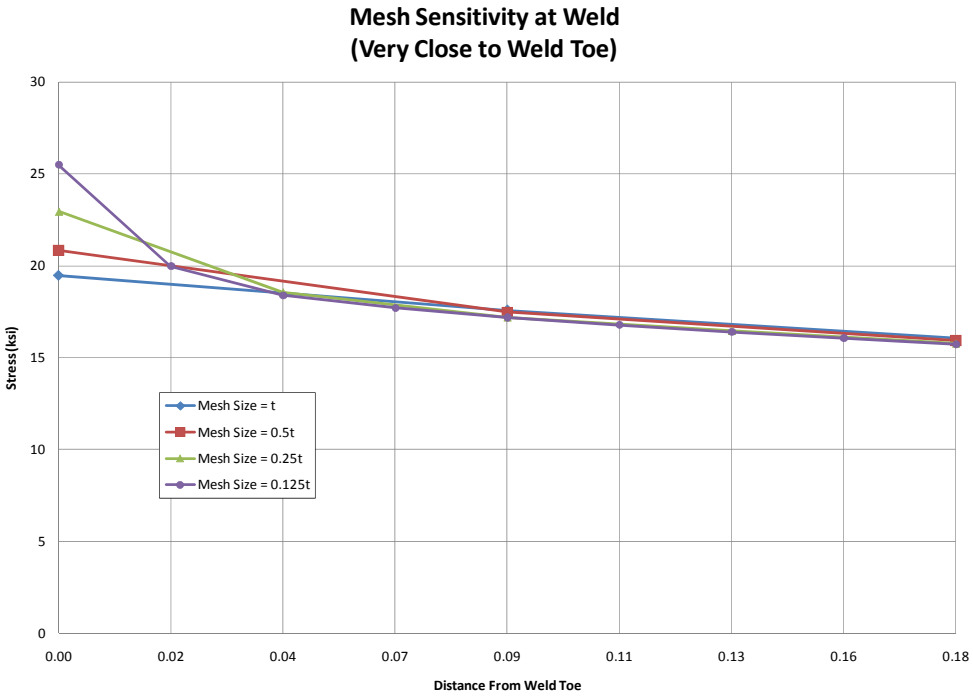

Figure 5-18: Close Up of Figure 9 near the Weld Toe

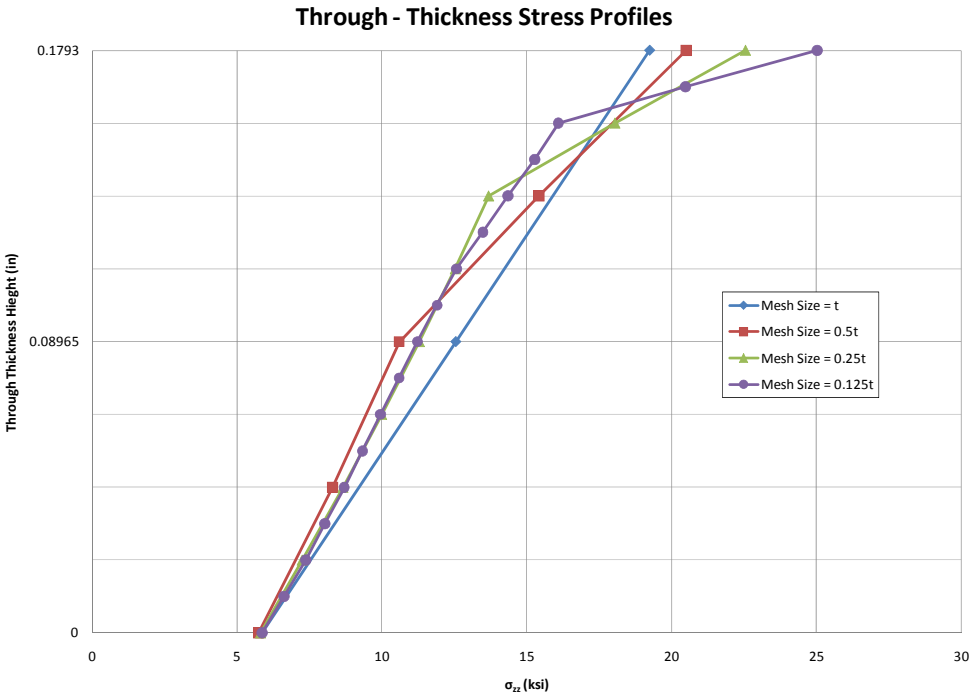

Figure 5-19: Mesh – Insensitivity shown in Through Thickness Stresses at the Weld Toe (Full Penetration)

Several methods are available to create a mesh – insensitive approximation of the hot spot stress. 2 methods were used in this study: the DNV Method (Det Norske Veritas 2008) and the Dong Structural Stress Method (Dong 2001). Both methods produce approximate hot spot stresses. These stresses do not include so called "notch effects" that are the product of variability in the weld profile, nor do they account for any residual stresses due to welding.

5.2.2 DNV Method

DNV stands for Det Norske Veritas, a maritime organization. The DNV Method was designed for use in offshore applications, where tubular structures are commonplace. Slightly away from the weld toe, the stress profile becomes mesh – insensitive at reasonable mesh sizes. Although the

stress profile near the weld toe increases nonlinearly, some distance away from the weld toe the stress profile resembles a linearly increasing function and can be approximated with a linear extrapolation. The DNV Method selects maximum principle stresses at points $t/2$ and $3t/2$ away from the weld toe, where *t* is the thickness of the tube wall, to linearly extrapolate the stress at the weld toe (Det Norske Veritas 2008).

An illustration of this method is shown in Figure 5-20.

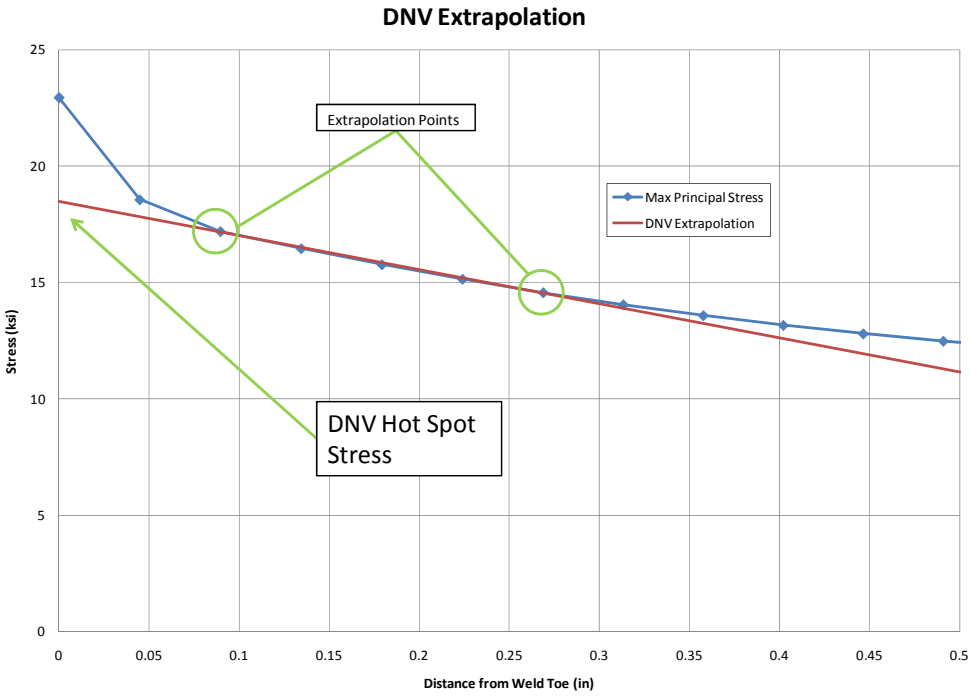

Figure 5-20: DNV Extrapolation

5.2.3 Dong Structural Stress Method

While the actual through thickness normal and shear stresses at the weld toe are mesh – sensitive, nearby the shear and normal stresses become mesh – insensitive. The Dong Method assumes a through thickness normal stress profile (σ_s) that can be broken up into two components: a constant membrane tensile stress (σ_m) and bending stress that varies linearly through the thickness (σ_b). The desired hot spot stress is at the surface of the pole at the weld toe. Using equilibrium of the pole between the weld toe and some nearby section where the stresses have become mesh – insensitive, equations can be formulated to determine the magnitudes of σ_m and σ_b. Equilibrium of force in the longitudinal (x in this case) direction requires that a constant membrane tension stress be equal to the average value of the tension stresses at the nearby section:

$$\sigma_m = \frac{1}{t}\int_0^t \sigma_x(y)dy$$

Equilibrium of moments about the inside of the pole at the weld toe yields:

$$\sigma_m \frac{t^2}{2} + \sigma_b \frac{t^2}{6} = \int_0^t \sigma_x(y)ydy + \delta\int_0^t \tau_{xy}(y)dy$$

where σ_x and τ_{xy} are the normal and shear stresses at a distance δ away from the weld toe. The assumed through thickness stress profile is determined by adding the membrane tension (σ_m) and the bending stresses (σ_b). The Dong Hot Spot Stress is the maximum tension stress that occurs in the assumed stress profile. This can be seen in Figure 5-21, where the maximum tension stress occurs at the weld toe.

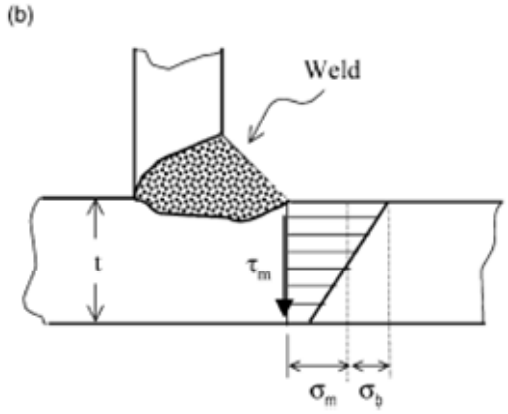

Figure 5-21: The Assumed Stress Profile in the Dong Method (Picture from Dong 2001)

This method is explained in great detail in (Dong 2001)**.**

5.2.4 Convergence Study

To determine what mesh size to use for the submodel, submodels were run with mesh sizes varying from $t/2$ to $t/10$. The 10-3R-WY detail was used for the global model and submodels since that was the first detail studied. Using the techniques described for determining hot spot stress, it was found that there was little difference between the global model (mesh size = *t*) and the submodels in terms of both hot spot stress and stress concentration factor, and no apparent change after the mesh size was reduced to $t/4$. For this reason, and in order to provide a reasonable amount of through – thickness nodes, a mesh size of $t/4$ was chosen. The results of this study are shown in Table 5-1and Figure 5-22. Both the DNV and Dong method of estimating the hot spot stress were utilized in the convergence study. A comparison is shown in Figure 5-23 and Figure 5-24. The difference in the extrapolated stress between these two methods was negligible at mesh size of $t/4$ and further refinement did not cause an appreciable change the

values of the hot spot stress for either method. In light of these results, the mesh size for submodels was set at $t/4$.

Mesh	Mesh	DNV Hot Spot Stress	Dong Hot Spot Stress	Nominal Stress	DNV SCF	Dong SCF
t	0.1793	19.082	19.639	12.405	1.54	1.58
t/2	0.08965	18.838	19.340	12.405	1.52	1.56
t/4	0.044825	18.494	18.763	12.405	1.49	1.51
t/8	0.022413	18.505	18.625	12.405	1.49	1.50
t/10	0.01793	18.494	18.608	12.405	1.49	1.50

Table 5-1: Results from Convergence Study

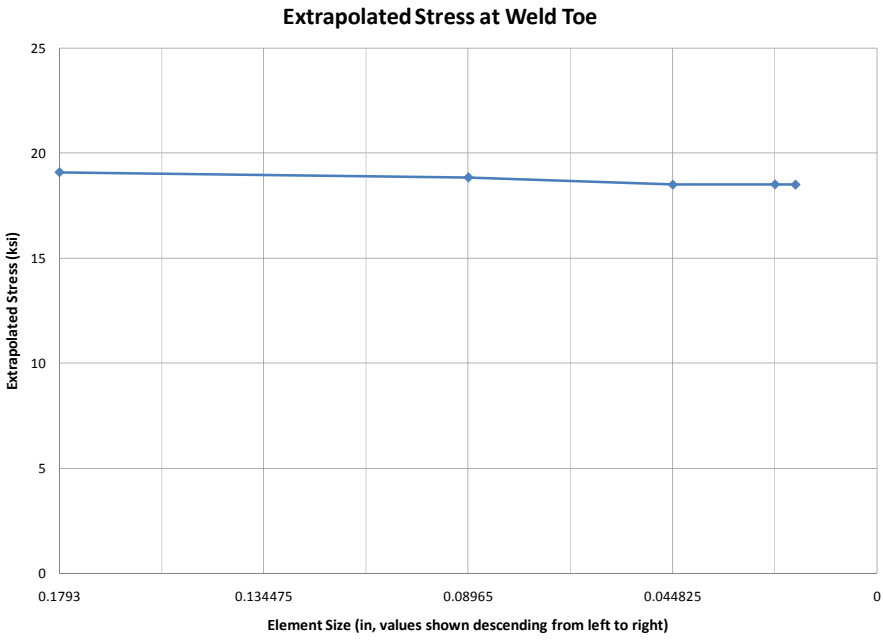

Figure 5-22: DNV Mesh Size Convergence

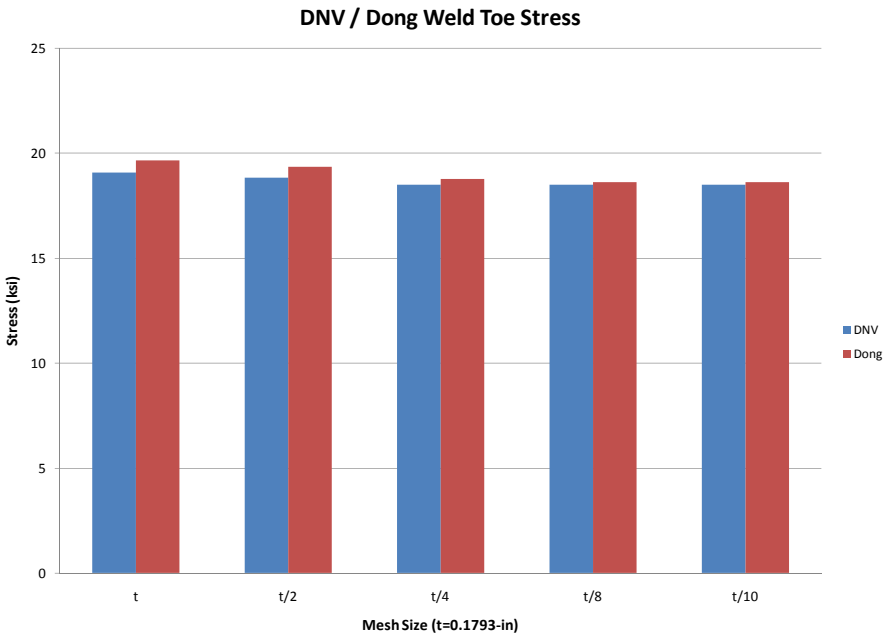

Figure 5-23: A Comparison of DNV and Dong Convergence (Hot Spot Stress)

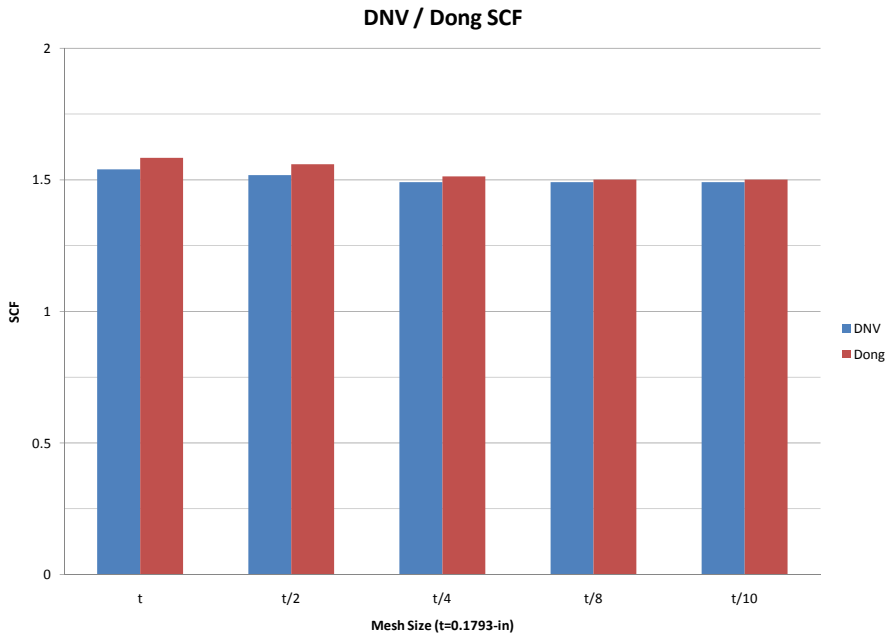

Figure 5-24: A Comparison of DNV and Dong Convergence (SCF)

Chapter 6

Results from Analytical Parametric Studies

The analysis work was divided into several parametric studies. The parametric studies changed one geometric variable while keeping others constant, to determine if there was a relationship between the given variable and the hot spot stress and stress concentration factor (SCF). Variables studied consisted of: base plate thickness, pole diameter, pole shape, pole – to – base plate connection detail, the presence of a fillet weld at the top of the backing ring in a full penetration detail, and the size of the hole in the base plate of a full penetration detail. The effect moment of inertia of the base plate, taken at the center of the hole in the base plate, was also examined. The moment of inertia is a function of the base plate thickness, detail, and hole size.

6.1 Nomenclature Used in Parametric Studies

The basic nomenclature that has been used throughout this thesis is kept with new variables added that are indicated at the end of the model name. The table below shows the nomenclature used in the analytical study. Several values of base plate thickness were studied for each model. An "X" is placed where the base plate thickness is usually called out to denote the range of base plate thicknesses that were studied. A key is given in Table 6-1.

X	All base plate thicknesses
Fillet	A fillet weld at the top of the backing ring in a full penetration connection
NH	No hole in the base plate
3H	A 3-in radius hole in the base plate
P2	Octagonal with 2-in bend radii
P(3/8)	Octagonal with 3/8-in bend radii
S#	A square base plate with bolt holes positioned at #-in by 12-in

Table 6-1: Key of New Nomenclature Variables

6.2 Results of Analytical Models

Computed hot spot stresses and SCFs for every model analyzed are presented in Table 6-2. Entries in the table are divided by model. Different hot spot locations on the same model, the base plate weld and the collar weld of an external collar model, for example, are presented as different entries.

	Name	8-XR-WY		10-XR-WY		10-XR-WY-Fillet		10-XR-WY-Fillet		10-XR-WY-P2		10-XR-WY-P(3/8)	
	Location	Base Plate Weld		Base Plate Weld		Base Plate Weld		Fillet Weld		Base Plate Weld		Base Plate Weld	
	$\sigma_{nominal}$ (ksi)	19.65		12.40		12.40		12.41		13.18		13.96	
	BP (in)	DNV	Dong	DNV	Dong	DNV	Dong	DNV	Dong	DNV	Dong	DNV	Dong
Hot Spot Stress	1.5	33.51	34.68	23.96	24.83	20.95	21.55	20.38	18.72	27.27	27.41	26.91	27.91
	2	28.60	29.50	20.88	21.63	17.07	17.56	20.02	19.14	23.02	23.12	22.78	21.94
	3	27.25	28.23	18.63	19.30	14.16	14.59	19.64	16.65	20.04	20.12	19.29	17.92
	4	26.40	27.28	17.84	18.48	13.15	13.55	19.36	9.84	19.01	19.09	18.76	18.36
	10	25.64	26.57	NA	NA	12.22	12.60	18.78	9.84	18.10	18.18	17.66	16.86
SCF	1.5	1.71	1.77	1.93	2.00	1.69	1.74	1.64	1.51	2.20	2.21	2.17	2.25
	2	1.46	1.50	1.68	1.74	1.38	1.42	1.61	1.54	1.85	1.86	1.84	1.77
	3	1.39	1.44	1.50	1.56	1.14	1.18	1.58	1.34	1.61	1.62	1.55	1.44
	4	1.34	1.39	1.44	1.49	1.06	1.09	1.56	0.79	1.53	1.54	1.51	1.48
	10	1.31	1.35	0.00	0.00	0.99	1.02	1.51	0.79	1.46	1.47	1.42	1.36

	Name	12-XR-WY		12-XR-WY-3H		12-XR-WY-NH		12-XS-EC		12-XS-EC	
	Location	Base Plate Weld		Base Plate Weld		Base Plate Weld		Base Plate Weld		Collar Weld	
	$\sigma_{nominal}$ (ksi)	8.54		8.54		8.54		8.54		7.94	
	BP (in)	DNV	Dong	DNV	Dong	DNV	Dong	DNV	Dong	DNV	Dong
Hot Spot Stress	1.5	16.31	16.83	13.75	14.22	12.95	13.42	10.94	NA	16.01	16.50
	2	14.50	14.96	12.84	13.27	12.33	12.76	9.13	NA	15.91	16.36
	3	13.08	13.50	12.19	12.59	11.91	12.30	9.03	NA	17.03	17.50
	4	12.54	12.94	11.99	12.38	11.78	12.17	9.37	NA	16.69	17.14
	10	11.99	12.75	11.71	12.09	11.65	12.03	9.49	NA	16.85	17.64
SCF	1.5	1.91	1.97	1.61	1.67	1.52	1.57	1.28	NA	1.88	1.93
	2	1.70	1.75	1.50	1.55	1.44	1.49	1.07	NA	1.86	1.92
	3	1.53	1.58	1.43	1.48	1.39	1.44	1.06	NA	1.99	2.05
	4	1.47	1.52	1.40	1.45	1.38	1.43	1.10	NA	1.96	2.01
	10	1.40	1.49	1.37	1.42	1.36	1.41	1.11	NA	1.97	2.07

	Name	10-2SX-WY			
	Detail	SR (9X15)	R10 (10X15)	R11(11X15	S
	Location	Base Plate Weld	Base Plate Weld	Base Plate Weld	Base Plate Weld
	$\sigma_{nominal}$ (ksi)	12.40	12.40	12.40	12.40

	BP	DNV	Dong	DNV	Dong	DNV	Dong	DNV	Dong
Hot Spot	2	18.649	19.36858	19.0552	19.85429	19.2592	20.05544	20.1199	20.88995
SCF	2	1.50	1.56	1.54	1.60	1.55	1.62	1.62	1.68

Table 6-2: Computed Hot Spot Stresses and Stress Concentration Factors (SCF)

Table 6-2 includes all results. thirteen different details which were studied at varying base plate thicknesses. Pole diameter, pole shape, and base plate geometry were studied in full penetration details. The presence of a fillet weld at the top of the backing ring in a full penetration detail as well as an external collar detail was also studied.

A discussion of each parametric study is given in the following sections.

6.3 Full Penetration Weld Connection Stiffness

The local bending of the pole plays a large role in the magnitude of the stress concentration. In simple beam theory, the bending moment is resisted by longitudinal stresses that are proportional to the distance from the neutral axis. Tension longitudinal stresses will be carried on the top side of the mast arm and compressive stresses on the bottom. The highest tension stresses will occur at the top of the mast arm at the weld toe. For a thin wall tube the stresses at any given point will be approximately constant through the thickness. Localized curvature in the pole wall will induce local bending stresses in the wall, increasing the tension stresses at one edge of the pole wall and decreasing the tension stresses (making them more compressive) on the other side. This is shown in Figure 6-1.

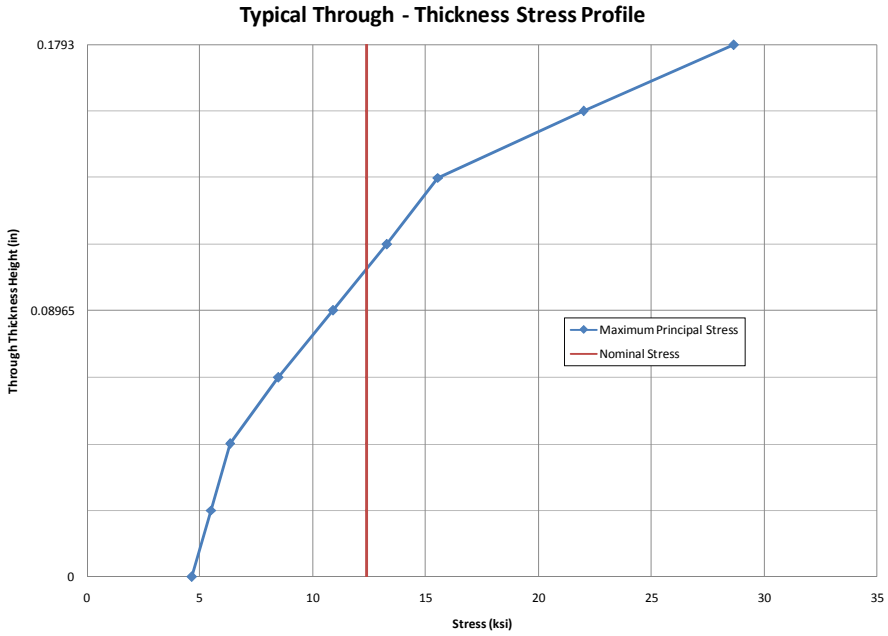

Figure 6-1: Typical Through Thickness Stress Profile

Previous studies found that a stiffer base plate reduced this local bending (M. T. Koenigs 2003) (Anderson 2007). Stiffness of the connection was a focus of much of the analytical work done in this phase of the research. Several variables were thought to contribute to the stiffness of the connection and were investigated in parametric studies. These were: base plate thickness, pole diameter, size of the hole in the base plate in full penetration details, pole shape (octagonal or round), and base plate geometry and bolt pattern. These are compared separately in the following sections.

An attempt to provide a simple rational comparison of the effect of connection stiffness on stress concentrations is provided in following sections.

6.3.1 Base Plate Thickness

Base plate thickness was varied for many details that were studied analytically. In nine of the full penetration details that were studied, base plate thickness was varied. In all full penetration details studied, the thickness of the base plate played a role in the stress concentration at the base plate weld toe. Results from two typical studies are shown in Figure 6-2 and Figure 6-3.

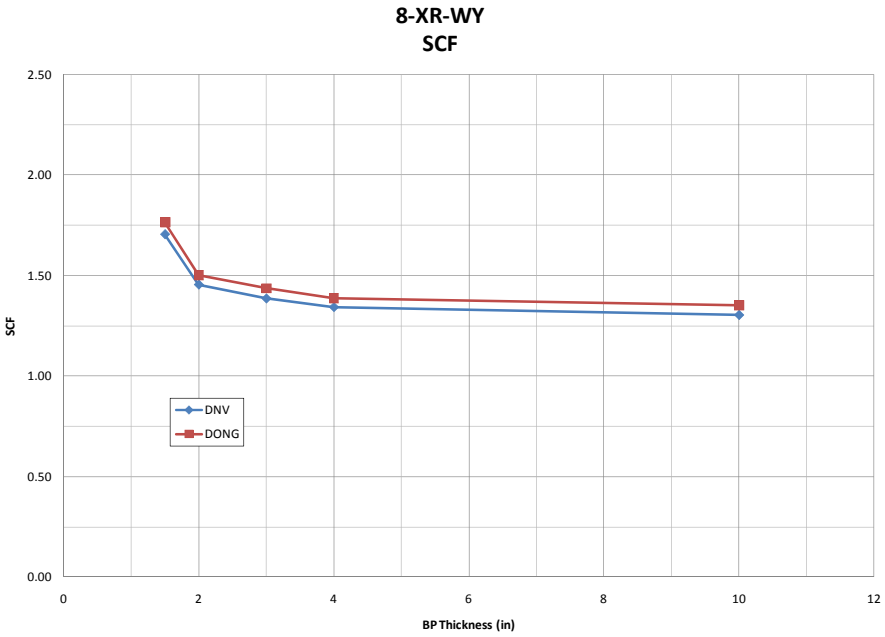

Figure 6-2: 8-XR-WY (SCF versus Base Plate Thickness)

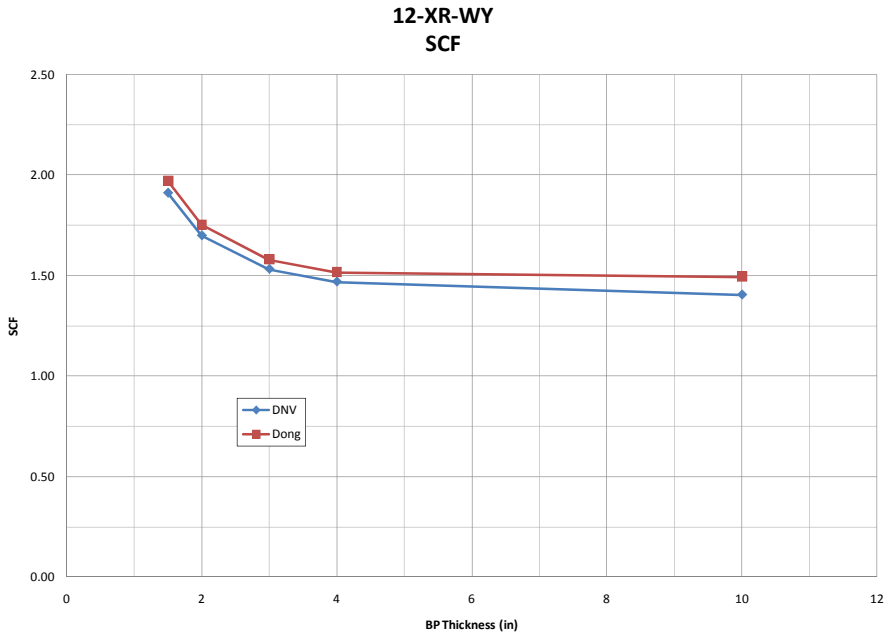

Figure 6-3: 12-XR-WY (SCF versus Base Plate Thickness)

As shown, there is a dramatic reduction of the SCF when increasing the base plate thickness from 1.5-in to 3-in. At about a 4-in base plate the SCF levels off and there is no additional benefit from increasing the base plate thickness. The difference between the SCF at a 1.5-in base plate (the maximum SCF) and the SCF at 10-in base plate (the minimum SCF) was not constant and depends on other variables, however the trend throughout full penetration details was that increasing the base plate thickness reduced the stress concentration at the base plate weld toe.

The role that the thickness of the base plate plays can be seen in Figure 6-4 and Figure 6-5. The thicker 3 in. base plate in Figure 6-5 is much stiffer and does not deflect nearly as much as the thinner 1.5 in. base plate shown in Figure 6-4. This translates to less bending in the pole wall and therefore a smaller stress concentration at the weld toe.

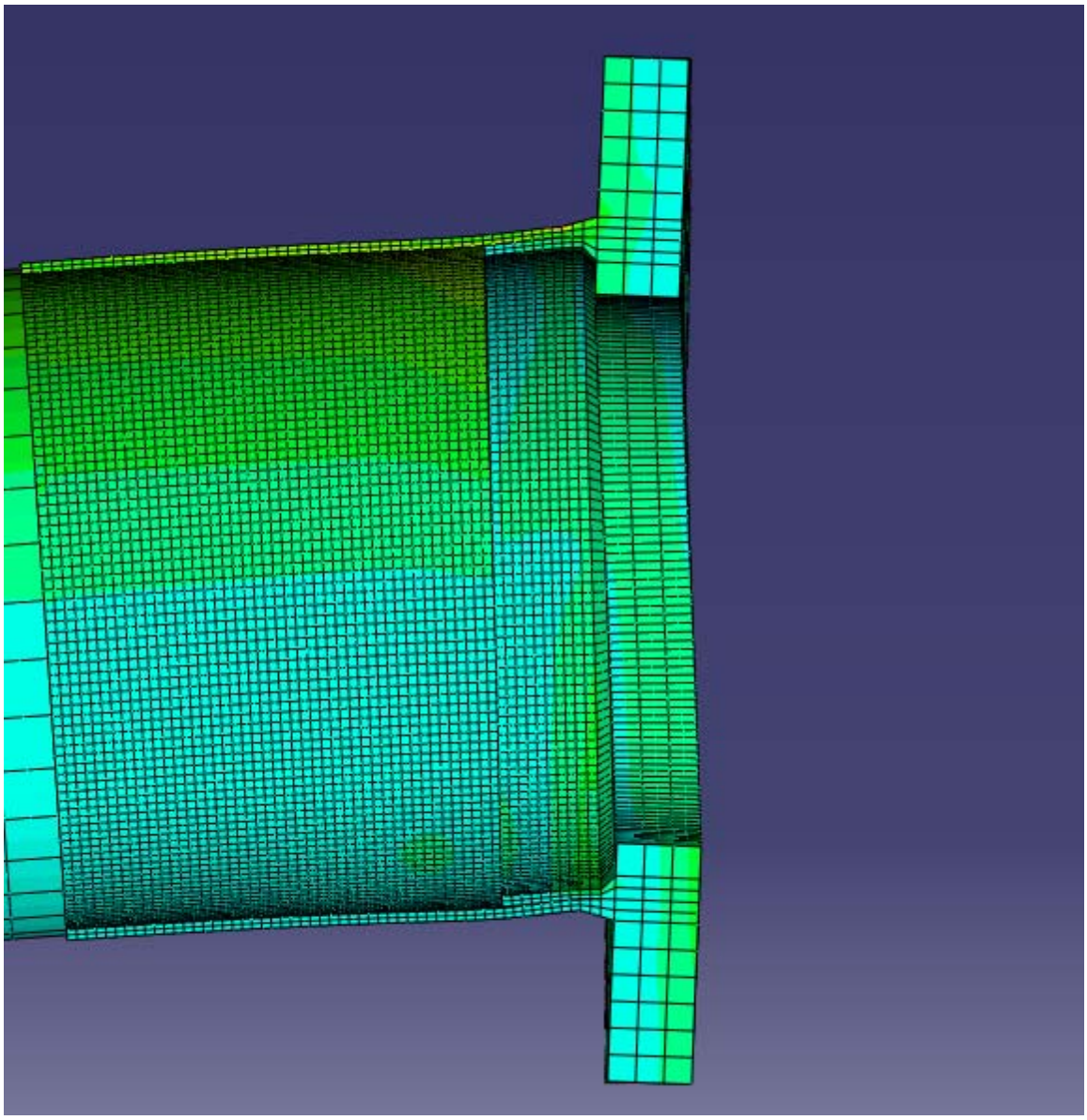

Figure 6-4: Bending of the Base Plate Connection (12-1.5R-WY)

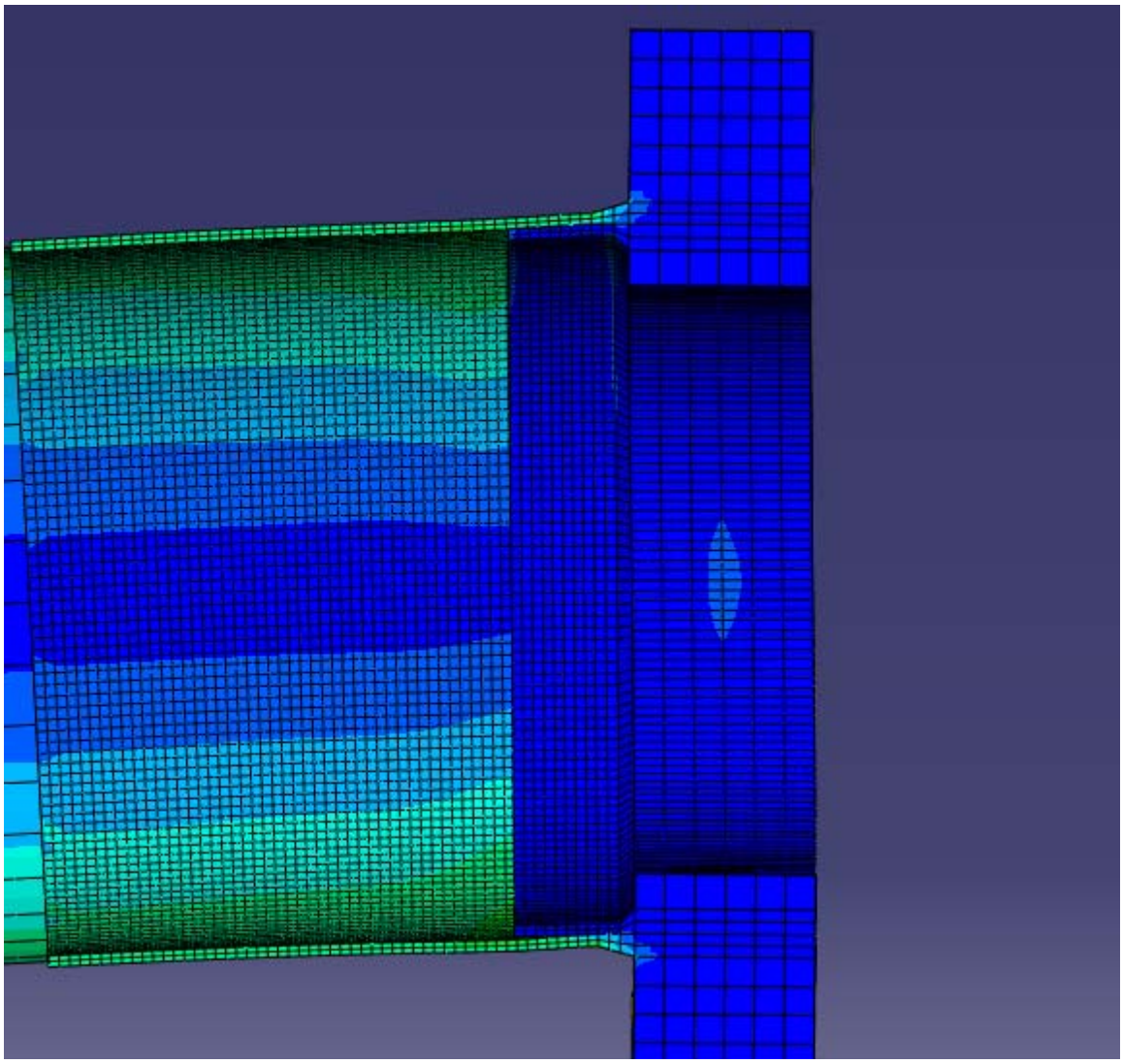

Figure 6-5: Bending in the Base Plate Connection (12-3R-WY)

6.3.2 Pole Diameter

The effect of pole diameter on the stress concentration at the weld toe was studied for rectangular (R) details. The results are presented in Figure 6-6 and Figure 6-7.

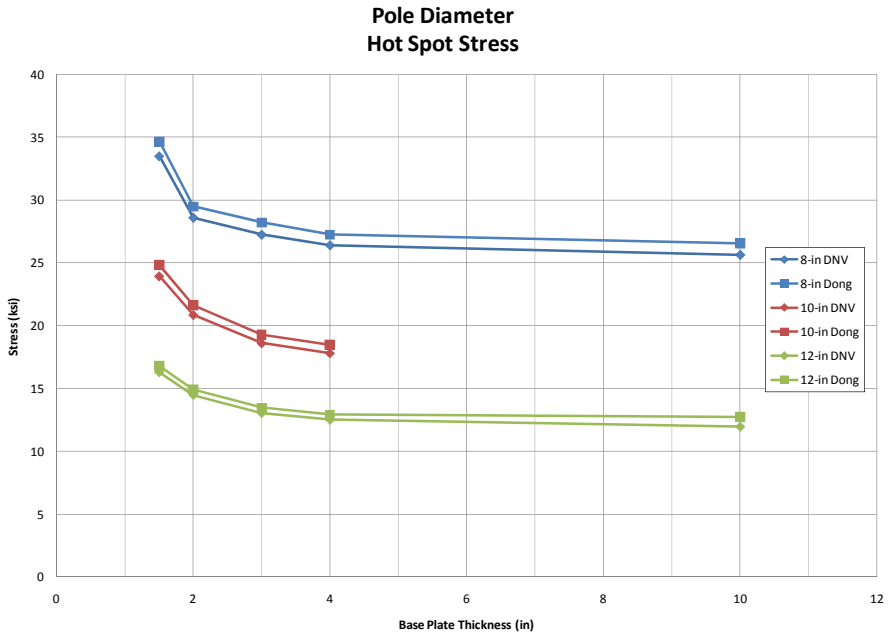

Figure 6-6: Pole Diameter Study (Hot Spot Stress versus Base Plate Thickness)

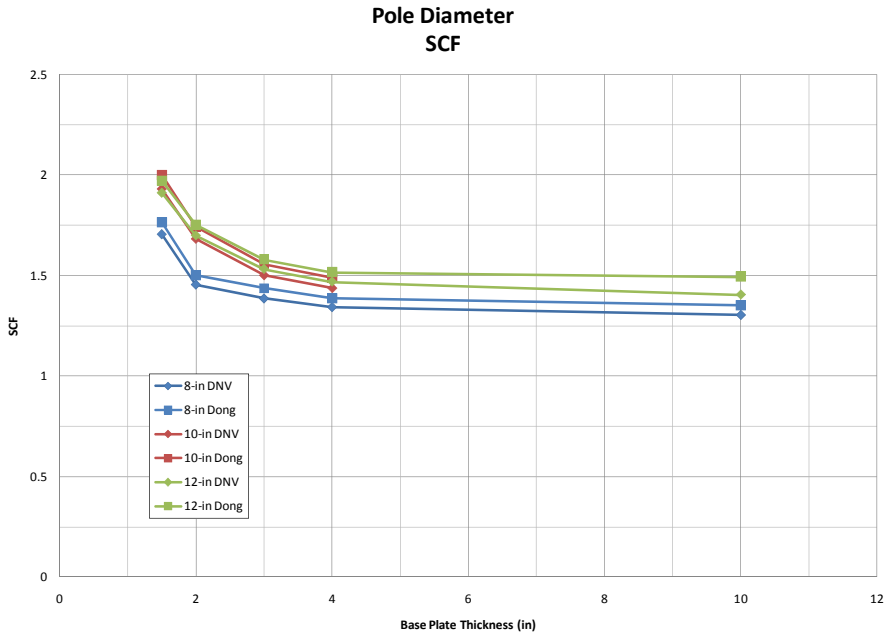

Figure 6-7: Pole Diameter Study (SCF versus Base Plate Thickness)

It is important to note that for the same applied moment, the stresses will vary for different diameter pole due to the change in moment of inertia. This is seen in Figure 6-6, where the hot spot stress is reduced in the larger diameter poles for the same applied bending moment. The SCF shown in Figure 6-7 does not significantly change with pole diameter, indicating that the diameter of the pole does not play a large role in the localized bending in the pole wall. There may be a small decrease in SCF in an 8-in diameter pole; however, this is at most a 10% reduction for a 1.5-in base plate in the SCF and could be conservatively ignored.

6.3.3 Pole Shape

A study of the effect of the shape of the pole was performed by comparing round and octagonal poles. A round pole was compared to octagonal poles with longitudinal bend radii of 3/8-in and

2-in. A cross section of the octagonal pole shape studied is shown in Figure 6-8. A survey of manufacturers indicated that the longitudinal bend radius of non – round poles (octagonal for mast arms) was not controlled during fabrication. Octagonal mast arms received for the experimental study had longitudinal bend radii of approximately 3/8-in. A 2-in radius was studied as an intermediate between the sharper bends of the samples received and a round pole. The results of the study are presented in Figure 6-9.

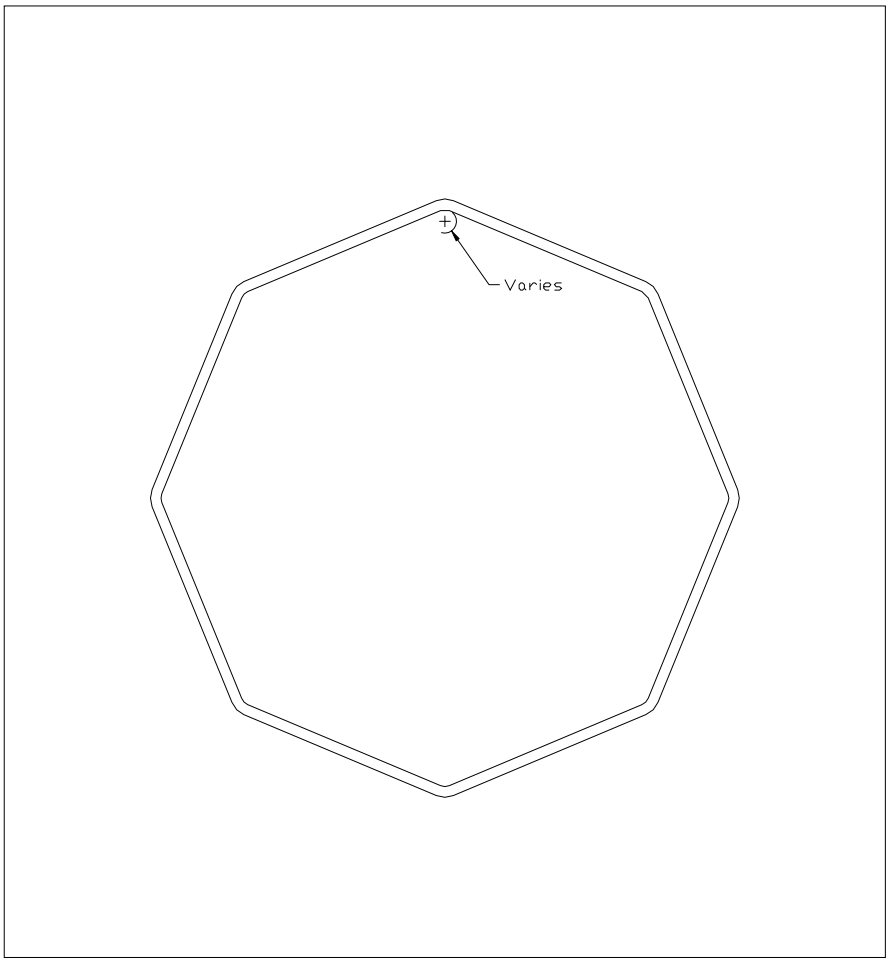

Figure 6-8: Typical Cross Section of Octagonal Pole

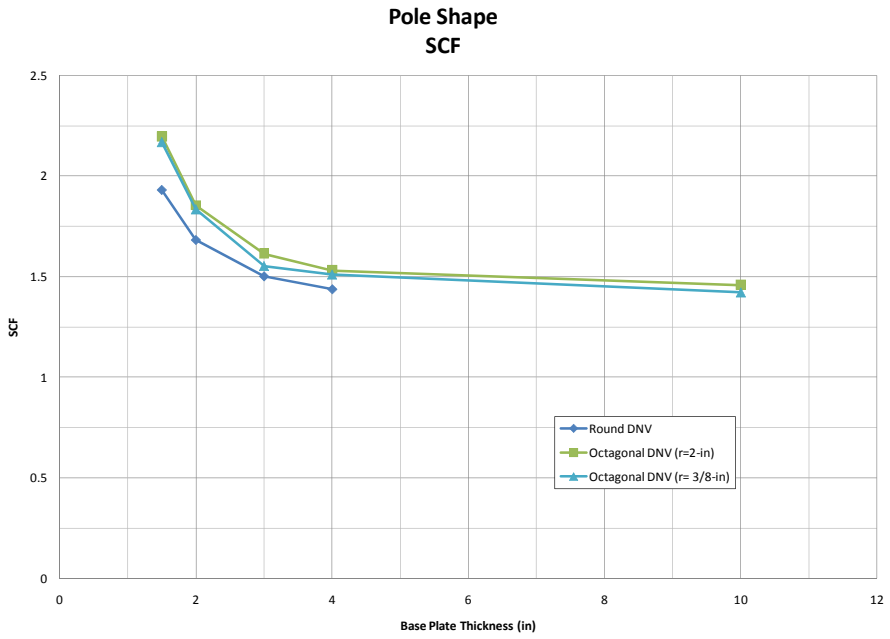

Figure 6-9: Pole Shape Study (SCF versus Base Plate Thickness)

Pole shape was found to have a small effect on the SCF. The difference is more pronounced at thinner base plates and at most amounts to a 12% increase in the stress concentration factor from the round mast arm. At 2-in and 3-in, the base plates studied experimentally, the change in shape results in a 7.1% and 3.3% increase, respectively. This slight increase in the stress concentration factor may have been seen in the experimental data, when comparing the better performing round samples (10-3R-WY-VG and 10-3R-WY-UG) with an octagonal sample (10-3R-WY-PG). Both round samples achieved slightly better fatigue performance than the octagonal sample; however the difference in performance was not great and the three mast arms all performed in the same AASHTO Category.

There is no noticeable effect due to a change in interior bend radius in the octagonal poles.

The stress distribution in an octagonal sample with a 3/8-in bend radius is shown in Figure 6-10.

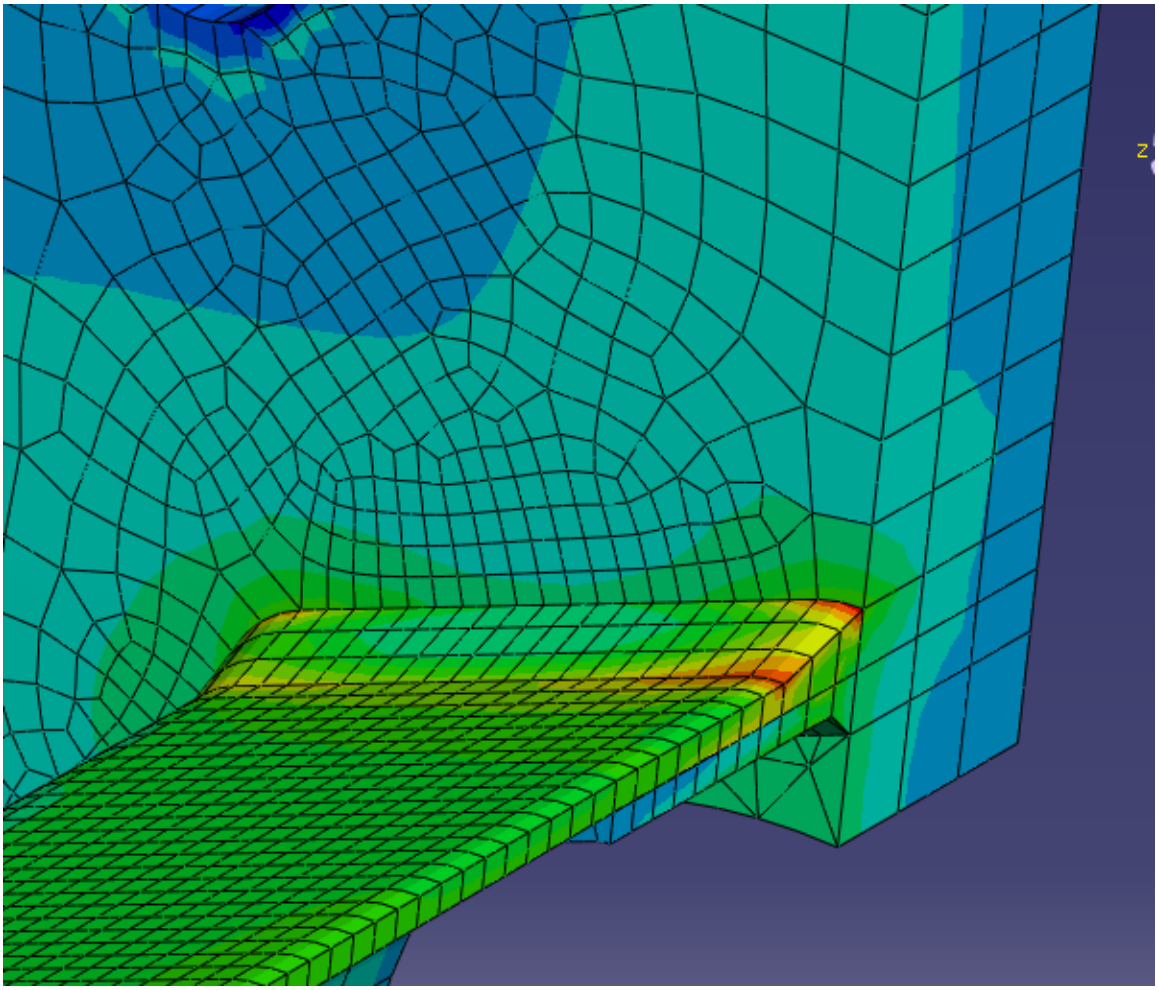

Figure 6-10: Stress Distribution of a Typical Octagonal Pole (10-1.5R-WY)

The corners of the octagonal pole are stiffer than the flat areas, and the stress accumulates at the corners. The slight increase in SCF in octagonal poles in relation to round poles is probably due to this effect.

6.3.4 Base Plate Geometry

A parametric study was performed to determine the effect of the base plate geometries tested in the experimental segment of this research. Across full penetration models with 10-in diameters and 2-in base plates, the base plate and bolt hole geometry was varied. In addition to the three geometries present in the experimental tests (*R*, *S*, and *SR*) models that had intermediate bolt patterns between *S* and *SR* were studied. The base plate geometries studied are shown in Figure 6-11. The results are plotted in Figure 6-12.

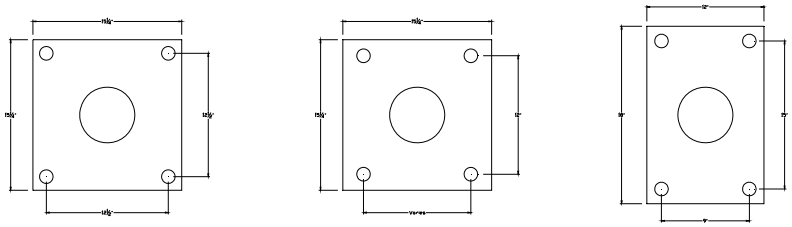

Figure 6-11: Base Plate Geometries Studied

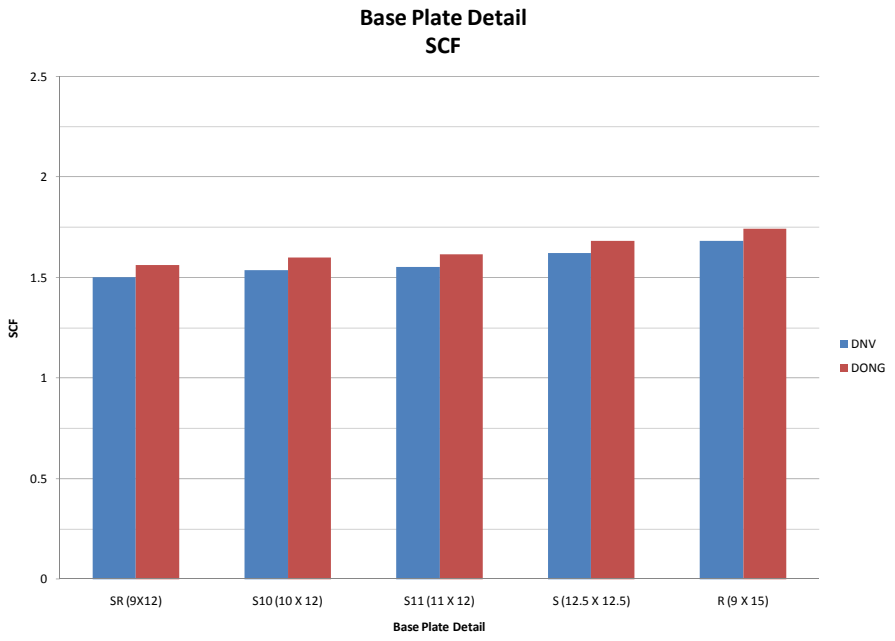

Figure 6-12: Base Plate Geometry Study (SCF)

The details all perform within 7% of the average. It is apparent that the SCF is influenced by the distance from the pole to the bolts. Also, the square details had slightly lower SCFs than the *R* detail. Both of these effects are small and do not influence the SCF to a great extent.

6.3.5 Size of the Base Plate Hole in a Full Penetration Connection

The hole in the base plate was varied for a 12-in diameter full penetration detail. Diameters of the hole that were studied were 9.64-in (the size of the hole for a 12-in Wyoming detail), 6-in, and 0-in (no hole). The results are presented in Figure 6-13.

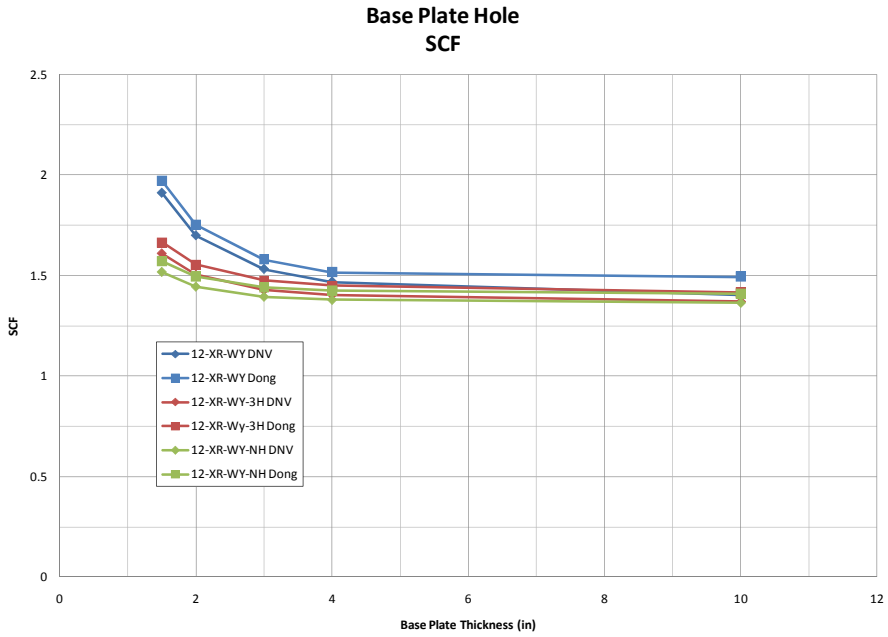

Figure 6-13: Base Plate Hole Study (SCF versus Base Plate Thickness)

Reducing the size of the hole in the base plate reduces the SCF at the weld toe. A larger hole in the base plate will reduce the base plate stiffness, since the presence of a hole reduces the moment of inertia of the base plate, in the direction of the moment. This effect is most pronounced in models with smaller base plate thicknesses. The effect of hole size diminishes as the base plate thickness increases.

6.3.6 Base Plate Stiffness

The local bending in the pole which results in high stress concentrations is due to bending of the base plate. As seen in the base plate thickness study, the stiffness of the base plate contributes a great deal to the magnitude of the stress concentration factor. Quantifying the actual stiffness of

the base plate is complicated, due to the complex geometries of the connections, presence of a hole in the base plate, and the three – dimensional nature of bending in the system.

In order to simplify the quantification of base plate stiffness, the base plate was assumed to behave like a simply supported beam loaded with a force couple. The "beam" was assumed to span between the top two bolts and the bottom two bolts. Bending was assumed to only occur in one direction, about the same axis as the applied moment. In this approximation, the width of the beam, b, is the horizontal width of the base plate, the height of the beam, h, is the thickness of the base plate, and the span length, L, is the distance between the top and bottom bolts. Figure 6-14shows a diagram of the assumed behavior under loading.

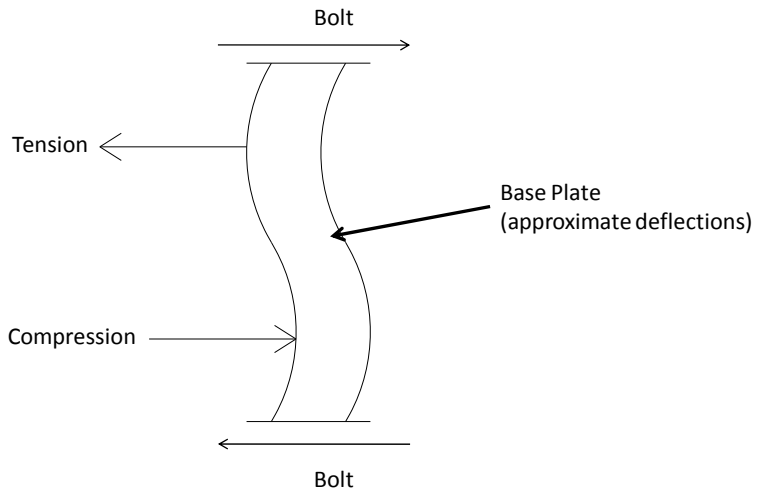

Figure 6-14: Approximate Behavior of Base Plate

In this case, the "stiffness" of the base plate is proportional to EI_B/L, where E is the modulus of elasticity (constant at 29,000-ksi), I_B is an average moment of inertia for the base plate that accounts for the reduction in stiffness due to the hole in the base plate, and L is the span length of the "beam" (the distance between the top and bottom bolts). Since E is constant, only I_B/L needs to be calculated. The moment of inertia of the base plate varies along the length, L. A simple way to account for the reduction in stiffness due to the hole in the base plate is to calculate the moment of inertia of the base plate through the center ($I = \frac{(b-d)h^3}{12}$) and average that with the moment of inertia of the base plate if there was no hole ($I = \frac{bh^3}{12}$).

The section that the moment of inertia will be calculated for is shown in Figure 6-15.

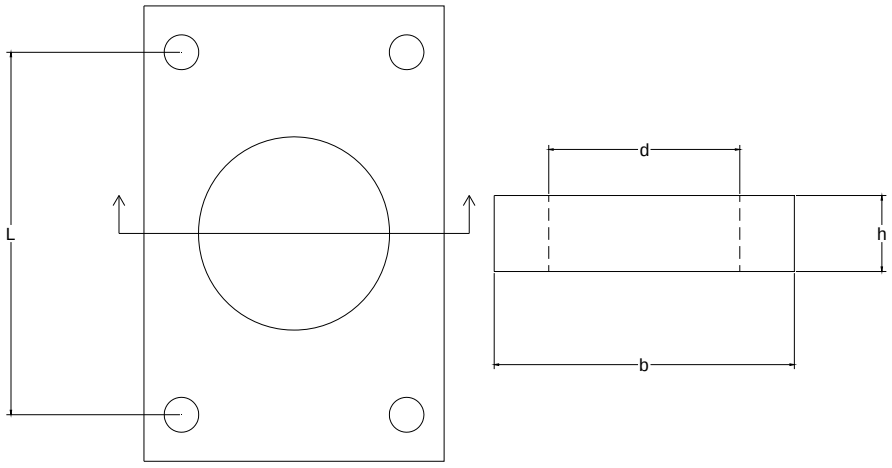

Figure 6-15: Base Plate Moment of Inertia is taken Through the Center of the Hole

Using the methods described above, values of the average moment of inertia were calculated for the full penetration models analyzed and were compared with the SCFs determined analytically. The results are presented in Table 6-3 and Figure 6-16. Figure 6-16 plots the flexibility of the base plate, L/I, the inverse of stiffness.

Model	B	Hole D	BP Thickness	L	MOI (Full)	MOI (Hole)	MOI (Average)	I/L	$(I/L)^{-1}$	SCF	
	(in)	(in)	(in)	(in)	(in^4)	(in^4)	(in^4)			DNV	Dong
8-XR-WY	12	5.64	1.5	15	3.375	1.789	2.582	0.172	5.810	1.706	1.765
	12	5.64	2	15	8.000	4.240	6.120	0.408	2.451	1.456	1.502
	12	5.64	3	15	27.000	14.310	20.655	1.377	0.726	1.387	1.437
	12	5.64	4	15	64.000	33.920	48.960	3.264	0.306	1.344	1.389
	12	5.64	10	15	1000.00	530.000	765.000	51.000	0.020	1.305	1.353
10-XR-WY	12	7.64	1.5	15	3.375	1.226	2.301	0.153	6.520	1.931	2.002
	12	7.64	2	15	8.000	2.907	5.453	0.364	2.751	1.683	1.744
	12	7.64	3	15	27.000	9.810	18.405	1.227	0.815	1.502	1.556
	12	7.64	4	15	64.000	23.253	43.627	2.908	0.344	1.438	1.490
	12	7.64	10	15	1000.00	363.333	681.667	45.444	0.022		
12-XR-WY	12	9.64	1.5	15	3.375	0.664	2.019	0.135	7.428	1.911	1.972
	12	9.64	2	15	8.000	1.573	4.787	0.319	3.134	1.699	1.753
	12	9.64	3	15	27.000	5.310	16.155	1.077	0.929	1.532	1.581
	12	9.64	4	15	64.000	12.587	38.293	2.553	0.392	1.469	1.516
	12	9.64	10	15	1000.00	196.667	598.333	39.889	0.025	1.405	1.494
12-XR-WY-3H	12	6	1.5	15	3.375	1.688	2.531	0.169	5.926	1.610	1.666
	12	6	2	15	8.000	4.000	6.000	0.400	2.500	1.504	1.555
	12	6	3	15	27.000	13.500	20.250	1.350	0.741	1.428	1.475
	12	6	4	15	64.000	32.000	48.000	3.200	0.313	1.405	1.450
	12	6	10	15	1000.00	500.000	750.000	50.000	0.020	1.372	1.417
12-XR-WY-NH	12	0	1.5	15	3.375	3.375	3.375	0.225	4.444	1.517	1.572
	12	0	2	15	8.000	8.000	8.000	0.533	1.875	1.445	1.495
	12	0	3	15	27.000	27.000	27.000	1.800	0.556	1.395	1.441
	12	0	4	15	64.000	64.000	64.000	4.267	0.234	1.380	1.425
	12	0	10	15	1000.00	1000.00	1000.000	66.667	0.015	1.365	1.410
10-2SR-WY	15.25	7.64	2	12	10.167	5.073	7.620	0.635	1.575	1.503	1.561
10-2S10-WY	15.25	7.64	2	12	10.167	5.073	7.620	0.635	1.575	1.536	1.601
10-2S11-WY	15.25	7.64	2	12	10.167	5.073	7.620	0.635	1.575	1.553	1.617
10-2S-WY	15.25	7.64	2	12.5	10.167	5.073	7.620	0.610	1.640	1.622	1.684
10-XR-WY-P2	12	7.64	1.5	15	3.375	1.226	2.301	0.153	6.520	2.198	2.209
	12	7.64	2	15	8.000	2.907	5.453	0.364	2.751	1.855	1.863
	12	7.64	3	15	27.000	9.810	18.405	1.227	0.815	1.615	1.621
	12	7.64	4	15	64.000	23.253	43.627	2.908	0.344	1.532	1.538
	12	7.64	10	15	1000.00	363.333	681.667	45.444	0.022	1.459	1.465
10-XR-WY-P3/8	12	7.64	1.5	15	3.375	1.226	2.301	0.153	6.520	2.169	2.249
	12	7.64	2	15	8.000	2.907	5.453	0.364	2.751	1.835	1.767
	12	7.64	3	15	27.000	9.810	18.405	1.227	0.815	1.554	1.444
	12	7.64	4	15	64.000	23.253	43.627	2.908	0.344	1.512	1.479
	12	7.64	10	15	1000.00	363.333	681.667	45.444	0.022	1.423	1.358

Table 6-3: Base Plate Stiffness and SCF

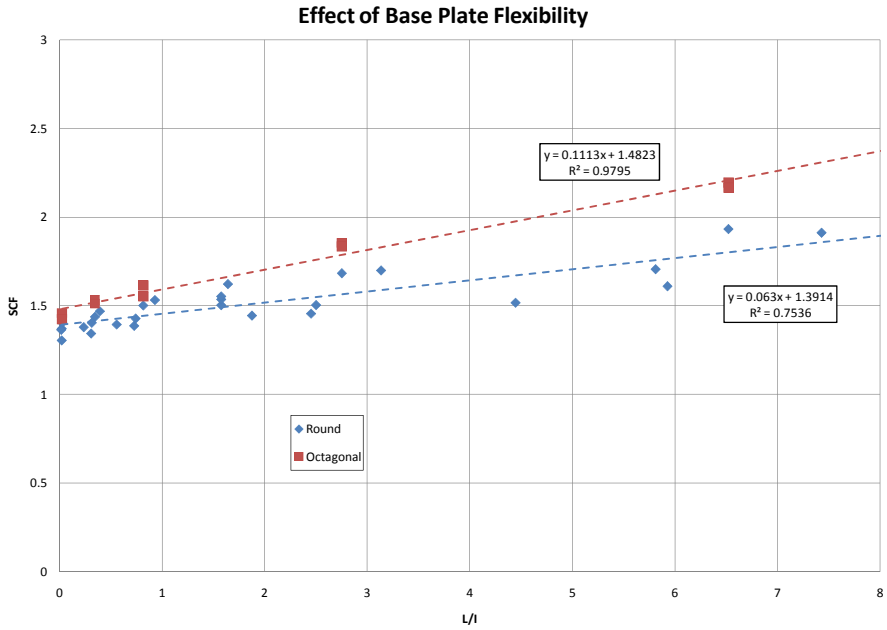

Figure 6-16: SCF versus Base Plate Flexibility (Constant Applied Moment)

The octagonal poles were separated from the round poles because of the difference in the way stress is distributed in the different pole shapes. The plot shows a linear correlation between flexibility of the base plate and the stress concentration factor for both round and octagonal poles. Another way to say this is that the SCF is inversely proportional to base plate stiffness. Trend lines were added using Excel. For round poles, excel produced the trend line: $SCF = 0.063\left(L/I\right) + 1.3914$. For round poles the R^2 value for this equation was 0.7536. For octagonal poles, excel produced the trend line: $SCF = 0.1113\left(L/I\right) + 1.4823$. The R^2 value for the octagonal pole trend line was 0.9795.

6.4 Failure Location

In the previous sections, the stress concentration occurred at the base plate full penetration weld. The stress concentration at that point was found to be highly influenced by the local bending in the pole due to the bending of the base plate. In the experimental tests, two types of details were tested that moved the failure location away from the base plate full penetration weld. These details are the full penetration weld with a fillet weld connecting the backing ring to the pole wall, and the external collar detail. Both details move the maximum stress concentration away from the base plate. In both connections the attachment stiffens the pole near the base plate weld and stress is split between two paths: the pole wall or the attachment (the collar or the backing ring), which reduces the stress concentration at the critical toe of the base plate weld.

6.4.1 Presence of Backing Ring Fillet Welds

The presence of a fillet weld connecting the top of the backing ring to the inside of the pole wall moved the failure location away from the base plate to the toe of that fillet weld in the experimental tests. The backing ring reduces the local bending near the weld toe and provides an extra path for stress to flow through the connection. The connection is shown in Figure 6-17.

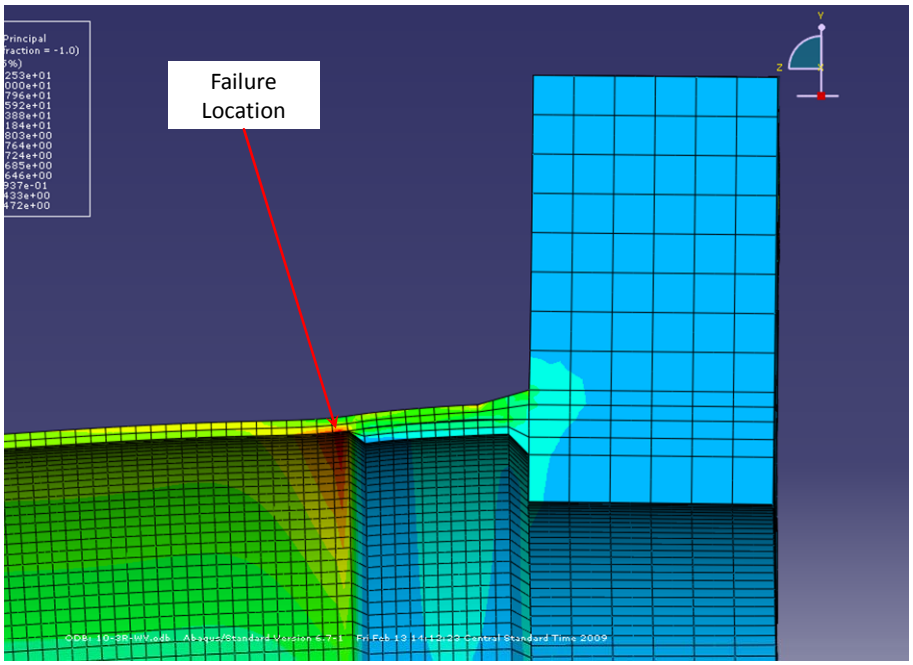

Figure 6-17: 10-3R-WY-FILLET Stress Distribution

A parametric study to determine the effect of base plate thickness on the stress concentration that occurs at the toe of the backing ring fillet weld was performed. The results for 10-XR-WY-FILLET are plotted in Figure 6-18.

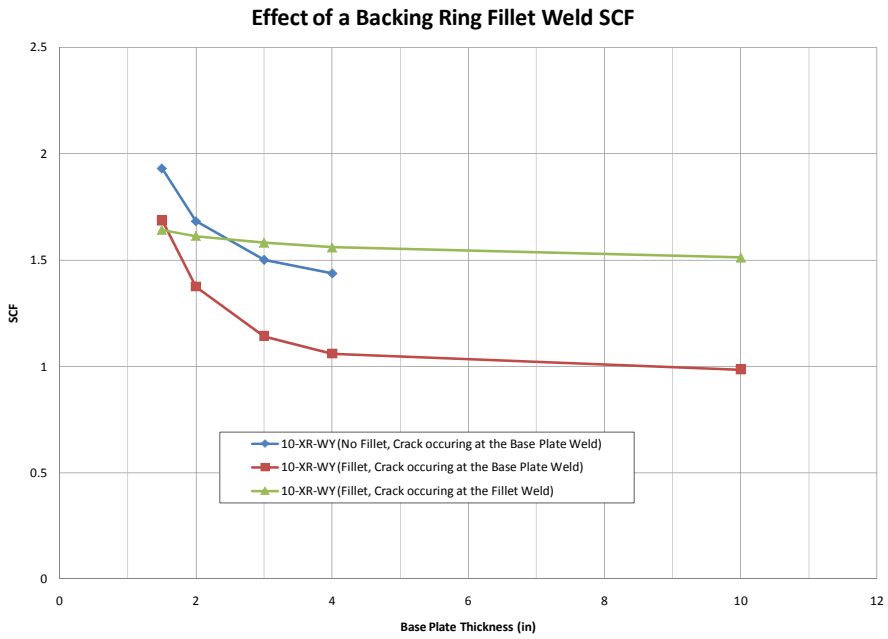

Figure 6-18: 10-XR-WY-FILLET (SCF versus Base Plate Thickness)

The results for 10-XR-WY are presented for comparison. The presence of a fillet weld reduces the stress concentration at the base plate weld. The fillet weld at the top of the backing ring acts to stiffen the connection and reduce the local bending that produces high stress concentrations. However, the stress concentration that occurs at the toe of the fillet weld is not affected to the same extent by increasing the base plate thickness, effectively staying constant across the variation of base plate thickness. At base plate thicknesses greater than 2-in, the SCF at the fillet weld at the end of the backing bar are greater than that at the base plate weld indicating that failure will occur at the end of the backing bar with thinner base plates.

6.4.2 External Collar Base Plate Study

A 12-XS-EC detail was studied and results are shown in Figure 6-19.

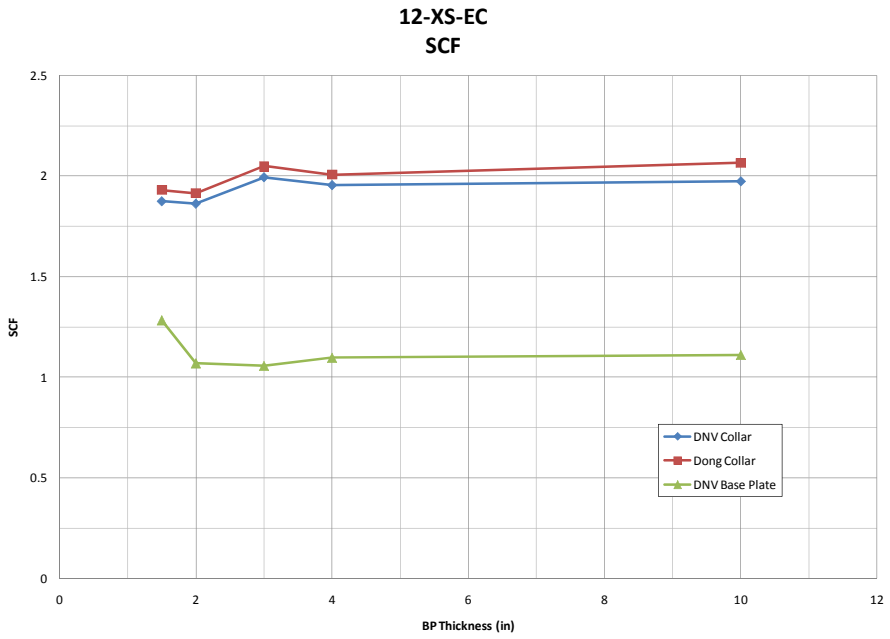

Figure 6-19: 12-XS-EC (SCF versus Base Plate Thickness)

The critical stress concentration (and where the fatigue crack would initiate) occurs at the fillet weld connecting the top of the collar to the pole wall. Increasing the base plate thickness has no significant effect on the SCF at this location. The local bending in the pole wall caused by the flexibility of the base plate largely occurs close to the base plate, far from the collar weld, and is spread between the collar and the pole wall.

An increase in base plate thickness does effect the stress concentration at the base plate weld toe, but this is not as critical as the collar weld. In the external collar detail studied, the stress flows

both through the collar and the pole wall and as such neither the collar nor the pole wall has as significant of a stress concentration as the fillet weld at the collar.

A comparison of the SCF values of 12-XS-EC and 12-XR-WY is given in Figure 6-20. The SCF of the 12-in external collar studied is comparable to the 12-in full penetration detail only at a 1.5-in base plate. At larger thickness base plates the increased stiffness of the base plate reduces the full penetration SCF. The SCF of the full penetration detail is about 23% less than the external collar detail at a base plate of 3-in.

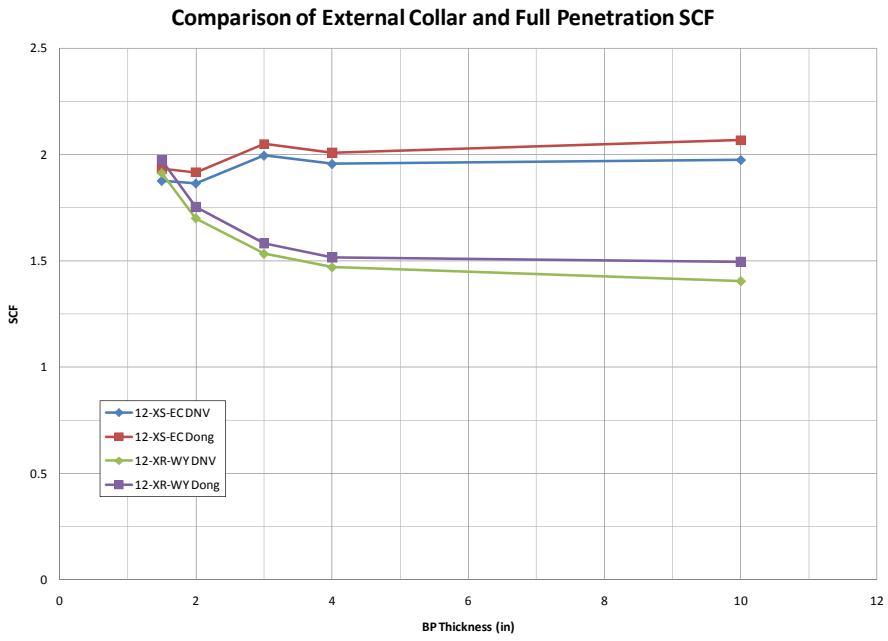

Figure 6-20: Comparison of External Collar and Full Penetration SCF

The stress in an external collar under load for two different base plate thicknesses can be seen in Figure 6-21 and Figure 6-22. Although there is a reduction of the stress concentration at the base plate weld when a 3-in base plate is used relative to a 1.5 in. base plate, there is no change in the stress concentration at the toe of the collar weld with this change in base plate thickness.

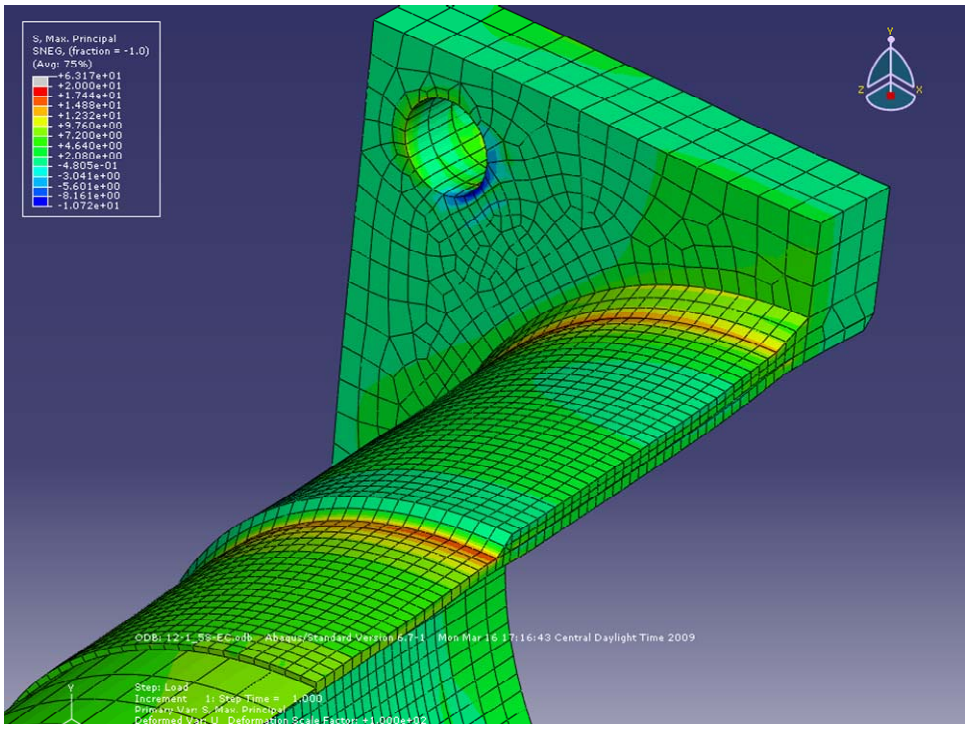

Figure 6-21: 12-1.5S-EC Stress Distribution

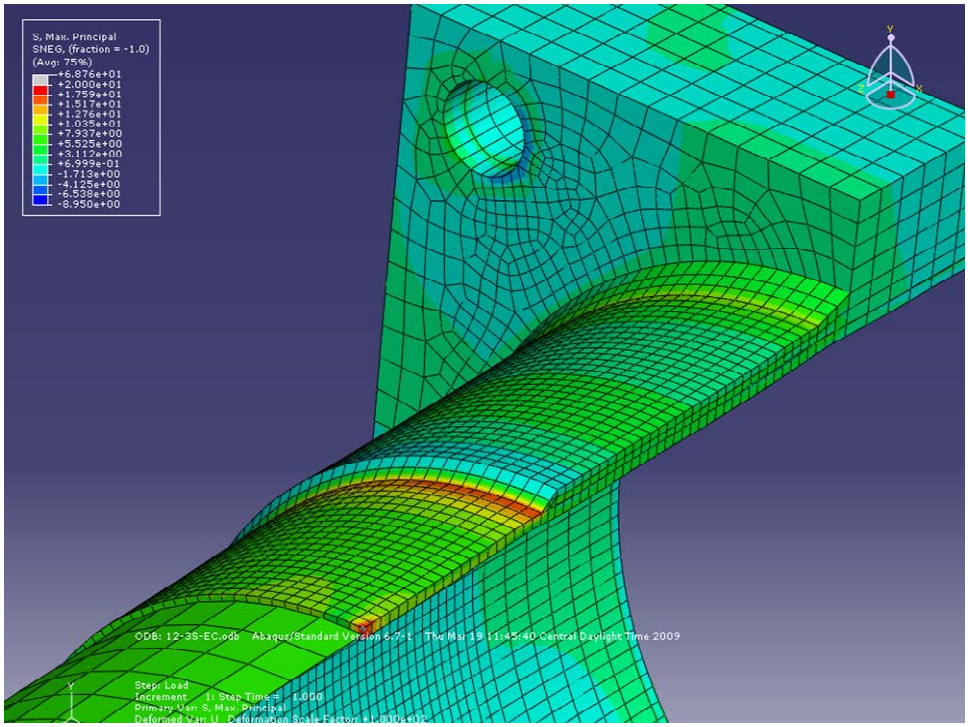

Figure 6-22: 12-3S-EC Stress Distribution

6.4.3 Effect of Base Plate Stiffness on SCF for Hot Spots Away From Base Plate

The base plate stiffness for the external collar and backing ring fillet models was calculated as before and compared to the controlling SCF determined from analysis. The results are presented in Table 6-4 and Figure 6-23.

Model	B	Hole D	BP Thickness	L	MOI (Full)	MOI (Hole)	MOI (Average)	I/L	$(I/L)^{-1}$	SCF	
		Diameter			(Full)	(Hole)	(Average)			DNV	Dong
10-XR-WY-F	12	7.64	1.5	15	3.375	1.226	2.301	0.153	6.520	1.642	1.508
	12	7.64	2	15	8.000	2.907	5.453	0.364	2.751	1.613	1.542
	12	7.64	3	15	27.00	9.810	18.405	1.227	0.815	1.583	1.342
	12	7.64	4	15	64.00	23.253	43.627	2.908	0.344	1.560	0.792
	12	7.64	10	15	1000	363.333	681.667	45.444	0.022	1.513	0.793
12-XS-EC	15.25	12	1.5	12.5	4.289	0.914	2.602	0.208	4.805	1.876	1.932
	15.25	12	2	12.5	10.17	2.167	6.167	0.493	2.027	1.863	1.916
	15.25	12	3	12.5	34.31	7.313	20.813	1.665	0.601	1.995	2.049
	15.25	12	4	12.5	81.33	17.333	49.333	3.947	0.253	1.955	2.008
	15.25	12	10	12.5	1270.8	270.833	770.833	61.667	0.016	1.974	2.066

Table 6-4: Base Plate Stiffness and SCF for External Collar and Full Penetration with Backing Ring Fillet

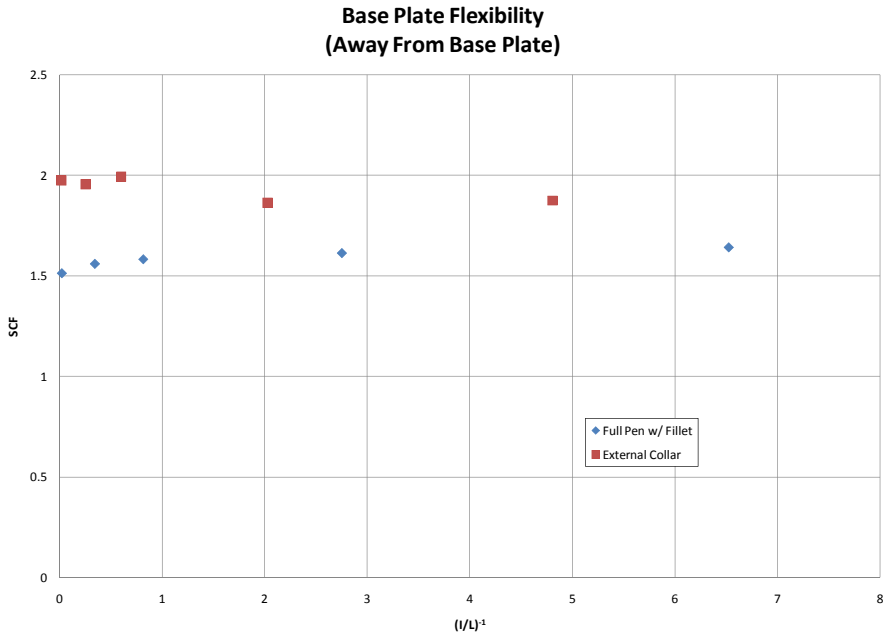

Figure 6-23: SCF versus Base Plate Flexibility for External Collar and Full Penetration with Fillet at Top of Backing Bar

Figure X shows no discernible trend between base plate flexibility and SCF for either 10-XS-EC or 10-XR-WY-FILLET.

6.5 Evaluation of Fatigue Life Using Hot Spot Stress

The experimental results in Chapter 4 were reported in terms of nominal stress range. The actual failures occurred at hot spots where the stress range was higher than the nominal stress due to a change in geometry and local bending in the pole wall. The reported experimental nominal stresses of the specimens can be multiplied by SCFs from analytical models with comparable geometries. Reporting fatigue data in this manner presents the micro behavior at discontinuities in the weld. For samples with welds of comparable quality, the data should collapse into a single AASHTO Category.

This was done for specimens that had corresponding analytical models. A table of all of the specimens that had analytical counterparts is shown in Table 6-5.

Specimen Code	S_r (ksi)	DNV SCF	$S_{hot\ spot}$ (ksi)	$N_{failure}$	A	Category	Crack Location	Backing Bar Weld Type
10-2S-WY-VG-A	12	1.62	19.44	**12,602,940**	**9.259E+10**	A	N/A	None
10-2S-WY-VG-B	12	1.62	19.44	**12,602,940**	**9.259E+10**	A	N/A	None
12-2S-EC-VG-A	18	1.86	33.48	**805,991**	**3.025E+10**	A	N/A	N/A
12-2S-EC-VG-B	18	1.86	33.48	468,601	1.759E+10	B	Collar	N/A
12-2S-EC-VG-B (flip)	18	1.86	33.48	337,390	1.266E+10	B	Collar	N/A
10-3R-WY-VG-A	18	1.5	27	**8,037,420**	**1.582E+11**	A	N/A	
10-3R-WY-VG-B	18	1.5	27	**8,037,420**	**1.582E+11**	A	N/A	
10-3R-WY-VG-A	24	1.5	36	439,511	2.051E+10	B	Weld Toe	None
10-3R-WY-VG-B	24	1.5	36	343,175	1.601E+10	B	Weld Toe	None
10-3R-WY-VP-A	24	1.5	36	**10,055,123**	**4.691E+11**	A	N/A	None
10-3R-WY-VP-B	24	1.5	36	**10,055,123**	**4.691E+11**	A	N/A	None
10-3R-WY-VB-A	19.07	1.5	28.605	2,232,742	5.226E+10	A	Weld Toe	None
10-3R-WY-VB-A (flip)	24	1.5	36	490,061	2.286E+10	B	Weld Toe	None
10-3R-WY-VB-B	21.14	1.5	31.71	3,516,775	1.121E+11	A	Shaft*	None
Ameron A	24	1.5	36	222,649	1.039E+10	C	Weld Toe	None
Ameron A (flip)	24	1.5	36	212,891	9.933E+09	C	Weld Toe	None
Union Metal A	24	1.5	36	1,873,499	8.741E+10	A	Weld Toe	None
ZZ88734-A	24	1.58	37.92	677,763	3.696E+10	A	Backing	Fillet
ZZ88734-B	24	1.58	37.92	633,458	3.454E+10	A	Backing	Fillet
ZZ88735-A	28	1.58	44.24	286,526	2.481E+10	B	Backing	Fillet
ZZ88735-B	28	1.58	44.24	123,072	1.066E+10	C	Backing	Fillet
ZZ88735-B (flip)	28	1.58	44.24	129,090	1.118E+10	C	Backing	Fillet
10-2SR-WY-VG-A	12	1.5	18	**9,881,390**	**5.763E+10**	A	Weld Toe	
10-2SR-WY-VG-B	12	1.5	18	3,051,996	1.780E+10	B	N/A	
10-3R-WY-PG-A	24	1.55	37.2	1,272,665	6.552E+10	A	Weld Toe	Tack
10-3R-WY-PG-B	24	1.55	37.2	1,210,499	6.232E+10	A	Backing Bar	Tack

Table 6-5: Fatigue Life and Hot Spot Stress Range

The data for specimens with corresponding analytical models is reported in Figure 6-24.

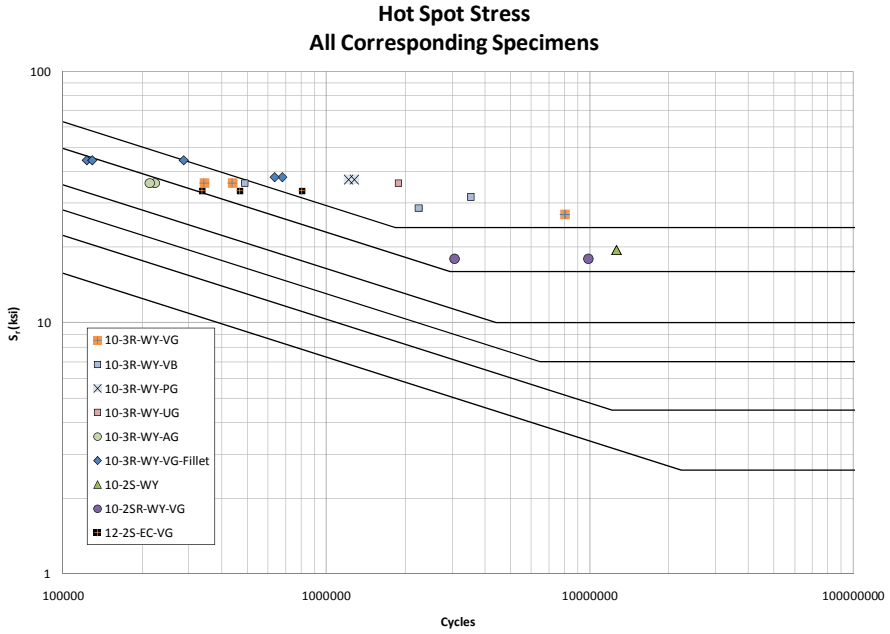

Figure 6-24: Fatigue Life Plotted Against Hot Spot Stress Range

For welded joints, a Category B represents full penetration welds connecting two equal size plates and is the best performance usable in design. In general the data lies somewhere between a Category B and a Category A, which indicates good quality to exceptional quality welds on the mast arms.

Two of the full penetration details that had fillet welds performed at a Category B, and two performed to a Category C. This variability is expected since the fillet weld on the top of the backing ring is basically a blind weld. Generally, load carrying fillet welds are given a Category C designation.

The 10-3R-WY specimens in general perform very well, with the exception of the two tests from Ameron, which performed at the level of a Category C detail. This suggests poor weld quality in the Ameron specimens.

The peened samples performed the best of all the specimens tested. In general the black specimens performed better than galvanized specimens, although one galvanized specimen ran out at a hot spot stress range of 27-ksi, which is very close to the hot spot stress ranges that the black samples experienced (28.6-ksi – 36-ksi).

The specimens with 2-in base plates, two full penetration details and an external collar, collapsed into a Category B, indicating that the quality of the welds in the different samples was similar.

As stated in Chapter 5, an approximation was made when modeling the bolts that the base plate attaches to. The bolts were modeled by fixing the edges of the bolt holes. This boundary condition resulted in slightly high reported SCF values. The actual stress that occurred was somewhat lower than what is reported. The same assumptions were made across all models, and the relative performance would be the same.

6.6 Summary of Results of Parametric Studies

- Stress concentrations at points very near to the base plate are highly influenced by local bending in the pole due to the flexibility of the base plate. This local bending affects the full penetration weld in Wyoming details and the base plate weld in external collar details. For welds far enough away from the base plate, like collar welds, the base plate stiffness does not affect the SCF.
- In this phase of the research, the base plates of external collars were relatively stiff, and the collar weld SCF controlled fatigue performance. The parametric study of external

collar SCF implied that if base plate stiffness was small enough, the SCF at the base plate weld of external collar details may be high enough to control fatigue performance. This was seen in concurrent research at the University of Texas at Austin, where high masts (very large mast arms) were tested. High mast external collars with stiffer base plates failed at the collar weld, while high masts with more flexible base plates failed at the base plate weld. (Stam 2009).

- For a full penetration details, the controlling stress concentration is at the toe of the weld connecting the pole to the base plate. The SCF is directly proportional to the flexibility of the base plate.
- For full penetration details, the base plate thickness affects the stress concentration factor more than any other variable. This is reasonable, since the moment of inertia of the base plate is proportional to the cube of the thickness.
- Other variables that affected the stress concentration factor in full penetration details were base plate geometry, the size of the hole in the base plate, the shape of the pole, and possibly the diameter of the pole, but these were smaller effects than the base plate thickness.
- In the external collar detail and the full penetration detail with a fillet weld at the top of the backing ring, the failure location moved away from the base plate to the fillet weld connecting the backing bar or collar. The pole near to the base plate was stiffened by the backup bar. The maximum stress concentration occurred at the toe of the weld connecting the collar or backing ring to the pole wall. There was no or little relationship between base plate thickness and this stress concentration. The comparison of base plate stiffness and SCF for these details shows no trend.

- At small base plate thickness, the external collar detail and full penetration detail perform comparably. As the base plate thickness is increased, the SCF of the full penetration detail is reduced but the SCF of the external collar detail remains the same. The effect of base plate stiffness on full penetration SCF can be used to size a full penetration mast arm to attain better fatigue performance than an external collar detail.

Chapter 7

Conclusions and Recommended Research

7.1 Conclusions

Based on the experimental testing and analytical studies, the following conclusions can be made:

- Full penetration, full penetration details with fillet welds at the top of the backing ring, and external collar details can achieve better fatigue performance compared to the socket details that that were previously studied at the University of Texas at Austin
- The critical stress concentration factor (SCF) for full penetration details is directly proportional to the flexibility of the base plate. The flexibility of the base plate is defined as the inverse of the stiffness of the base plate which is proportional to $\frac{bh^3}{12}\frac{1}{L}$, where b is the width of the base plate, L is the distance from the top bolts to the bottom bolts, and h is the thickness of the base plate. The thickness of the base plate plays a major role in the fatigue performance of a full penetration connection.
- Introducing a change in the connection geometry away from the base plate (i.e. an external collar, or a fillet weld at the top of the backing ring) moves the hot spot stress away from the base plate and reduces the dependence of fatigue life on base plate stiffness. The addition of some sort of collar to the pole near the base plate stiffens the pole and reduces the local bending that causes high SCFs near the base plate, but the fillet weld at the top of the collar introduces a new SCF that is not dependent on the base plate thickness. The parametric studies that were conducted indicate that for flexible enough base plates, the SCF at the base plate weld will become high enough to control the fatigue behavior.

- Because of the reduction of SCF possible in full penetration details due to an increase in the base plate stiffness, a full penetration detail can achieve lower SCFs than a comparable external collar detail. This will translate to the full penetration details achieving better fatigue performance.
- The shape of the pole (round or octagonal) affects the SCF to a small degree. The longitudinal bends of an octagonal pole are stiffer than the flat portions and act as sinks for the stress. There was no discernible change in the fatigue performance of the round and octagonal full penetration poles tested.
- No significant difference was found in the fatigue performance of full penetration details with 10-in and 12-in poles. Full penetration details with8-in poles may perform slightly better, but the difference in performance was minor and it can be conservatively assumed that 8-in full penetration details perform at the same level as 10-in and 12-in full penetration details.
- Peening the base plate weld on a full penetration detail greatly improves the fatigue life of the specimen.
- The presence of a tack weld on the backing ring of a full penetration detail may or may not affect the fatigue performance. Several variables come in to play, including the position of the tack weld relative to the tension stress and the quality of the weld. This variability made it impossible to predict whether the mast arm would fail at the tack weld or not.

7.2 Recommendations for Future Research

- This phase of research studied a large amount of variables, and in many cases no comparison could be made between different specimens due to multiple differences

between the specimens. It is recommended that further studies limit their scope in order to achieve a large sample size of comparable specimens.

- Analytical studies indicated that the fatigue performance of external collar details was not related to base plate stiffness. This resulted in the full penetration detail being able to achieve lower SCFs and therefore better fatigue performance, simply by increasing the base plate thickness. A study of the effect of base plate stiffness (mainly in the form of base plate thickness) on external collar fatigue performance is recommended.
- It is necessary to seal off the top of the backing ring to moisture, since zinc does not penetrate the space between the backing ring and the pole during the galvanization process. The Wyoming Detail calls for a field caulk to be applied after galvanization. Another option is to connect the top of the backing ring to the inside of the pole with a fillet weld. The full penetration details with fillet welds at the top of the backing ring that were tested in the research presented in this thesis performed at the level of an AASHTO Category C, which is an improvement the socket details that were previously tested by Anderson and Koenigs. These details may be a viable alternative to a field caulk. A study of the performance of full penetration details with backing ring fillet weld is recommended.

7.3 Recommendations for Design of Mast Arm Structures

- The base plate thickness of a mast arm should be as large as possible, preferably 3-in. Much of the cost of fabrication is due to welding of the mast arm, and using a thicker base plate is a cheap way to improve the fatigue life.
- The thickest base plates on socket connections tested at the University of Texas at Austin were 3-in. These mast arms performed at the level of a Category D (Anderson 2007). Full penetration details and external collar details can be used to improve the fatigue life.

- If a higher performance connection detail is desired, the full penetration detail with no weld at the top of the backing ring (Wyoming Detail) should be used. The external collar detail cannot take advantage of an increase in base plate stiffness, whereas the full penetration Wyoming detail can be paired with a thick base plate to significantly improve fatigue life.

Appendix A

Measured Dimensions of Specimens

The measured dimensions of all specimens are given in Tables A-1 and A-2. Several specimens were unintentionally cut or disposed of before dimensions could be measured. Dimensions that were not available are marked as "not available" or "NA".

Measured General Dimensions:

Full Penetration	Length	Base Plate Thickness				Pole Wall Thickness				Outside Pole Diameter at Base								
Specimen										Round			Octagonal Flat to Flat			Octagonal Corner to Corner		
		1	2	3	Average	1	2	3	Average	1	2	Average	1	2	Average	1	2	Average
10-2S-WY-PB-A	86.688	2.035	2.028	2.035	2.033	0.192	0.194	0.190	0.192				9.750	10.000	9.875			
10-2S-WY-PB-B	86.688	2.035	2.030	2.035	2.033	0.190	0.190	0.183	0.188				9.188	10.000	9.594			
10-2S-WY-VG-A	86.688	2.016	2.012	2.014	2.014	0.195	0.183	0.190	0.189	10.000	9.938	9.969						
10-2S-WY-VG-B	86.625	2.014	2.016	2.031	2.020	0.186	0.186	0.185	0.186	10.000	10.000	10.000						
8-2S-WY-VG-A	86.625	2.016	2.017	2.008	2.014	0.170	0.168	0.170	0.169	8.000	7.938	7.969						
8-2S-WY-VG-B	86.625			2.017	2.017	0.163	0.166	0.168	0.166	8.000	7.938	7.969						
12-2S-WY-VG-A	86.000	2.058	2.058	1.988	2.035	0.174	0.179	0.176	0.176	12.063	11.875	11.969						
12-2S-WY-VG-B	85.938	2.055	1.989	2.010	2.018	0.178	0.179	0.177	0.178	12.000	11.875	11.938						
10-3R-WY-VG-A	86.688	3.025	3.024	3.027	3.025	0.177	0.175	0.174	0.175	9.938	9.938	9.938						
10-3R-WY-VG-B	86.750	3.021	3.019	3.025	3.022	0.176	0.170	0.175	0.174	9.938	9.875	9.906						
10-3R-WY-VP-A	86.688	3.025	3.014	3.025	3.021	0.177	0.178	0.177	0.177	9.938	9.938	9.938						
10-3R-WY-VP-B	86.688	3.007	3.007	3.016	3.010	0.177	0.178	0.176	0.177	10.000	9.938	9.969						
10-3R-WY-VB-A	86.750	2.994	2.990	2.992	2.992	0.182	0.179	0.176	0.179	9.938	9.938	9.938						
10-3R-WY-VB-B	86.750	2.992	2.997	2.990	2.993	0.175	0.176	0.178	0.176	10.000	10.000	10.000						
10-3R-WY-AG	86.750	3.030	3.030	3.050	3.037	NA	NA	NA	NA	10.000	10.000	10.000						
10-3R-WY-UG	86.875	3.050	3.055	3.040	3.048	NA	NA	NA	NA	9.938	10.000	9.969						
ZZ88734-A	86.500	3.000	3.000	3.000	3.000	NA	NA	NA	NA	9.938		9.938						
ZZ88734-B	NA	NA	NA	NA	NA	NA	NA	NA	NA	NA	NA	NA						
ZZ88735-A	NA	3.063	3.063	3.000	3.042	NA	NA	NA	NA	NA	NA	NA						
ZZ88735-B	NA	NA	NA	NA	NA	NA	NA	NA	NA	NA	NA	NA						
10-2SR-WY-VG-A	86.625	2.000	2.000	1.938	1.979	NA	NA	NA	NA	9.938	9.938	9.938						
10-2SR-WY-VG-B	86.625	2.000	2.000	2.000	2.000	NA	NA	NA	NA	10.000	9.938	9.969						
10-3R-WY-PG-A	86.313	3.000	3.000	3.000	3.000	0.196	0.196	0.198	0.197				9.375	9.250	9.313	10.000	9.938	9.969
10-3R-WY-VG-B	86.750	3.000	3.000	3.000	3.000	0.193	0.196	0.198	0.196				9.250	9.188	9.219	9.938	9.938	9.938
12-3R-WY-VG-A	86.813	3.000	3.000	3.000	3.000	0.196	0.199	0.196	0.197				11.000	11.063	11.031	11.938	11.875	11.906
12-3R-WY-VG-B	86.625	3.000	3.000	3.000	3.000	0.194	0.198	0.194	0.195				11.000	11.000	11.000	11.813	11.813	11.813

External Collar	Length	Base Plate Thickness				Pole Wall Thickness				Inside Pole Diameter at Base								
Specimen										Round			Octagonal Flat to Flat			Octagonal Corner to Corner		
		1	2	3	Average	1	2	3	Average	1	2	Average	1	2	Average	1	2	Average
8-2S-EC-VG-A	86.625	1.997	1.996	2.044	2.012	0.186	0.190	0.194	0.190	7.563	7.563	7.563						
8-2S-EC-VG-B	86.688	1.992	1.991	1.990	1.991	0.186	0.188	0.181	0.185	7.625	7.625	7.625						
12-2S-EC-VG-A	85.938	2.003	1.999	2.008	2.003	0.178	0.179	0.180	0.179	11.625	11.688	11.656						
12-2S-EC-VG-B	85.875	1.996	1.994	2.010	2.000	0.179	0.174	0.177	0.177	11.625	11.563	11.594						
10-2SR-EC-VG-A	Dimensions Not Available																	
10-2SR-EC-VG-B	Dimensions Not Available																	
10-2R-EC-PG-A	86.500	2.000	2.000	2.000	2.000	0.195	0.194	0.194	0.194				8.750	8.875	8.813	9.313	9.500	9.406
10-2R-EC-PG-B	86.625	2.000	2.000	2.000	2.000	0.196	0.198	0.198	0.197				8.813	8.750	8.781	9.500	9.375	9.438
12-2R-EC-PG-A	86.750	2.000	2.000	2.000	2.000	0.196	0.202	0.194	0.197				10.625	10.750	10.688	11.438	11.375	11.406
12-2R-EC-PG-B	86.750	2.000	2.000	2.000	2.000	0.198	0.196	0.202	0.199				10.750	10.625	10.688	11.500	11.375	11.438

External Collar	Collar Thickness				Collar Height		
Specimen							
	1	2	3	Average	1	2	Average
8-2S-EC-VG-A	0.238	0.235	0.239	0.237	4.063	4.125	4.094
8-2S-EC-VG-B	0.242	0.240	0.237	0.240	4.000	4.000	4.000
12-2S-EC-VG-A	0.240	0.242	0.239	0.240	6.000	6.000	6.000
12-2S-EC-VG-B	0.240	0.238	0.238	0.239	6.125	6.125	6.125
10-2SR-EC-VG-A	Dimensions Not Available						
10-2SR-EC-VG-B	Dimensions Not Available						
10-2R-EC-PG-A	0.454	0.483	0.490	0.476	5.500	5.750	5.625
10-2R-EC-PG-B	0.483	0.485	0.479	0.482	5.875	5.750	5.813
12-2R-EC-PG-A	0.492	0.476	0.474	0.481	4.875	4.875	4.875
12-2R-EC-PG-B	0.491	0.481	0.505	0.492	4.875	4.875	4.875

Table A-1: General Dimensions

Measured Weld Dimensions:

Full Penetration	Full Penetration Weld							
Specimen	Pole Wall				Base Plate			
	1	2	3	Average	1	2	3	Average
10-2S-WY-PB-A	0.563	0.625	0.563	0.583	0.250	0.250	0.250	0.250
10-2S-WY-PB-B	0.563	0.625	0.625	0.604	0.250	0.250	0.250	0.250
10-2S-WY-VG-A	0.750	0.688	0.688	0.708	0.406	0.375	0.344	0.375
10-2S-WY-VG-B	0.625	0.813	0.750	0.729	0.313	0.438	0.438	0.396
8-2S-WY-VG-A	0.438	0.438	0.438	0.438	0.813	0.875	0.813	0.833
8-2S-WY-VG-B	0.438	0.438	0.438	0.438	0.813	0.875	0.875	0.854
12-2S-WY-VG-A	0.813	0.750	0.750	0.771	0.531	0.438	0.438	0.469
12-2S-WY-VG-B	0.813	0.813	0.813	0.813	0.500	0.438	0.438	0.458
10-3R-WY-VG-A	0.719	0.750	0.781	0.750	0.281	0.344	0.375	0.333
10-3R-WY-VG-B	0.750	0.750	0.719	0.740	0.281	0.344	0.281	0.302
10-3R-WY-VP-A	0.781	0.781	0.813	0.792	0.281	0.281	0.313	0.292
10-3R-WY-VP-B	0.719	0.750	0.781	0.750	0.313	0.344	0.375	0.344
10-3R-WY-VB-A	0.781	0.844		0.813	0.375	0.375		0.375
10-3R-WY-VB-B	0.813	0.688		0.750	0.281	0.344		0.313
10-3R-WY-AG	0.688	0.625		0.656	0.250	0.281		0.266
10-3R-WY-UG	0.469	0.531		0.500	0.313	0.313		0.313
ZZ88734-A	0.750	0.750		0.750	0.438			0.438
ZZ88734-B	Dimensions Not Available							
ZZ88735-A	0.813			0.813	0.625			0.625
ZZ88735-B	Dimensions Not Available							
10-2SR-WY-VG-A	0.750			0.750	0.375			0.375
10-2SR-WY-VG-B	0.688			0.688	0.375			0.375
10-3R-WY-PG-A	0.313	0.500		0.406	0.250	0.250		0.250
10-3R-WY-VG-B	0.625	0.563	0.500	0.563	0.250	0.250	0.250	0.250
12-3R-WY-VG-A	0.625	0.625	0.625	0.625	0.375	0.375	0.250	0.333
12-3R-WY-VG-B	0.688	0.625	0.625	0.646	0.375	0.375	0.313	0.354

External Collar	External Collar Base Plate Weld								External Collar Top Weld							
Specimen	Pole Wall				Base Plate				Pole Wall				Collar			
	1	2	3	Average	1	2	3	Average	1	2	3	Average	1	2	3	Average
8-2S-EC-VG-A	0.813	0.813	0.813	0.813	0.406	0.438	0.406	0.417	0.625	0.563	0.625	0.604	0.250	0.250	0.250	0.250
8-2S-EC-VG-B	0.750	0.688	0.750	0.729	0.313	0.375	0.313	0.333	0.563	0.625	0.563	0.583	0.188	0.313	0.188	0.229
12-2S-EC-VG-A	0.688	0.688	0.625	0.667	0.313	0.313	0.281	0.302	0.625	0.625	0.625	0.625	0.250	0.250	0.250	0.250
12-2S-EC-VG-B	0.750	0.813	0.875	0.813	0.438	0.500	0.469	0.469	0.625	0.500	0.563	0.563	0.250	0.281	0.250	0.260
10-2SR-EC-VG-A	Dimensions Unavailable															
10-2SR-EC-VG-B	Dimensions Unavailable															
10-2R-EC-PG-A	0.563	0.625	0.688	0.625	0.438	0.438	0.375	0.417	0.500	0.563	0.500	0.521	0.375	0.313	0.313	0.333
10-2R-EC-PG-B	0.688	0.563	0.625	0.625	0.313	0.250	0.313	0.292	0.563	0.500	0.500	0.521	0.375	0.375	0.375	0.375
12-2R-EC-PG-A	0.688	0.625	0.625	0.646	0.313	0.313	0.313	0.313	0.500	0.500	0.563	0.521	0.375	0.313	0.313	0.333
12-2R-EC-PG-B	0.625	0.688	0.625	0.646	0.375	0.375	0.250	0.333	0.438	0.500	0.500	0.479	0.375	0.375	0.313	0.354

Table A-2: Measured Weld Dimensions

Appendix B

Summary of Results from Experimental and Analytical Research

Experimental Test Results:

Specimen Code	S_r	$N_{failure}$	A	Category	Crack Location	Backing Bar Weld Type
10-2S-WY-PB-A	12	6,734,487	1.164E+10	C	Weld Toe	Fillet
10-2S-WY-PB-B	12	5,219,304	9.019E+09	C	Weld Toe	Fillet
10-2S-WY-VG-A	12	**12,602,940**	**2.178E+10**	**B**	N/A	None
10-2S-WY-VG-B	12	**12,602,940**	**2.178E+10**	**B**	N/A	None
8-2S-WY-VG-A	12	**12,464,800**	**2.154E+10**	**B**	Weld Toe	Tack
8-2S-WY-VG-B	12	**12,464,800**	**2.154E+10**	**B**	Weld Toe	Tack
8-2S-WY-VG-A	24	856,122	1.184E+10	C	Backing	Tack
8-2S-WY-VG-A (flip)	24	747,510	1.033E+10	C	Weld Toe	Tack
8-2S-WY-VG-B	24	**1,603,632**	**2.217E+10**	**B**	N/A	Tack
8-2S-EC-VG-A	18	512,860	2.991E+09	D	Collar	N/A
8-2S-EC-VG-B	18	653,208	3.810E+09	D	Collar	N/A
12-2S-WY-VG-A	18	1,053,554	6.144E+09	C	Weld Toe	Tack
12-2S-WY-VG-B	18	880,807	5.137E+09	C	Weld Toe	Tack
12-2S-EC-VG-A	18	**805,991**	**4.701E+09**	**C**	N/A	N/A
12-2S-EC-VG-B	18	468,601	2.733E+09	D	Collar	N/A
12-2S-EC-VG-B (flip)	18	337,390	1.968E+09	E	Collar	N/A
10-3R-WY-VG-A	18	**8,037,420**	**4.687E+10**	**A**	N/A	
10-3R-WY-VG-B	18	**8,037,420**	**4.687E+10**	**A**	N/A	
10-3R-WY-VG-A	24	439,511	6.076E+09	C	Weld Toe	None
10-3R-WY-VG-B	24	343,175	4.744E+09	C	Weld Toe	None
10-3R-WY-VP-A	24	**10,055,123**	**1.390E+11**	**A**	N/A	None
10-3R-WY-VP-B	24	**10,055,123**	**1.390E+11**	**A**	N/A	None
10-3R-WY-VB-A	19.07	2,232,742	1.548E+10	B	Weld Toe	None
10-3R-WY-VB-A (flip)	24	490,061	6.775E+09	C	Weld Toe	None
10-3R-WY-VB-B	21.14	3,516,775	3.322E+10	A	Shaft	None
10-3R-WY-AG-A	24	222,649	3.078E+09	D	Weld Toe	None
10-3R-WY-AG-A (flip)	24	212,891	2.943E+09	D	Weld Toe	None
10-3R-WY-UG-A	24	1,873,499	2.590E+10	A	Weld Toe	None
ZZ88734-A	24	677,763	9.369E+09	C	Backing	Fillet
ZZ88734-B	24	633,458	8.757E+09	C	Backing	Fillet
ZZ88735-A	28	286,526	6.290E+09	C	Backing	Fillet
ZZ88735-B	28	123,072	2.702E+09	D	Backing	Fillet
ZZ88735-B (flip)	28	129,090	2.834E+09	D	Backing	Fillet
10-2SR-WY-VG-A	12	**9,881,390**	**1.708E+10**	**B**	Weld Toe	
10-2SR-WY-VG-B	12	3,051,996	5.274E+09	C	N/A	
10-2SR-EC-VG-A	12	**10,652,284**	**1.841E+10**	**B**	N/A	N/A
10-2SR-EC-VG-B	12	**10,652,284**	**1.841E+10**	**B**	N/A	N/A
10-3R-WY-PG-A	24	1,272,665	1.759E+10	B	Weld Toe	None
10-3R-WY-PG-B	24	1,210,499	1.673E+10	B	Backing Bar	Tack
10-2R-EC-PG-A	24	137,220	1.897E+09	E	Collar	N/A
10-2R-EC-PG-B	24	244,763	3.384E+09	D	Collar	N/A
12-3R-WY-PG-A	24	292,468	4.043E+09	D	Weld Toe	Tack
12-3R-WY-PG-B	24	328,833	4.546E+09	C	Weld Toe	Tack
12-2R-EC-PG-A	24	169,059	2.337E+09	D	Collar	N/A
12-2R-EC-PG-B	24	119,289	1.649E+09	E	Collar	N/A

Table B-1: Experimental Test Results

Base Plate Stiffness and Stress Concentration Factor:

Model	B	Hole D	BP Thickness	L	MOI (Full)	MOI (Hole)	MOI (Average)	I/L	$(I/L)^{-1}$	SCF	
	(in)	(in)	(in)	(in)	(in^4)	(in^4)	(in^4)			DNV	Dong
8-XR-WY	12	5.64	1.5	15	3.375	1.789	2.582	0.172	5.810	1.706	1.765
	12	5.64	2	15	8.000	4.240	6.120	0.408	2.451	1.456	1.502
	12	5.64	3	15	27.000	14.310	20.655	1.377	0.726	1.387	1.437
	12	5.64	4	15	64.000	33.920	48.960	3.264	0.306	1.344	1.389
	12	5.64	10	15	1000.000	530.000	765.000	51.000	0.020	1.305	1.353
10-XR-WY	12	7.64	1.5	15	3.375	1.226	2.301	0.153	6.520	1.931	2.002
	12	7.64	2	15	8.000	2.907	5.453	0.364	2.751	1.683	1.744
	12	7.64	3	15	27.000	9.810	18.405	1.227	0.815	1.502	1.556
	12	7.64	4	15	64.000	23.253	43.627	2.908	0.344	1.438	1.490
	12	7.64	10	15	1000.000	363.333	681.667	45.444	0.022		
12-XR-WY	12	9.64	1.5	15	3.375	0.664	2.019	0.135	7.428	1.911	1.972
	12	9.64	2	15	8.000	1.573	4.787	0.319	3.134	1.699	1.753
	12	9.64	3	15	27.000	5.310	16.155	1.077	0.929	1.532	1.581
	12	9.64	4	15	64.000	12.587	38.293	2.553	0.392	1.469	1.516
	12	9.64	10	15	1000.000	196.667	598.333	39.889	0.025	1.405	1.494
12-XR-WY-3H	12	6	1.5	15	3.375	1.688	2.531	0.169	5.926	1.610	1.666
	12	6	2	15	8.000	4.000	6.000	0.400	2.500	1.504	1.555
	12	6	3	15	27.000	13.500	20.250	1.350	0.741	1.428	1.475
	12	6	4	15	64.000	32.000	48.000	3.200	0.313	1.405	1.450
	12	6	10	15	1000.000	500.000	750.000	50.000	0.020	1.372	1.417
12-XR-WY-NH	12	0	1.5	15	3.375	3.375	3.375	0.225	4.444	1.517	1.572
	12	0	2	15	8.000	8.000	8.000	0.533	1.875	1.445	1.495
	12	0	3	15	27.000	27.000	27.000	1.800	0.556	1.395	1.441
	12	0	4	15	64.000	64.000	64.000	4.267	0.234	1.380	1.425
	12	0	10	15	1000.000	1000.000	1000.000	66.667	0.015	1.365	1.410
10-2SR-WY	15.25	7.64	2	12	10.167	5.073	7.620	0.635	1.575	1.503	1.561
10-2S10-WY	15.25	7.64	2	12	10.167	5.073	7.620	0.635	1.575	1.536	1.601
10-2S11-WY	15.25	7.64	2	12	10.167	5.073	7.620	0.635	1.575	1.553	1.617
10-2S-WY	15.25	7.64	2	12.5	10.167	5.073	7.620	0.610	1.640	1.622	1.684
10-XR-WY-P2	12	7.64	1.5	15	3.375	1.226	2.301	0.153	6.520	2.198	2.209
	12	7.64	2	15	8.000	2.907	5.453	0.364	2.751	1.855	1.863
	12	7.64	3	15	27.000	9.810	18.405	1.227	0.815	1.615	1.621
	12	7.64	4	15	64.000	23.253	43.627	2.908	0.344	1.532	1.538
	12	7.64	10	15	1000.000	363.333	681.667	45.444	0.022	1.459	1.465
10-XR-WY-P3/8	12	7.64	1.5	15	3.375	1.226	2.301	0.153	6.520	2.169	2.249
	12	7.64	2	15	8.000	2.907	5.453	0.364	2.751	1.835	1.767
	12	7.64	3	15	27.000	9.810	18.405	1.227	0.815	1.554	1.444
	12	7.64	4	15	64.000	23.253	43.627	2.908	0.344	1.512	1.479
	12	7.64	10	15	1000.000	363.333	681.667	45.444	0.022	1.423	1.358

Table B-2: SCF and Base Plate Stiffness

Bibliography

AASHTO. *Standard Specifications for Structural Supports for Highway Signs, Luminaires and Traffic Signals.* American Association of State Transportation Officials, 2006 Interim to.

Anderson, Thomas Henry. *Fatigue Life Investigation of Traffic Signal Mast-Arm Connection Details.* Master's Thesis, Austin: The University of Texas at Austin, 2007.

Det Norske Veritas. *Fatigue Design of Offshore Steel Structures.* Recommended Practice DNV-RP-C203, Norway: Det Norkse Veritas, 2008.

Dong, P. "A Structural Stress Definition and Numerical Implentation for Fatigue Analysis of Welded Joints." *International Journal of Fatigue*, May 2001.

Koenigs, Mark T., Tamer A. Botros, Dylan Freytag, and Karl H. Frank. *Fatigue Strength of Signal Mast Arm Connections.* Research Report, Austin: Texas Department of Transportation, 2003.

Koenigs, Mark Thomas. *Fatigue Resistance of Traffic Signal Mast-Arm Connection Details.* Master's Thesis, Austin: The University of Texas at Austin, 2003.

Stam, Andrew P. *Fatigue Performance of Base Plate Connections Used in High Mast Lighting Towers.* Master's Thesis, Austin: The University of Texas at Austin, 2009.

Vita

Nicholas Bogart Richman was born in Silver Spring, Maryland on June 20, 1985. Nicholas is the son of Gerald L. Richman and Suzanne B. Richman. He attended Bethesda – Chevy Chase High School in Bethesda, Maryland, graduating in 2003. After graduating high school, Nicholas attended Tulane University in New Orleans, Louisiana where he studied Civil Engineering and developed a love of fried seafood and roast beef po' boys. During the fall of 2005, he attended the University of Maryland, while Tulane University was shut down due to Hurricane Katrina. Nicholas returned to the city of New Orleans the following semester and graduated from Tulane University summa cum laude with a Bachelor's Degree in Civil Engineering.

Nicholas enrolled at the University of Texas at Austin to pursue his Master's Degree in Engineering and shortly after graduating from Tulane, Nicholas came to Austin, Texas, to begin working on research.

Permanent Address: 4712 Overbrook Rd

Bethesda, Maryland 20816

This thesis was typed by the author.